UNIVERSITÉ DE MONTRÉAL

DISCOVERY AND CORRECTION OF SPATIAL NON-UNIFORMITY IN OPTICAL FIBERS: TOWARDS THE FABRICATION OF PERFECT ULTRA-LONG FIBER BRAGG GRATINGS FOR APPLICATIONS IN NON-LINEAR OPTICS

SÉBASTIEN LORANGER

DÉPARTEMENT DE GÉNIE PHYSIQUE

ÉCOLE POLYTECHNIQUE DE MONTRÉAL

THÈSE PRÉSENTÉE EN VUE DE L'OBTENTION

DU DIPLÔME DE PHILOSOPHIAE DOCTOR

(GÉNIE PHYSIQUE)

JANVIER 2018

UNIVERSITÉ DE MONTRÉAL

ÉCOLE POLYTECHNIQUE DE MONTRÉAL

Cette thèse intitulée:

DISCOVERY AND CORRECTION OF SPATIAL NON-UNIFORMITY IN OPTICAL FIBERS: TOWARDS THE FABRICATION OF PERFECT ULTRA-LONG FIBER BRAGG GRATINGS FOR APPLICATIONS IN NON-LINEAR OPTICS

présentée par : LORANGER Sébastien

en vue de l'obtention du diplôme de : Philosophiae doctor

a été dûment acceptée par le jury d'examen constitué de :

M. GODBOUT Nicolas, Ph. D., président

M. KASHYAP Raman, Ph. D., membre et directeur de recherche

M. LEBLOND Frédéric, Ph. D., membre

M. RUSSELL Philip, Ph. D., membre externe

DEDICATION

To my mother, Claire, who would have been proud to see me finish this PhD.

Thank you for all your love.

ACKNOWLEDGEMENT

I would like to give a very special thanks to Raman, who has been a great mentor and has led me into this great adventure of research and science. Thanks to him, I have high hopes for my future career.

I would also like to give a special thanks to my close friend and colleague Victor, with whom I have shared most of my years here at Polytechnique. Our work together has been very fun and instructive and I hope that our paths will cross on many future occasions!

I would like to thank my friends and colleagues Jean-Sébastien Boisvert, Jérome Lapointe, François Parent, Mathieu Gagné, Elton Soares, Mamoun Wahbeh, Amir Tehranchi, Frédéric Monet, Antoine Drouin and Meenu Ahlawat. Working with all of those friends has made this PhD very interesting, fun and instructive.

I wish to give a special thanks to our devoted technicians Jules Gauthier, Steve Dube, Jean-Paul Lévesque, Mikael Leduc, Jean-Sébastien Décarie and Traian Antonescu, without which none of this work would have been possible.

I would also thank the Vanier Canada Graduate Scholarship and the Natural Sciences and Engineering Research Council of Canada for the funding and support during my PhD.

Finally, a special thanks to my family and friends who have supported me during those long studies, especially my dad, André, who has always been there for me.

RÉSUMÉ

Les réseaux de Bragg (FBGs) sont des dispositifs tout-fibre communs en photonique et très utilisés en télécommunications comme filtres, réflecteurs sélectifs, compensateurs de dispersions et bien plus. Le sujet de cette thèse concerne les réseaux de Bragg ultra-longs, soit plus longs que la longueur typique des masques de phase (>20 cm). Les FBG ultra-longs ont la particularité d'avoir une très petite bande passante, un long temps de vie pour les modes de cavités distribués (DFB, cavité dont le champ des modes est distribué sur toute la longueur du réseau) et un grand *chirp* pour des FBG *chirpé*. Cette thèse étudie les cavités DFB ultra-longues à saut de phase, idéalement de π. Celles-ci comportent un seul mode de cavité à très haut facteur de qualité qui peut être utilisé comme laser lorsqu'un gain est présent. De tels lasers ont la propriété d'être monomode avec une largeur d'émission très fine en fréquence. Lorsqu'un gain non linéaire est présent, tel que du Brillouin ou Raman stimulé, ce qui est possible avec des FBGs ultra-longs, de tels lasers n'ont pas de restriction bande de longueurs d'onde, ce qui n'est pas le cas du gain des terres rares. En d'autres mots, ils peuvent être opérés à n'importe quelle longueur d'onde.

Ces dispositifs ultra-longs spécialisés ont toujours été très difficiles à produire. Même avec les meilleurs systèmes, la reproductibilité de fabrication de FBGs ultra-longs de haute qualité était absente. À cause de cela, de tels dispositifs n'ont jamais été développés pour des applications commerciales. Cette thèse étudie les difficultés d'écriture de FBGs ultra-longs et démontre des solutions permettant une reproductibilité de haute qualité. La méthode d'écriture utilisée et étudiée au long de cette thèse est l'écriture en continu par modulateur électro-optique avec interféromètre de Talbot. La principale difficulté trouvée dans l'écriture de FBGs ultra-longs est la haute non-uniformité dans toutes les fibres optiques, une caractéristique difficile à mesuré et hautement néfaste pour les FBG ultra-longs. La solution proposée : faire une correction de phase pendant l'écriture afin de permettre un réseau parfait dans toute fibre. La thèse présente 4 articles montrant les limitations et solutions de la fabrication de FBGs ultra-longs ainsi que l'opération de laser DFB à fibre par gain Brillouin et Raman dans de tels FBGs.

La thèse montre, dans la première publication, l'avantage de FBGs ultra-longs en démontrant un laser DFB avec un gain Brillouin dans de la fibre standard (SMF-28), au lieu de fibre hautement non linéaire typiquement utilisé pour de tels lasers. En effet, en utilisant des FBGs ultra-longs, le seuil laser peut être réduit grandement grâce au très long temps de vie des photons dans la cavité

monomode, permettant ainsi l'utilisation de fibres faiblement non linéaires d'être utilisées. Une nouvelle technique est aussi démontrée afin d'écrire des sauts de phase reproductible avec une écriture en continu utilisant des modulateurs électro-optiques : en générant un saut temporaire en longueur d'onde de Bragg écrite. Cette technique résout un des problèmes du manque de rétroaction sur les modulateurs de phase, un problème décrit dans la thèse.

Bien que les FBGs DFB ultra-longs ont été démontrés dans la SMF-28, la production reproductible de tels réseaux dans d'autres types de fibres se montrait impossible. Cette thèse identifie le problème: la non-uniformité des fibres optiques. Une nouvelle méthode de caractérisation est décrite afin de mesurer cette non-uniformité, un sujet du second article présenté dans cette thèse. La méthode comprend l'écriture de FBGs sondes à différentes longueurs d'onde dans la même région d'intérêt de la fibre, puis l'utilisation de réflectométrie optique dans le domaine fréquentiel afin de mesurer la longueur d'onde de Bragg vs la position. Étant donné que tous les paramètres d'écritures sont bien contrôlés et que les fluctuations aléatoires dues à l'environnement sont moyennées par plusieurs FBGs, la déviation de longueur d'onde de Bragg observée est une mesure directe de la variation de l'indice de réfraction effective du mode guidé.

Une méthode de correction est alors proposée et démontrée afin de corriger cette non-uniformité et ainsi écrire des FBGs ultra-longs de façon reproductible. Cela est présenté dans le 3^{e} article, où les résultats de FBGs produits sont comparés avant et après la correction. La méthode consiste à utiliser la mesure de déviation de longueur d'onde de Bragg afin d'écrire un FBG final où la phase est compensée selon cette mesure. La méthode s'est montré un grand succès.

Une fois qu'une méthode de production reproductible a été démontrée, une vaste étude de lasers DFB à fibre utilisant le gain Raman a été menée, soit le sujet du 4^{e} article décrit dans la thèse. D'abord, une nouvelle méthode de simulation a été développée afin de permettre une résolution plus rapide des équations de modes-couplés. Une étude détaillée des paramètres des FBGs DFB a été menée et ces dispositifs ont été optimisés dans les conditions idéales. La simulation a été comparée avec des dispositifs expérimentaux, ce qui a mené à des conclusions intéressantes. Bien que de tels lasers DFB peuvent être très efficaces avec des seuils lasers très faibles, ils sont limités par l'apparition d'un gradient thermique due au chauffage du cœur de la fibre par la présente des champs internes de haute intensité. Des solutions sont proposées dans la thèse afin d'adresser le problème, telles que le contrôle dynamique du saut de phase pendant l'opération.

ABSTRACT

Fiber Bragg gratings (FBGs) are common all-fiber devices in photonics and have been widely used in telecommunications as filter, selective reflectors, dispersion compensators and more. The subject of this thesis is specialised Ultra-long FBGs, which are defined as longer then the typical length of a phase mask (>20 cm). Ultra-long FBGs have the particularity of having very narrow bandwidth, long lifetime for distributed feedback (DFB) cavity modes and high chirp for chirped FBGs. A DFB cavity is a single-longitudinal-mode long cavity, as the photon is trapped along the entire length of the FBG. This thesis studies ultra-long DFB cavities known as "phase-shifted" or "π-shifted" and have a single phase defect inside the FBG to create the high Q cavity mode, which can then be used as a laser if an active gain medium is present. Such lasers would have the property of narrow linewidth single-frequency operation. When used with non-linear gain, such as Stimulated Raman or Brillouin gain, which can be done with ultra-long FBGs, those lasers have no specific band of operation restriction, contrary to rare-earth gain. In other words, they can be operated at any wavelength.

Those specialised ultra-long FBG devices have long been difficult to produce. Even with the best systems, reproducibility of high quality ultra-long FBGs has always been absent. Because of this, such device was never fully developed for commercial applications. This thesis studies the difficulties of ultra-long FBG writing and demonstrates solution for reproducible high-quality fabrication. Stimulated Brillouin and Raman scattering gain phase-shifted DBF ultra-long FBGs are then modeled, optimized and tested. The writing method is continuous writing using an electro-optic modulator driven Talbot interferometer. The main difficulty found in ultra-long FBG writing, is high non-uniformity found in *all* optical fibers, a characteristic difficult to measure and very detrimental for ultra-long FBGs. A solution was proposed for this: make a phase correction during writing to allow perfect FBGs in any fibers. The thesis presents 4 articles relating ultra-long FBG fabrication limitations and solutions as well as Brillouin and Raman DFB fiber laser operation in ultra-long FBGs.

The thesis shows, in the first publication, the advantage of ultra-long FBG by DFB lasers using non-linear gain (Stimulated Brillouin Scattering) in standard fiber (SMF-28), instead of typical highly non-linear fibers. Indeed, by using ultra-long FBGs, the lasing threshold can be significantly reduced thanks to the very long lifetime of photon in the long single-mode cavity, therefore

allowing low-non-linear fibers to be used. A new technique is also shown to ensure reproducible phase-shift with a modulator-based continuous writing system: by generating a temporary shift in written Bragg wavelength. This technique solves the issue of lack of feedback on modulators, a problem described in this Thesis.

Although ultra-long DFB FBG were demonstrated in SMF-28, reproducible production of ultra-long FBGs in other types of fiber was proven impossible, as stated above. This thesis identifies the issue: non-uniformity of fibers. A new characterisation method is described to measure this non-uniformity, a subject of the second paper described in the thesis. This method involves writing weak probe gratings at different wavelengths in the same length of interest of fiber, and then using optical frequency domain reflectometry to measure the Bragg wavelength vs position. As all writing parameters are well controlled, and environmental random fluctuation are averaged out by multiple probe FBGs, the observed Bragg wavelength deviation is directly related to a variation in the effective refractive index.

A correction method is then proposed and demonstrated to correct for this fiber non-uniformity and therefore write ultra-long FBGs in a reproducible way. This was demonstrated in a third paper, where production results are compared before and after correction with dramatic effect. The method consists in using the measured Bragg wavelength deviation from probe FBGs to write a final phase compensated FBG. The method proved very successful.

Once a reproducible production method was demonstrated, a vast study on DFB lasers using Raman gain was conducted, the subject of the 4^{th} paper described in the thesis. First, a new simulation method was developed to allow a much faster solving of the couple-mode equation, compared to previous work on the subject. A detailed study on all parameters of ultra-long DFB FBG was undertaken and such devices were optimized in the ideal conditions. The simulation was compared with experimental data, which led to interesting conclusions. Although such DFB lasers could potentially be very efficient with low threshold, they are limited by non-linear thermal gradient due to heating from the high internal fields. Solutions are proposed in the thesis to address this, such as dynamically control the phase shift through heating or cooling, during laser operation.

TABLE OF CONTENT

LIST OF TABLE

LIST OF FIGURES

LIST ACRONYMS AND ABBREVIATIONS

CFBG	Chirped fiber Bragg grating
DFB	Distributed feedback
EO	Electro-optic
EOM	Electro-optic modulator
ESA	Electrical spectrum analyser
FBG	Fiber Bragg grating
FFT	Fast Fourier transform
FSR	Free spectral range
FUT	Fiber under test
MFD	Mode field diameter
NA	Numerical aperture
NL	Non-linear
OBR	Optical back-reflectometer
OCT	Optical coherence tomography
OFDR	Optical frequency domain reflectometry
OSA	Optical spectrum analyser
PS	Phase shifted
RE	Rare earth
RI	Refractive index
RIU	Refractive index units
RK4	Runge-Kutta, 4^{th} order
SBS	Stimulated Brillouin scattering
SRS	Stimulated Brillouin scattering

LIST OF APPENDIX

CHAPTER 1 INTRODUCTION

Optical fibers play an important role in our society: from the backbone of our telecommunication network to advanced laser sources and sensing applications. One type of device has accompanied researchers and engineers since 1978, a decade after the beginning of the grand adventure of optical fiber: fiber Bragg gratings (FBGs). These devices are an inscribed periodic change in the effective refractive index inside a waveguide, which acts as a wavelength selective reflective filter. Although such filters had been predicted in the mid 70^{ies} [1], it remained a difficult device to fabricate. This issue was resolved purely by accident, as many discoveries are, at the Canadian Communication Research center in 1978 by Hill, Fujii, Johnson and Kawasaki [2]. When injecting light from an argon ion laser into a germanium-doped-core silica fiber, Hill *et al.* noticed a reflection which grew over time. They then discovered that this reflection was permanent: a narrow-band filter had been successfully imprinted on the fiber. This was caused by a 4% back-reflection between the fiber output-ends, which generated a standing wave and slowly wrote a grating inside the core. When the Ar-ion laser mirror facing the fiber was removed, the authors realised that the laser kept oscillating, thanks to the reflection from the newly formed FBG, as shown in Figure 1.1. Photosensitivity in optical fiber was therefore discovered and the first FBG was thus demonstrated.

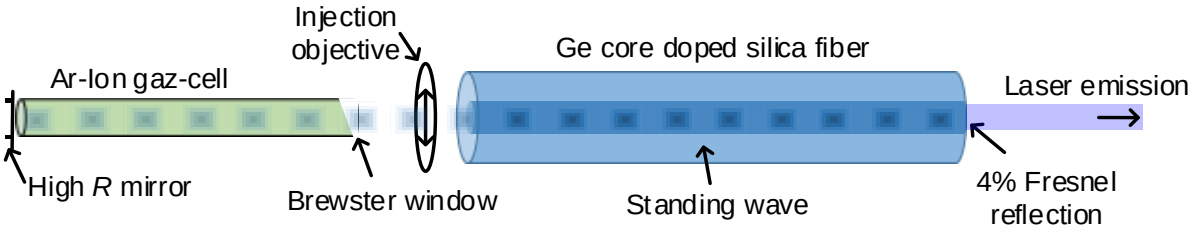

Figure 1.1: Hill et al.'s experiment discovering photosensitivity and how to make FBGs using an Ar-ion laser. A Fresnel reflection caused a standing wave in a Ge-doped silica fiber, which in turn wrote a permanent grating in the fiber through photosensitivity.

Unfortunately, this method of writing a grating is restricted to the photosensitive wavelength region, and with periods that cannot be altered to arbitrary wavelengths. Since then, writing techniques and more complex and optimized designs of FBGs have appeared. Present day FBGs are written using holographic techniques [3], a more convenient way which allows writing at

virtually any wavelengths. FBGs have become a crucial part of the telecommunication infrastructure for implementing narrow-band selective filters to select and separate channels [4]. Complex designs were also proposed to select multiple channels at once [5, 6]. FBGs have also had an important role in solving a major long-distance communication issue: dispersion of light in optical fibers. By chirping the FBG (CFBGs), i.e. linearly changing the resonance wavelength along the position, such filters could be used as dispersion compensators [6-8]. Being small and customizable devices, they have been used ever since the beginning of the telecoms explosion. Today, thanks to phase encoding, electronic [9] or digital [10] post-processing techniques are used for dispersion compensation, which does not require any physical device and has reduced the need for CFBGs.

FBGs have been also used as laser cavity reflectors and later, as distributed feedback (DFB) lasers, a type of laser where the feedback happens all along the FBG, i.e. in which a mode oscillates inside the grating. The very first proposed application of FBG by Hill *et al.* was as a reflector for their argon-ion laser [2]. Since FBGs offer tunable reflectivity and wavelength, and thanks to their narrow band, they can be used to select a specific lasing wavelength in a broad-band gain medium. FBG based DFB lasers have also shown exceptional performance as a single-frequency laser source, as will be described in section 2.3 of the next chapter.

Since their invention, FBG fabrication techniques and applications have increased in number immensely. Indeed, FGB applications can be found in almost all fields where optical fiber is used: telecommunications, sensing, laser sources, biomedical and quantum optics and more. Many of these areas were addressed during the course of my PhD, as my work focused on developing new fiber tools based on FBGs which can be applied, and have been applied, to the above applications. Several new ideas and complex designs of FBGs have been proposed and investigated throughout my years of research, but here we focus on the main contributions, the subject of this thesis: the fabrication of perfect ultra-long FBGs.

"Ultra-long" is of course a relative term but is typically defined as being >20 cm long. This is compared to the current typical gratings length (<10 cm) which are limited by the length of the phase-masks used to write them. The characteristics of such long-length gratings have been known and pursued for a long time, but the technology and known techniques at the time could not produce such gratings. My predecessors at Polytechnique had solved some of the problems, such as high-

speed writing, perfect apodization, high tunability on written wavelength and phase and reduced phase noise from vibrations [11, 12] by implementing a novel system which will be presented in the next chapter. However, by attempting various complex devices on specialty fibers, new problems specific to ultra-long FBG fabrication were revealed. This has led to the development of new fabrication techniques and new devices, which will be described in this thesis.

Ironically, the best writing technique which yields the highest quality FBGs (no chirp nor phase noise or defect) remains the very first technique developed by Hill *et al.*, since the grating is written by a perfect standing wave. As mentioned before, such a technique is unfortunately not suitable for all operating wavelengths and generally limited to the UV. All writing techniques have tried to reproduce such high quality FBGs, which could never be completely achieved. When going into ultra-long FBGs, such difficulties only tend to increase. The goal of this thesis is therefore to return to the top-quality FBGs produced by Hill *et al.*, while applying it to fully tunable, ultra-long FBGs. Such an accomplishment could, as we have already started to demonstrate, lead to new types of devices in non-linear optics.

1.1 The Motivation and problem

A type of FBG structure which will be studied in this thesis, and which gains much from ultra-long length is a phase-shifted DFB grating. As stated earlier, a DFB mode resonates throughout the FBG length. Uniform FBGs have intrinsic DFB modes, which appear spectrally on either side of the stop-band (central resonance band) and come from a Fabry-Perot-like oscillation from the abrupt ends of the FBG. A DFB mode can be created inside the stop-band, which would offer a much higher confinement and therefore quality-factor. To do so, the phase of the FBG must be shifted by a half-period of the grating (π-shift, also considered as quarter-wavelength). More details on phase-shifted DFB structures will be given in the next chapter.

Ultra-long FBGs have the advantage of enhancing grating characteristics, especially in terms of frequency bandwidth and in the case of DFB modes, their linewidth. For a constant strength (constant transmission, losses), a FBG will see its bandwidth reduced inversely with its length. The same goes for the linewidth of DFB resonance modes of a phase-shifted FBG. This brings a highly reduced linewidth of laser emission from such structures. It can also be pointed out that ultra-long FBGs will have a reduced requirement on the coupling constant (refractive index change) with

increasing length for a constant overall reflectivity, as this strength is the product of coupling constant, κ_{ac}, and length, L (called $\kappa_{ac}L$). However, one must remain cautious when pointing out this advantage: short FBGs may have a higher requirement on coupling constant, therefore on laser writing exposure, but the UV exposed-length is also shorter, therefore total fabrication time can be equivalent to an ultra-long FBG with weak UV exposure. Therefore, it is better to compare FBGs at constant strength. Nevertheless, the lower requirement on refractive index change for ultra-long FBGs allows the use of a wider range of writing techniques and fibers.

These advantages offer new possibilities for applications: ultra-narrow filters, long photon lifetime cavities, high-internal optical fields for non-linear processes, low thresholds for lasers, narrow linewidth lasers etc. For instance, these properties can allow optically pumped stimulated Raman scattering (SRS) narrow linewidth fiber lasers to be fabricated, which can be implemented at any wavelength, since Raman gain is not specific to a spectral band, contrary to rare-earth dopants. Such lasers could be useful in many applications, one of which is the laser guide-star [13] which requires a narrow-line (high coherence) laser to lock on the 589 nm sodium line. However, there is little choice for amplification at this wavelength. On the other hand, the second harmonic of a SRS DFB fiber laser at 1178 nm could accomplish that task easily, while offering fine tunability. This is just one of the many potential applications for such a technology.

Despite these advantages, the ultra-long FBGs is not available in the market: only specialised labs, including ours, can fabricate such gratings. Even then, the specifications are difficult to achieve. The reason for this is that fabrication of ultra-long gratings is very difficult: a continuous writing system with top-of-the-line air-bearing stages are required. The best system was developed in our lab before my PhD: a modulator-based interferometer for high-speed, with zero vibration and perfect apodization [12]. Despite this, several problems remained unsolved, as were progressively discovered at the beginning of this PhD:

- Phase shift was not reproducible and difficult to control on the modulator system. This was found to be because of lack of feedback on the phase applied by the modulator.
- Difficult writing conditions due to environment change (noise, reproducibility issues, etc.)
- FBG are not reproducible in specialised fibers (in most fibers except standard SMF-28).

These issues were therefore quite limiting for studying specialised structures and had to be solved to properly attack the initial goal set at the beginning of my PhD: to design and optimize special structures for non-linear optical applications, such as stimulated Brillouin and Raman scattering laser based on DFB phase-shifted FBGs. Designing new structures also requires good modeling and simulation. Models already existed for such lasers, however the proposed simulation methods were so time consuming, that very little study was possible with varying parameters. Also, except for a few demonstrations, which did not fit the prevailing models, there were no experimental studies on an extended set of FBGs due to severe limitations in their reproducibility. Due to these obstacles, the objectives of my PhD had to be redefined as will be described in the next sub-section.

1.2 Objectives

Considering the problems described above, we can state four objectives for the PhD described below.

1. **Understanding the limitations of ultra-long FBG writing:**

The first objective of this Thesis is to understand the problems that limits the fabrication of perfect gratings. Understanding the limitations is useful not only for improving fiber fabrication technique, but also to understand what structures (phase, amplitude) can be inscribed in which fibers.

2. **Develop fabrication technique for perfect and reproducible Ultra-long FBG**

The goal of this objective is to reach the perfect gratings, as demonstrated by Hill *et al*. in 1978, while maintaining complete tunability on the wavelength and flexibility on the structure (phase, amplitude) to inscribe.

3. **Develop a DFB model and simulation scheme for understanding and optimizing Raman DFB lasers**

Understanding the physics of a device is crucial before any design can take place. This objective is to develop a proper model representing what is observed experimentally, simulate the effect of all potential parameters on performance to understand device operation and develop an optimization method.

4. **Design, optimize and demonstrate high performance Raman and Brillouin gain DFB lasers**

This objective is the experimental realisation of optimized and high-performance Raman and Brillouin gain DFB lasers. To do so, experimental FBGs must be tested with varying parameters and compared with the model. High performance (low threshold, high efficiency) is aimed or at least a better understanding on the requirements for optimal future performance.

1.3 Organisation of thesis

As a start for the thesis, a detailed literature review will be made on various subjects covered in the thesis or during my PhD. First, a review of FBG theory and simulation methods. Second, a review of FBG writing techniques, including, of course, a state-of-the-art on ultra-long writing. Third, various applications related to work done during my PhD will be reviewed. Those are not directly linked to the subject presented in the articles of this thesis, but they were instrumental in achieving the first objective by identifying problems of the writing technique. Finally, theory and state-of-the-art will be presented concerning DFB Raman and Brillouin fiber laser, the subject of the 1st and 4th article and of the two last objectives.

After this literature review, an introduction chapter to the presented article will be made. This chapter will describe the methodology and link between each article. Following this, 4 articles are presented:

- The first article will present my initial work on ultra-long DFB lasers, where issues of phase-shift and writing stability were resolved. A Brillouin gain DFB fiber laser in SMF-28 is also presented and brings some insights on Raman and Brillouin DFB fiber laser which has been useful for the study of Raman gain DFB fiber laser.
- The second article is directly related to the first objective and describe the cause of why ultra-long FBGs in specialised fibers are not reproducible and often suffer from bad quality. This cause is fiber non-uniformity. A measurement method for the fiber's effective refractive index is presented in the paper.

- The third article describes the solution to the problem explained in the second article. This is directly related to the second objective. A new ultra-long FBG fabrication technique is presented which can adapt to any fiber non-uniformity.
- The fourth and last article is on a vast study, both theoretically and experimentally, on Raman gain DFB fiber lasers. The FBGs in this article are inscribed using the technique described in the 3rd article. This paper answers the two last objectives.

Following these 4 papers, a general discussion will be made concerning the overall work presented in this thesis. This discussion will be followed by a concluding chapter.

CHAPTER 2 LITERATURE REVIEW

In this chapter, a detailed literature review is presented on fiber Bragg gratings (FBGs). First, a description of FBG theory and how they are fabricated will be shown. Then, some specialised application which were studied during my PhD will be described and reviewed. As the main subject of this thesis is ultra-long phase-shifted DFB FBGs for laser applications, the literature review focuses on this subject in the last section.

2.1 Modeling of fiber Bragg gratings

2.1.1 Theory of fiber Bragg gratings

This section will describe the theory of FBGs. For clarity purpose, this description will be simplified to the relevant expressions. For a more detailed demonstrations of those expressions, various work can be explored more thoroughly such as Gloge's [14] for weakly guided mode theory and Kashyap's [15] for grating coupling mode theory.

A fiber Bragg grating is a periodic variation of the refractive index (RI) in a guided medium, usually an optical fiber, as shown in Figure 2.1. There are several techniques that can be used to inscribe this structure, as will be discussed in the next section, which usually require interferometric methods as the period of the RI variation is sub-micron. The general mathematical description of a Bragg grating in terms of RI variation is as follows [15]:

$$n(z) = n_0 + \overline{\Delta n}(z) + \sum_{N=-\infty}^{\infty} \Delta n_N(z) \cos\left(\frac{2\pi N z}{\Lambda} + \phi_N(z)\right) \tag{2.1}$$

Where n_0 is the effective RI of the guided mode before an FBG is inscribed, $\overline{\Delta n}(z)$ is the average RI increase after the FBG is inscribed, N is an integer order of the decomposed Fourier harmonic component of the RI modulation, $\Delta n_N(z)$ the modulation amplitude for N^{th} harmonic, Λ is the grating period and $\phi_N(z)$ is any other phase variation along the grating of the N^{th} harmonic. During fabrication, the average index rises, and the modulation RI and phase are parameters which can be engineered along the propagation axis of the fiber. Note that some fabrication techniques generate higher-order FBGs, which have several resonances at higher harmonic frequencies (shorter wavelengths). For example, a 2nd -order FBG with a first order resonance wavelength at 3 µm, will

also have a resonance at ~1550 nm and for the third order, possibly at ~775 nm ($\Delta n_{N=3}$). Using most fabrication techniques, FBGs can usually be approximated, with good reliability, by a perfect 1st order sinusoidal modulation, therefore simplifying Eq. (2.1) by neglecting other harmonics as:

$$n(z) = n_0 + \overline{\Delta n}(z)\left(1 + v(z)\cos\left(\frac{2\pi z}{\Lambda} + \phi(z)\right)\right) \tag{2.2}$$

Where $v(z)$ represents the visibility of the modulation ($0 \leq v \leq 1$), which can be controlled by a process called apodization. The inscribed modulation $\overline{\Delta n}$ is generally small and can be considered as a perturbation of the RI.

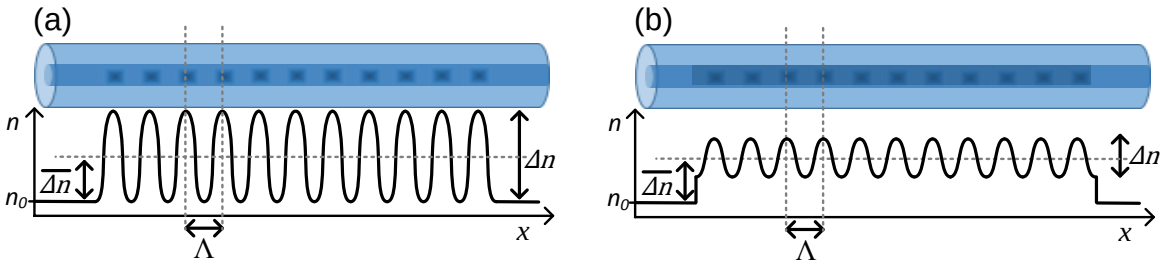

Figure 2.1: Schematic representation of a uniform FBG for (a) perfect visibility (v = 1) and (b) reduced visibility (v ~ 0.5)

To consider the effect of such a periodic RI change on a propagating light wave, we must first consider the constitutive equation of polarisation:

$$P = \varepsilon_0\big(\varepsilon_r - 1 + \Delta\varepsilon(z)\big)E \tag{2.3}$$

Where ε_r is the relative permittivity and the term in parenthesis the first order susceptibility $\chi^{(1)}$ perturbed by the periodic modulation in the permittivity, $\Delta\varepsilon(z)$. Using the relationship between RI and permittivity ($n^2 = \varepsilon_r$), we have:

$$\big(n_0 + \delta n(z)\big)^2 = \varepsilon_r + \Delta\varepsilon(z) \tag{2.4}$$

Where $\delta n(z)$ is the RI perturbation term in Eq. (2.2). considering this perturbation to be very small, the effect on the permittivity can be simplified as:

$$\Delta\varepsilon(z) \approx 2n\delta n(z) = 2n\overline{\Delta n}(z)\left(1 + v(z)\cos\left(\frac{2\pi z}{\Lambda} + \phi(z)\right)\right) \tag{2.5}$$

By placing equation (2.5) inside the constitutive relation, equation (2.3), the effect of the grating inscription on the induced polarisation is:

$$P = \varepsilon_0 \left(\varepsilon_r - 1 + 2n\overline{\Delta n}(z) \left(1 + v(z) \cos\left(\frac{2\pi z}{\Lambda} + \phi(z) \right) \right) \right) E \tag{2.6}$$

Let us now define the total transverse field in the fiber as:

$$E_t = \frac{1}{2} \left(A_v(z) \xi_{vt}(x,y) e^{i(\omega t - \beta_v z)} + B_\mu(z) \xi_{\mu t}(x,y) e^{i(\omega t + \beta_\mu z)} \right) + cc \tag{2.7}$$

Where ξ_{vt} and ξ_{ut} are the normalised transverse electrical fields distribution of the μ^{th} and ν^{th} guided coupled-modes orders, A_v and B_μ the forward and backward fields, respectively, along the propagation axis and β_v and β_μ the propagating constants of the two guided modes. From the field definition of equation (2.7), we can define the forward reference field (R) and the coupled backward signal field (S) as:

$$\begin{aligned} R &= A_v e^{-\frac{i}{2}(\Delta\beta z - \phi(z))} \\ S &= B_\mu e^{-\frac{i}{2}(\Delta\beta z - \phi(z))} \end{aligned} \tag{2.8}$$

In which $\Delta\beta$ represents the phase mismatch:

$$\Delta\beta = \beta_v + \beta_\mu - \frac{2\pi}{\Lambda} \tag{2.9}$$

Coupling will therefore occur when this $\Delta\beta$ tends to zero. For a FBG in a single mode fibre, the coupled waves are counter-propagating and are of the same order ($v = \mu$), therefore the resonance wavelength, i.e. the Bragg wavelength, can be defined as:

$$\lambda_B = 2n_{eff}\Lambda \tag{2.10}$$

Where n_{eff} is the effective RI of the guided mode.

Considering weakly guided mode theory as developed by Gloge [14] and well described in many subsequent works [15, 16], the RI perturbation of equation (2.6), and differentiating the defined fields of equation (2.8), the coupled-mode equations can be expressed as:

$$\frac{dR}{dz} = -i\left[\kappa_{dc} + \frac{\Delta\beta}{2} - \frac{1}{2}\frac{d\phi(z)}{dz}\right]R - i\kappa_{ac}^{*}S$$
$$\frac{dS}{dz} = i\left[\kappa_{dc} + \frac{\Delta\beta}{2} - \frac{1}{2}\frac{d\phi(z)}{dz}\right]R + i\kappa_{ac}S \quad (2.11)$$

Where κ_{ac} and κ_{dc} are the modulation and dc coupling constants, respectively. κ_{ac} is linked to the RI modulation depth, Δn and influences the strength of the coupling. κ_{dc} is linked to the average RI variation $\overline{\Delta n}$. Its effect is adding a local phase, thus altering the phase matching condition. If κ_{dc} increases, it will simply move the resonance wavelength and is therefore the reason why strong FBGs tend to be red-shifted in wavelength for the same period Λ. If κ_{dc} is varied spatially, it will induce a chirp, having the same effect as a non-linear phase variation $\phi(z)$. Based on equations (2.1) and (2.2), the coupling constants are defined by:

$$\kappa_{ac} = \beta c \varepsilon_0 \iint_{-\infty}^{+\infty} \frac{\Delta n}{2} \xi_{vt} \xi_{ut} dx dy = \frac{2\pi n_{eff} \Delta n}{\lambda} \eta$$
$$\kappa_{dc} = \frac{4\pi n_{eff} \overline{\Delta n}}{\lambda} \eta = \frac{2\kappa_{ac}}{v} \quad (2.12)$$

Where η (dimensionless) represent the overlap integral of fields with index modulation Δn in the core cross-section. The coupled-mode equations (2.11) can be solved by using standard eigenvalue techniques [17] for a uniform FBG (constant κ_{ac}, κ_{ac} and ϕ) of length L. The ratio between the reflected field $S(0)$ and the reference input field $R(0)$ can be expressed analytically by [15]:

$$\rho = \frac{S(0)}{R(0)} = -\frac{\kappa_{ac} \sinh(\alpha L)}{\delta \sinh(\alpha L) - i\alpha \cosh(\alpha L)} \quad (2.13)$$

Where δ represents the resonance mismatch:

$$\delta = \kappa_{dc} + \frac{\Delta\beta}{2} - \frac{1}{2}\frac{d\phi(z)}{dz} \quad (2.14)$$

And α, the coupling term:

$$\alpha = \sqrt{|\kappa_{ac}|^2 - \delta^2} \quad (2.15)$$

Equation (2.13) represents the entire spectral characteristics of a uniform FBG, as can be seen in Figure 2.2. The peak reflectivity of the FBG (where $\Delta\beta = 0$) depends only on the modulation depth and on the length and is simply:

$$|\rho_{\delta=0}|^2 = \tanh^2(\kappa_{ac}L) \tag{2.16}$$

Where the product $\kappa_{ac}L$ is often considered as the strength of the FBG. The reflection spectra between the first zeros around the central resonance is considered as the stop-band (in reference to a band-gap of a periodic structure, as a FBG is effectively a weak 1D photonic crystal). The width of this stop-band can be calculated as:

$$\Delta\lambda = \frac{\lambda_B^2}{2\pi n_{eff}L}\sqrt{(\kappa_{ac}L)^2 + \pi^2} \tag{2.17}$$

Examples of reflection, transmission and group-delay spectra are shown in Figure 2.2. As can be seen, uniform FBGs have important side-structure outside of the stop-band. This side-structure comes from high frequency variations, such as the abrupt square shape of the uniform FBG, but can also appear due to noise along the FBG as will be discussed in Section 2.2. The side-lobes are normally minimised through apodization: a process by which the κ_{ac} (more specifically, the visibility of fringes) is slowly varied along the grating. As this thesis focuses on ultra-long FBGs, a comparison is given in Figure 2.2 between a typical 5 cm length grating and a 30 cm ultra-long version, for a similar $\kappa_{ac}L$ strength. As can be seen, the main interest of the ultra-long version is a narrowing in the spectral characteristics of the FBG, such as it's band-width, and an increase in the photon trap-time within the structure, strongly influencing group delay.

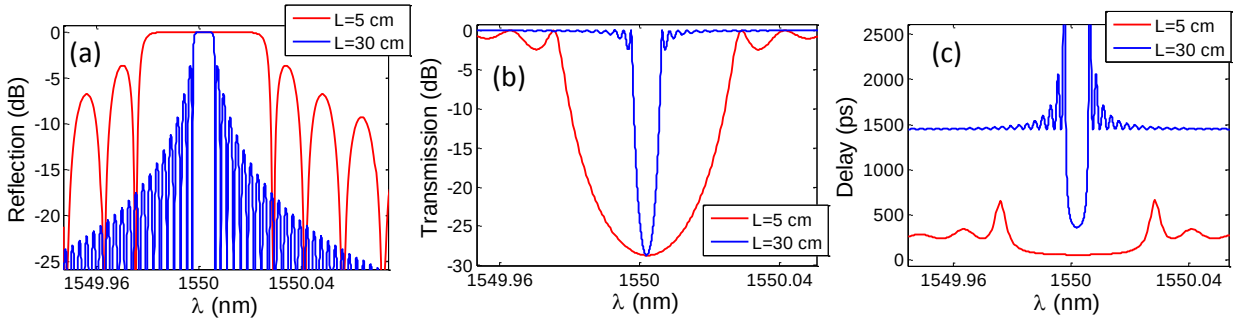

Figure 2.2: Example of FBG (a) reflection, (b) transmission and (c) group delay of reflection spectra as calculated by the transfer-matrix method (section 2.1.2). A typical 5-cm short FBG is compared with an ultra-long 30-cm FBG for the same strength ($\kappa_{ac}L$ = 4).

Long-period gratings (LPGs), on the other hand, scatter the guided light in the forward direction. As their name suggests, these structures have much longer periods (tens of µm to mm) instead of the sub-µm periods of FBGs. These structures can couple different propagation modes in a wave-guide in the same direction, such as a core-mode with cladding modes in an optical fiber. The model is similar to FBGs, except that equation (2.7) must now describe modes in the same direction with different n_{eff}, therefore different propagation constants β. The resonance condition (2.9) remains the same, but depends on a difference of effective refractive index ($n_{eff_\mu} - n_{eff_\nu}$). Since LPGs were not studied during my PhD they have not been considered in depth in this thesis.

The above gives a general idea of the behavior of a uniform FBG. However, in this thesis, complex structures of FBGs are studied. To understand these structures, simulating their behavior is a crucial step in their design. Simulation techniques will therefore be reviewed in the next section.

2.1.2 Simulation techniques for non-uniform FBG

The most common and flexible technique used to simulate a non-uniform FBG structure is called the Transfer-Matrix Method (TMM) [15]. This method consists in separating the FBG into *M* uniform sections for which the exact analytical solution is known (equation (2.13)). Each section can be represented in the form of a matrix, as shown schematically in Figure 2.3 and represented by:

$$\begin{bmatrix} R(0) \\ S(0) \end{bmatrix} = T \begin{bmatrix} R(\Delta z) \\ S(\Delta z) \end{bmatrix} = \begin{bmatrix} T_{11} & T_{12} \\ T_{21} & T_{22} \end{bmatrix} \begin{bmatrix} R(\Delta z) \\ S(\Delta z) \end{bmatrix} \tag{2.18}$$

With the matrix elements:

$$T_{11} = \cos(\alpha \Delta z) + \frac{i\delta \sin(\alpha \Delta z)}{\alpha} \tag{2.19}$$

$$T_{22} = \cos(\alpha \Delta z) - \frac{i\delta \sin(\alpha \Delta z)}{\alpha} \tag{2.20}$$

$$T_{12} = \frac{i\kappa_{ac} \sin(\alpha \Delta z)}{\alpha} \tag{2.21}$$

$$T_{21} = \frac{i\kappa_{ac} \sin(\alpha \Delta z)}{\alpha} \tag{2.22}$$

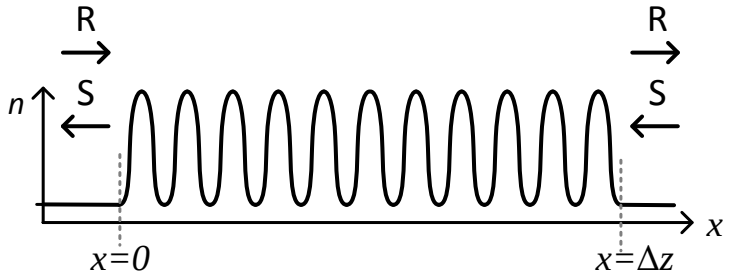

Figure 2.3: Schematic representation of a uniform FBG Δz section represented by a single matrix, with an integer number of periods.

Any phase variation in the grating between two sections can be calculated by adding a phase matrix between the twin section matrix, as shown below in equation (2.23) below. This is extremely useful to model phase-shifted distributed feedback structure, the main subject of this thesis, as discussed by Haus and Lai [18].

$$T_{\phi} = \begin{bmatrix} e^{-i\Delta\phi/2} & 0 \\ 0 & e^{i\Delta\phi/2} \end{bmatrix} \tag{2.23}$$

As light propagates from one section to another, which need not be identical (different κ_{dc}, κ_{ac} and ϕ), a transfer matrix can be calculated which represents the FBG as a whole:

$$\begin{bmatrix} R(0) \\ S(0) \end{bmatrix} = T^1 T^2 \ldots T^N \begin{bmatrix} R(L) \\ S(L) \end{bmatrix} = T \begin{bmatrix} R(L) \\ S(L) \end{bmatrix} \tag{2.24}$$

With this transfer matrix, the input (z = 0) and output fields (z = L), R and S may be calculated. By assuming a normalised input reference (R(0) = 1) and zero signal back-propagating input from the other end (S(L) = 0), the reflected and transmitted field solutions are found as:

$$R(L) = \frac{1}{T_{11}} \tag{2.25}$$

$$S(0) = \frac{T_{21}}{T_{11}} \tag{2.26}$$

Each transfer matrix is considered for one particular wavelength. Therefore, to calculate a reflection and/or transmission spectrum, a transfer matrix must be calculated for each wavelength. From these values, both the amplitude and phase of the reflected/transmitted signals can be calculated, thus characterising the behavior of a complex FBG. Knowing the phase, the group velocity can be calculated as its derivative, as shown in Figure 2.2(c). Once the solution at position

L is found, the FBG's internal field can also be determined by applying successively the matrix multiplication in equation (2.18) from $z = L$ to $z = 0$ from the definition of R and S as shown in equation (2.8). Gain and loss can be added either in the phase matrix of equation (2.23) as a real exponent, or directly in the coupled-mode equations (2.11) as an imaginary κ_{dc} (this was used in the simulation of article 4).

This TMM is extremely powerful and has been used for all simulations shown in this thesis. However, there are limitations, as discussed by Yamada *et al.*[19]. Indeed, the transfer-matrix supposes each section is an analytical solution to an integer number of grating period uniform FBG. The phase error can become important (will mostly affect the side-lobes) for short sections in which this condition is not respected. However, by maintaining the sections long ($dz \gg \Lambda$), this phase error becomes negligible. The transfer-matrix method is shown schematically Figure 2.4(a) and compared with other methods described below.

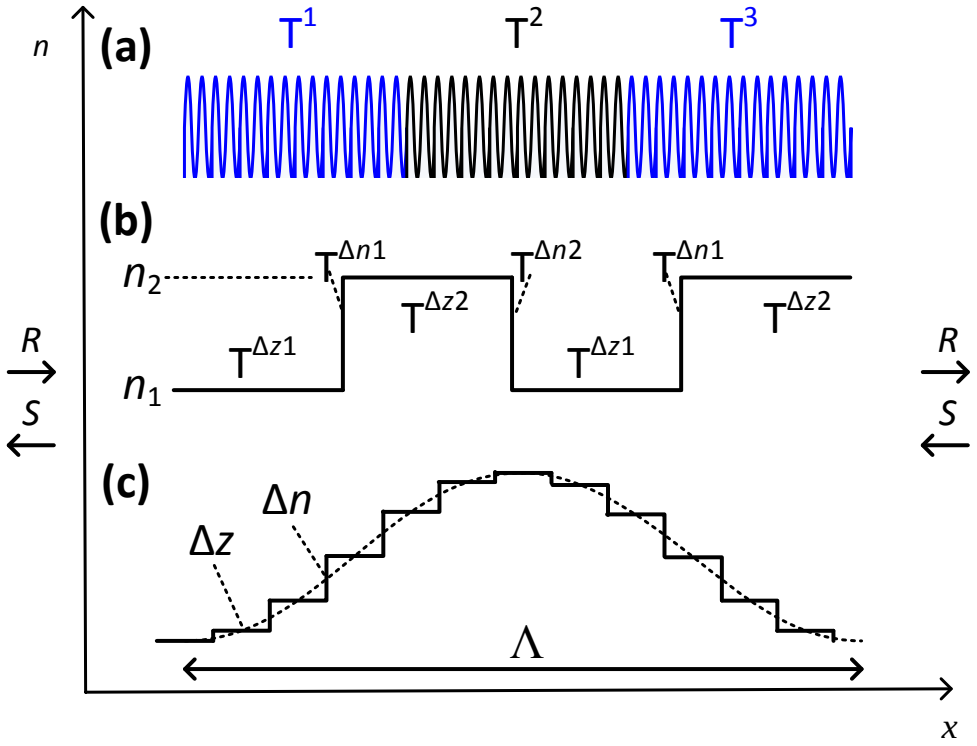

Figure 2.4: Schematic representation of the 3 simulation techniques for simulating a FBG: (a) transfer matrix method (TMM), (b) thin-film method and (c) Rouard's method.

When dealing with small structures, another technique can be used: the thin-film method [15], as shown schematically in Figure 2.4(b). In this method, the FBG is approximated as a stack of thin

films, therefore considering a square-shaped periodic structure for the RI instead of a sinusoidal structure proposed in equation (2.2). In such a case, each step is considered as a simple Fresnel reflection followed by a propagation matrix. A grating half-period is therefore represented by:

$$\begin{bmatrix} R(0) \\ S(0) \end{bmatrix} = T_{\Delta n} T_{\Delta z} \begin{bmatrix} R(\Delta z) \\ S(\Delta z) \end{bmatrix} \tag{2.27}$$

$$T_{\Delta n} = \frac{1}{t_1} \begin{bmatrix} r_1 & 1 \\ 1 & r_1 \end{bmatrix}, \qquad T_{\Delta z} = \begin{bmatrix} e^{-i2\pi n_2 \Delta z/\lambda} & 0 \\ 0 & e^{i2\pi n_2 \Delta z/\lambda} \end{bmatrix} \tag{2.28}$$

$$r_1 = \frac{(n_1 - n_2)}{n_1 + n_2} \tag{2.29}$$

$$t_1 = \frac{2n_1}{n_1 + n_2} \tag{2.30}$$

Where n_1 is the index before the step and n_2 is the index on the Δz step. When the propagation matrix matches a quarter wavelength, constructive interference occurs in reflection, creating a resonance in reflection/transmission spectra, the same as that shown in Figure 2.2. As the name suggests, this method is useful for simulating thin-films, but has limited applications for FBGs, as the RI modulation seldom has a square spatial profile in most FBGs. However, it can be useful to consider the approximate behavior of mm length FBGs with a fast RI variation, such as short superimposed CFBGs, where the transfer-matrix method becomes limited and the Rouard's method, described below, is much slower.

A third technique is called the Rouard's method [20], shown schematically in Figure 2.4(c). This technique is the most accurate, as it takes as the input the exact RI profile with its modulation, but requires an enormous number of matrix sections to be accurate. Like the thin-film method, Rouard's method considers steps of Fresnel reflection followed by a propagation step. However, instead of dividing the FBG period into two steps of high and low RI, Rouard's method divides it into as many steps required to properly model the RI variation. Therefore, a good approximation of a sinusoidal FBG structure would require an order of at least ~10 steps (ideally more) to properly model the sine-wave and reduce the effect of higher harmonics and phase accumulation errors. This method is therefore very useful when simulating actual writing of FBGs and has been used to evaluate the effect of defects which occur during writing of the RI modulation (noise, bad beam shape, quality of apodization) and short superimposed chirped cavities, discussed in section 2.3.2. However, it is extremely heavy in terms of calculation time: a 10 mm FBG at 1550 nm would

require at least 37 380 matrices per wavelength step. This method is therefore very slow for calculating a detailed spectrum of a cm-range FBG, which is not practical for optimizing a design where several simulations with different parameters are necessary. Also, the method introduces phase error when the RI modulation is strong, therefore is should be used only for weak gratings.

It should be noted that in this thesis, most of the spectra of ultra-long FBG will be shown as a function of wavelength difference ($\Delta\lambda$), instead of absolute wavelength. The central wavelength will be defined for each spectra. This is because ultra-long FBGs exhibit very narrow bandwidths (~0.01 nm) compared to the central wavelength (~1550 nm). This allows for more representative tick marks with units in pico-meters.

2.2 FBG writing techniques

The first consideration one must have in mind when writing FBGs is how to change the refractive index of the glass fiber core. There are two methods to do so: UV exposure of a photosensitive fiber, or through femto-second laser pulse induced plasma generation. The second method was not used for the Thesis, so it will be described only briefly.

2.2.1 Photosensitivity of glass

The main technique that will be reviewed here is UV photo-induced RI change since it was used throughout this Thesis. This method requires a photosensitive material in the fiber core, one that will react to UV light exposure. Pure fused silica, the base material of common optical fiber (cladding of standard fiber) is not sufficiently photosensitive to UV light, but transparent down to a wavelength of 190 nm. The most commonly used photosensitive material is germanium oxide (GeO_x), which is used as a core dopant in standard fibers. The photo-induced electronic defects (electron trap, hole trap and oxygen vacancy), of GeO_x dopants in a SiO_2 matrix was first described by Friebele *et al.* [21] and then further developed in pure GeO_2 glass by Tsai *et al.* [22]. Those defects are called type I photorefractive change. Type II RI variation is a damage grating and should be avoided, while Type IIa is a negative RI change (opposite sign from type I) caused by stress relaxation inside the glass. Type IIa generally appears after longer exposure and can reach much larger Δn than Type I.

Other materials have also shown to be photosensitive such as phosphorus-germanium (GeP), rare-earths with aluminium oxides (AlO_3-Yb-Er) and others. However, depending on the photosensitive dopant concentration and its nature, some fibers may be only weakly or not at all photosensitive. For example, SMF-28 has a low Ge concentration and FBGs are difficult to make with UV wavelengths above 250 nm, but gratings have been demonstrated with 213 nm exposure after ~ 1 hour by Gagné *at al*. [23].

There are several ways to increase the photosensitivity of the typical fiber core. One method consist of adding a co-dopant to the standard Ge oxide such as boron (B) [24] or tin (Sn) [25]. Although each co-dopant has some practical advantage, in that the fibre is rendered permanently photosensitive, co-doping can only be done during the fiber pre-form fabrication. Another technique to enhance the photosensitivity of any Ge, Al or other core dopants is with hydrogen loading. This consists of placing the fiber in a high pressure (room temperature or heated) hydrogen chamber to in-diffuse the atoms into the core [26-29]. The presence of hydrogen around the Ge atoms significantly increases the probability of defect formation under UV irradiation. However, the use of hydrogen generates extra OH defects which absorbs around 1.4 μm, close enough to the C-band to induce undesirable loss. Replacing hydrogen with deuterium has the same photosensitivity enhancement, but the OD defect absorption is shifted to ~1.9 μm instead, reducing loss between 1 and 1.6 μm [30]. All the loading done during the PhD was done with deuterium to minimise such losses.

RI change can also be induced by femtosecond laser pulses. The high intensity of the focused light leads to multi-photon absorption, generating a local plasma. There are various routes to RI change, such as multi-photon avalanche ionisation, self-focussing induced dielectric breakdown, physical damage and thermal effects [31-33]. The advantage of such a method is that it can be used with almost any glass and it does not require the removal of the fiber's primary polymer coating, allowing the fiber to retain most of its tensile strength [34]. Femtosecond laser written gratings have proven to be more resistant to decay at high-temperatures, and are finding applications in high temperature sensing [35].

2.2.2 Laser sources for FBG fabrication

FBG writing requires a suitable laser to interact with the photosensitive fiber. UV writing for FBGs is normally performed with laser wavelengths between 190 and 270 nm. However, it has been

shown that the photosensitivity varies considerably within this band. Also, a pulsed laser typically induces a larger index modulation [36] due to the higher photon flux. Pulsed excimer lasers were the first to be used in the 240 nm band [37] for FBG inscription. However, excimer lasers suffer from low temporal and spatial coherence (difficult to use in an interferometer) and often have a poor beam quality. High-coherence lasers such as CW frequency doubled argon ion-gas lasers operating at 244-257 nm soon became the lasers of choice [38-40], as well as the 4th harmonic Nd:YLF, Nd:YAG or Nd:VO_4 Q-switched lasers in the 262-266 nm band [41, 42]. A 5th harmonic of a Q-switched Nd:VO_4 laser operating at 213 nm was only recently demonstrated in our laboratory showing possibly the highest photosensitive response [23] from fibers. In this Thesis a 213 nm laser was used as often as possible as well as the 4th harmonic of the Nd:YAG operating at 266 nm laser.

As for femtosecond sources, they can be either 800 nm Ti:Saph lasers for very short pulses (~10 fs) or infrared lasers at 1μm or 1.5 μm for 100-300 fs pulses. Infrared lasers have the advantage of a better penetration through the acrylic coating, but have longer pulses, and require a larger number of photons for multi-photon absorption due to their lower energy, compared to shorter wavelengths.

2.2.3 Writing techniques for short FBGs

For FBG writing, a fringe pattern must be generated in the core of the fiber. Although LPGs of periods in the 100μm to mm range can be directly written by programmable point-by-point or even by physical clamping of a mask onto a fiber, as was demonstrated with plastic 3D printed masks [43], FBGs are more challenging due to their sub-μm periods. To write such structures, interferometric methods are normally used to create a fringe pattern of the right period. Point-by-point inscription, is also possible using a pulsed laser, but suffer from poorer quality of the FBGs.

The simplest and robust method is called behind-the-mask [44], as shown in Figure 2.5. In this technique, the fiber is placed directly behind a phase mask designed for a specific wavelength and a UV beam is scanned along the mask length. The interference between the +1 and -1 orders create a fringe pattern in the beam overlap region imprinting in the fiber core a grating with a period half that of the phase mask, with a Bragg wavelength of:

$$\lambda_B = n_{eff}\Lambda_{mask} \tag{2.31}$$

Where Λ_{mask} is the period of the phase mask. The beam can be scanned across the phase mask [45] to write longer gratings. The length of the phase mask limits the length of the FBG that can be inscribed, and a different phase mask is required for different wavelengths. Complex structures can be inscribed in the phase-mask, such as a linear chirp [46], which is also imprinted in the fiber. Phase mask may have phase errors which will be copied into the core of the fiber, therefore the quality of the grating is dependent on the uniformity of the phase mask. Various methods were proposed to correct for non-uniformities during the lithography process [47], or during the writing [48]. A phase correction technique was recently proposed by writing a test grating and characterising it via frequency domain reflectometry [49]. That technique was the inspiration to develop our ultra-long, phase-correction writing-scheme as described in article 3.

Femtosecond writing has been also demonstrated with good success using a behind-the-mask technique, although the larger diffraction angles from longer wavelength does cause complication. Also, great care must be taken to optimise the overlap of the writing region due to the tight focusing with the core by scanning the fringe pattern across the core. Despite these difficulties, FBGs have been reported in several fibers, such as non-hydrogenated [50] and hydrogenated [51] SMF-28, ZBLAN fiber [52], pure silica fiber [53], rare-earth doped fiber [54] and others.

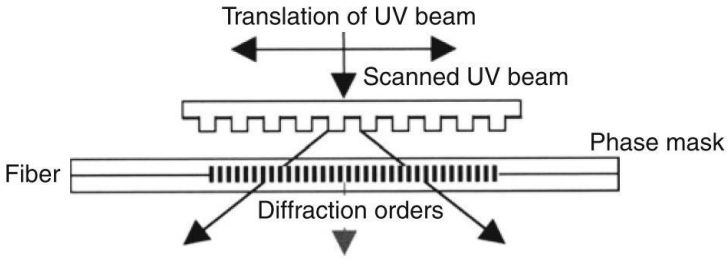

Figure 2.5: Behind the mask technique. The phase mask used as a scanned interferometer. The quality of the grating is dependent on the uniformity of the phase mask. [15] © Elsevier 2010, reproduced with permission.

A second general technique involves generating the same fringe pattern by holographic techniques. To do so, an interferometer consisting of mirrors to adjust the interference angle can be used. The beam can be divided by a beam splitter [3], or by a phase mask, as shown in Figure 2.6(a), which is called a Talbot interferometer [55]. The same effect can be also achieved with a glass block (Figure 2.6(b)) [46], a fold mirror (Figure 2.6(c)) [56] or a prism (Figure 2.6(d)) [57], the last two being in the form of Lloyd interferometers. The beam can be scanned across phase-mask, beam-

splitter or prism for longer FBG length, as this simulates a larger beam. In each case a tunability of the written wavelength is possible by changing the interference angle as shown by:

$$\lambda_B = \frac{n_{eff}\lambda_{uv}}{\sin\left(\frac{\theta}{2}\right)} \tag{2.32}$$

Interferometer systems such as those shown in Figure 2.6 require a minimum of coherence length from the laser. Therefore, a femtosecond source, which usually has a coherence length of less than 1 mm, is difficult to use limiting the FBG length severely. Each the those writing methods are limited in terms of FBG length to the length of beam splitting component. As phase mask are generally limited to less then 100 mm due to fabrication cost issues, this is generally considered as the limit for short gratings.

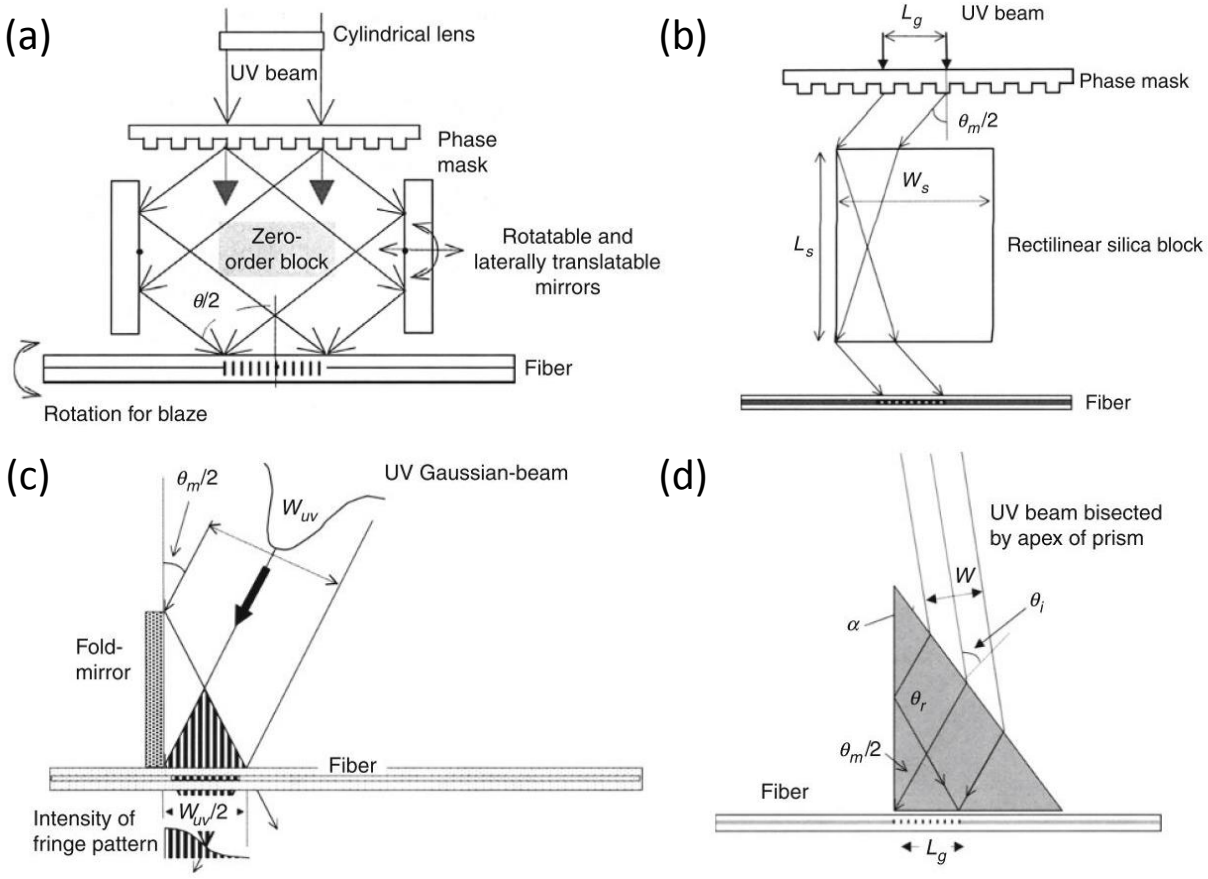

Figure 2.6: Tunable interferometer writing techniques: (a) Talbot interferometer using mirrors and (b) using a silica block and (c) Lloyd interferometer using a fold mirror and (d) a prism. [15]

2.2.4 Unlimited length FBG writing techniques

As a general rule, ultra-long FBGs will require the fiber to be moved over the desired length (200-1000 mm or longer) without any phase shift or phase error. This has always been the main challenge for such techniques and the most limiting factor is the fiber moving method itself. Mechanical bearing stages have proved to be problematic as frequent phase errors occur due to friction and vibrations. Rolling fiber drums have also been used, but because of slippage of the fiber on the drum (friction and variation in tension during rolling), phase errors are impossible to avoid. This has nevertheless led to the discovery of ultra-long random gratings by our group, which offers ultra-low lasing threshold with physically interesting operating characteristics [58, 59]. The best early results for ultra-long gratings were achieved using air-bearing stages, which offers a smooth movement and reduces the effects of vibrations significantly.

The first unlimited length method we will address is point-by-point inscription. This can be done with a UV laser source, as the diffraction limited spot size is small enough to inscribe half-period of a FBG. This can also be done by femtoseconds pulses, where the nonlinear interaction area is smaller than the diffraction limited spot size. However, it has been shown to be difficult to write long or ultra-long FBGs as the precision of the pulse position inside the core is difficult to maintain. It was proposed to use amplitude masks to control illumination with large beams, with relatively good results [60], as shown in Figure 2.7(a). Methods using a preliminary fiber position mapping to allow a correction on the writing point are possible, as shown in Figure 2.7(b). Although this technique is rather difficult to implement for ultra-long FBG due to the precision required, it has been highly useful for LPGs where the period is >10 μm [61]. Using fs writing in point-by-point usually increases scatter loss due to formation of scattering centers and bad overlap of the RI change region with the core. However, with better care, this problem can be overcome [34]. Point-by-point FBGs tend to form high order resonances (N>1 in equation (2.1)), which can be helpful as a high-order resonance reduces diffraction limitations (the required period is multiplied by the order).

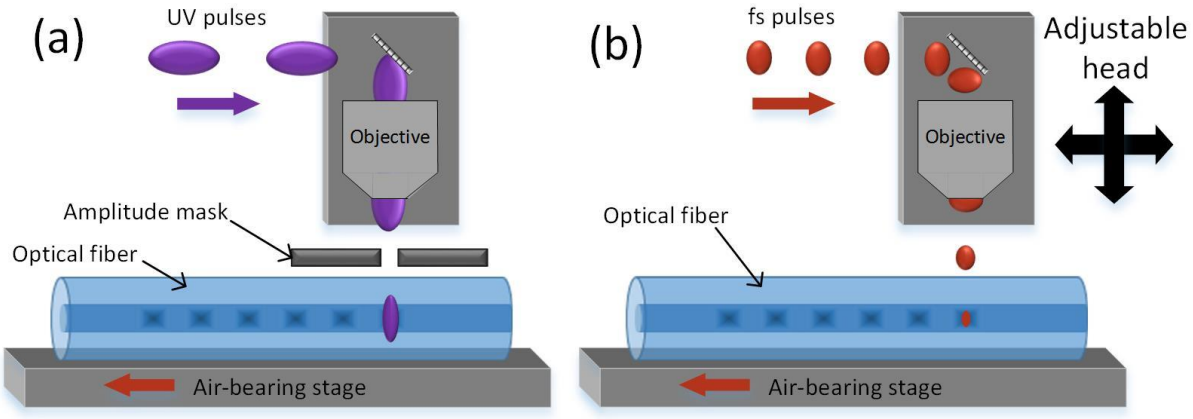

Figure 2.7: Point-by-point inscription using (a) an amplitude mask with UV pulses and (b) using no mask with a fs infrared. When no mask is present, the head must be adjusted according to the exact core position along the fiber.

Another technique involves FBG stitching [62, 63]. Small FBG sections are written using the previously shown techniques (Figure 2.5 and Figure 2.6). After each sectional inscription, which can be done in a single pulse, the fiber is moved precisely by an integer number of periods, then the FBGs are written once more, as is shown in Figure 2.8. However, the absolute accuracy of even the best stages is insufficient to ensure exact positioning, therefore phase errors are frequent. A continuously moving stage offer better result, but then the exposure is limited to a single pulse, which limits the maximum κ_{ac}. This technique was successful in writing ultra-long chirped FBGs, as the requirements of exact phase are not as critical [64].

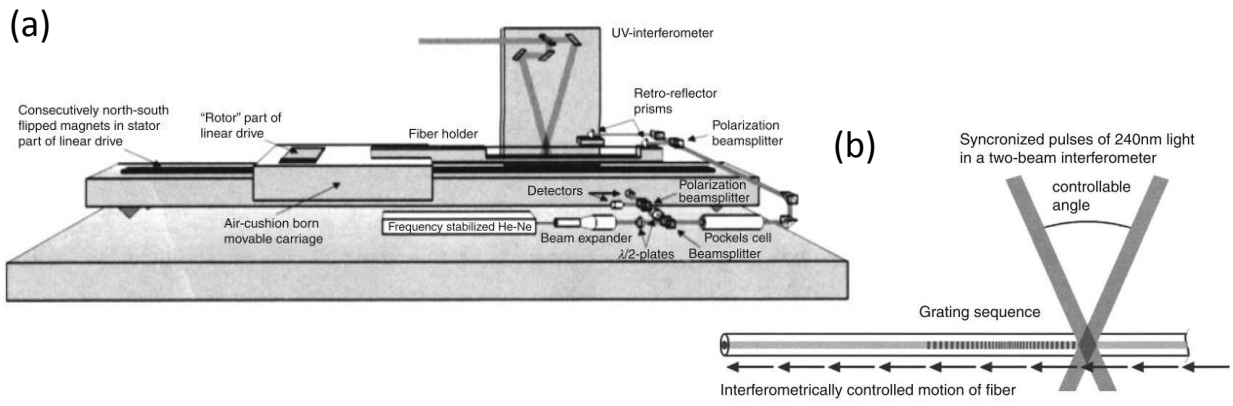

Figure 2.8: The multiple printing in fiber (MPF) technique where multiple FBGs are stitched together to conserve phase. [15] © Elsevier 2010, reproduced with permission.

The most successful technique involves continuous writing of an interference fringe pattern. The first method for this consists in moving the phase-mask synchronously along with the fiber through a piezo-electric element in a saw-tooth wave function, which "folds" the fringe back to an integer number of periods, as shown in Figure 2.9(a) [65-67]. We will refer to this saw-tooth wave as "folding wave". However, such method is limited in speed, due to the inertia and resonant frequency of the piezo mass. Also, due to the mechanical movement of the piezo and its limited frequency, vibrations are present and the saw-tooth wave's higher harmonics are cut (the edge of the wave function is smoothed), leading to slight phase errors, which accumulate. A second method consists in using a rotating circular phase-mask [68]. Such technique requires hard-to-fabricate phase-mask, as the fringes must be in a perfectly radial geometry, which is generally incompatible with electron beam x-y coordinate inscription method. The third method, shown in Figure 2.9(b), was been proposed by Gagné *et al.* [12] in our lab and involves two phase modulators to change the phase between the two UV beams in a push-pull configuration using a Talbot interferometer. By doing so, the fringe pattern can be moved in the same way as a phase mask, without its mechanical limitation, as the electro-optic modulation is much faster and does not generate vibration. This method has been demonstrated to write outstanding ultra-long (up to 1 m) FBGs, also by Gagné *et al.* [11]. Both of these methods were used during this PhD, the second one being used in all 4 articles presented in this thesis.

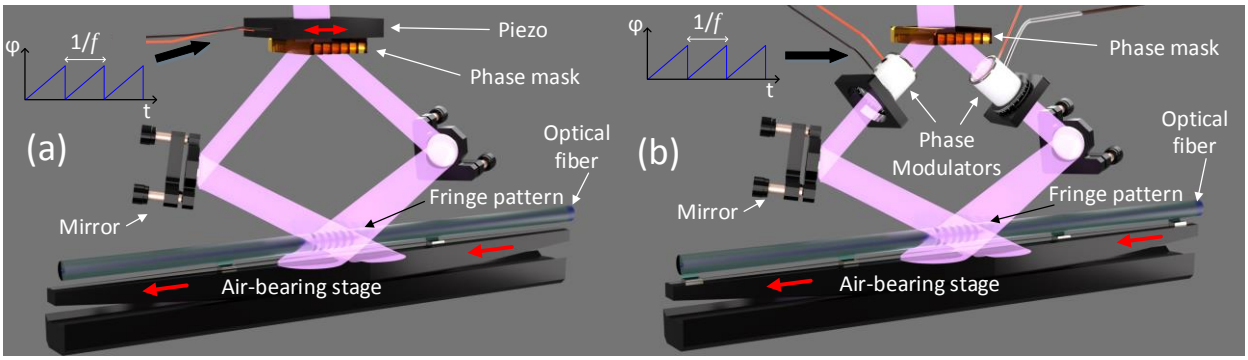

Figure 2.9:Continuous writing scheme for ultra-long FBG using a Talbot interferometer. (a) A scanning phase mask or (b) phase modulators are required to move the fringe pattern synchronously with the fiber.

Continuous FBG writing has one particularity: the actual written period (therefore Bragg wavelength) does not depend on the fringe pattern as defined by the Talbot interferometer described by equation (2.32). Instead, it depends on the synchronous relationship between the moving fiber

and fringe pattern frequency. To demonstrate this, the refractive index change in the fiber through continuous writing can be modeled by supposing a moving phase-mask and beam (at position z_b) relative to a fixed fiber:

$$\Delta n(z) = \int_0^L f(z, z_b) \left\{ 1 + \cos\left[\frac{2\pi}{\Lambda} \left(z + z_b \left(\frac{\delta z f}{v} - (M\Lambda - \delta z)\frac{f}{v} - 1 \right) \right) \right] \right\} dz_b \qquad (2.33)$$

Where $f(z, z_b)$ is a function representing the beam shape, z_b the position of the beam, Λ the fringe period determined by the Talbot interferometer and M the number of periods which are intended to be jumped at each period of the folding wave. The last 3 parameters, i.e. f, δz and v, are the writing parameters corresponding to the frequency and amplitude of displacement of the saw-tooth folding wave and to the speed of fiber respectively. A good example for the beam function is a gaussian of amplitude A and width at half-maximum Δz:

$$f(z, z_b) = A e^{-4 \ln 2 \left(\frac{z - z_b}{\Delta z}\right)^2} \qquad (2.34)$$

The parenthesis of z_b of equation (2.33) contains 3 phase terms which model the moving fringe pattern vs the moving fiber. The first term (red) represents the movement of the fringe pattern from the folding wave sent to the modulators. The second term (blue) represents the phase jump which would happen if the saw-tooth amplitude is not equal to an integer number of M period. Although this term is represented in equation (2.33) as a linearly evolving phase, it is rather a step function which "jumps" every folding period. Ideally, δz should be maintained as close as possible to $M\Lambda$ because those instantaneous phase jump contribute to phase noise. The third term (green) represents the movement of the fringe pattern in respect with the fiber. Ideally, the second term should be zero (integer-period phase jumps), and the 1st and 3rd term should cancel each other (fringe pattern moves at the same speed as the fiber).

If we suppose an infinitely small spot size ($f(z, z_b)$ represented by a Dirac function), the effective period will be:

$$\Lambda_{eff} = \Lambda \left(\frac{\delta z f}{v} - (M\Lambda - \delta z)\frac{f}{v} \right)^{-1} \qquad (2.35)$$

The displacement is controlled by the applied voltage (V) in respect with the full period voltage ($V_{2\pi}$), therefore we pose:

$$b = \frac{\delta z}{\Lambda} = \frac{V}{V_{2\pi}} \tag{2.36}$$

By replacing equation (2.36) in (2.35) and converting to Bragg wavelength using equation (2.10), we can find the Bragg wavelength for continuous writing, which is independent of the period Λ as defined by the Talbot interferometer angles :

$$\lambda_B = \frac{2n_{eff}v}{f(2b - M)} \tag{2.37}$$

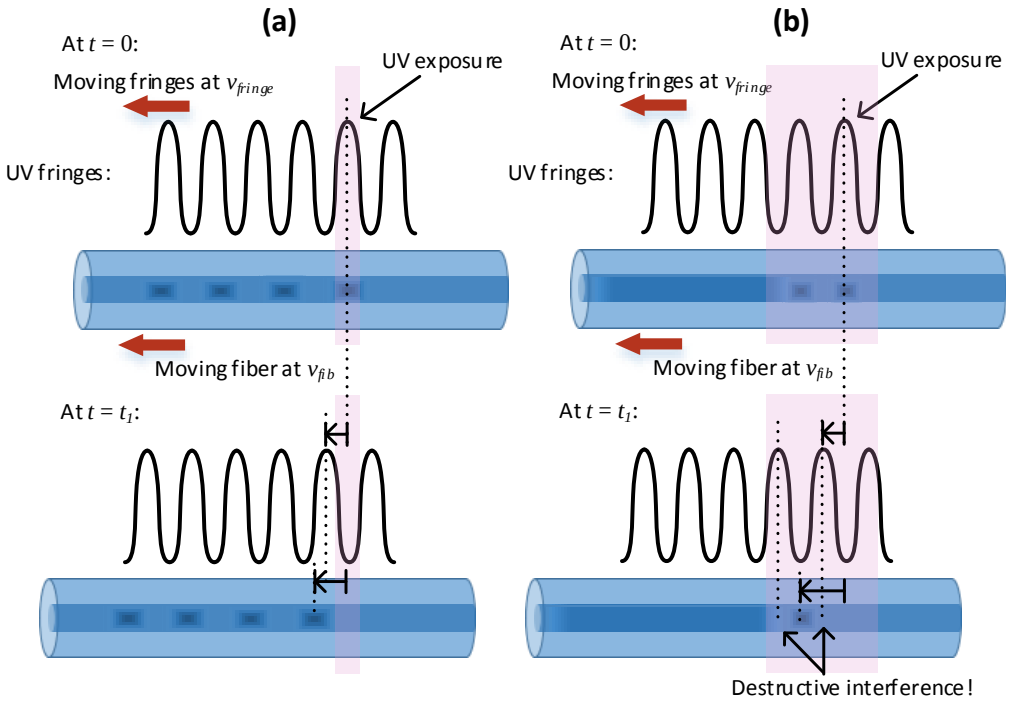

Figure 2.10: Schematic description of the tunability ($v_{fringe} \neq v_{fiber}$) of continuous writing. (a) Ideal case of infinite tunability where a half-period or less is illuminated. (b) Practical case where tunability is limited by spot size where a de-synchronised fringe pattern vs fiber will erase the written FBG.

Where *b* should be equal to *M* in an ideal case. Asynchronous writing is schematically shown in Figure 2.10(a), where a spot size of less then half period can allow an infinite tuning of the Bragg wavelength. In practice, such a small spot size is not possible. Indeed, the tuning shown in equation (2.37) is only possible within a certain bandwidth of the Talbot-defined-Bragg-wavelength, beyond which the FBG will erase itself, as shown in Figure 2.10(b). This tuning bandwidth between the

first zeros (when a π phase difference is reached between the written fringe and the Talbot fringe) is:

$$\Delta\lambda_{tuning} = \frac{2\lambda_{B0}^2}{4n_{eff}\Delta z - \lambda_{B0}} \quad (2.38)$$

Where Δz is the exposed fiber length (illumination spot size), or full-width-at-half-maximum of $f(z, z_b)$. Our own writing scheme has a spot size of ~100µm, which includes ~200 periods. At 1550nm, this gives a tuning bandwidth of ~7 nm.

2.2.5 Effect of refractive index variation

With the technologies described above, ultra-long chirped gratings have been demonstrated abundantly, as phase defects in such FBG have much less impact. However, the only ultra-long uniform FBG that was demonstrated to be all-in-phase for a length of 1 m was reported by Gagné *et al.* in our laboratory in SMF-28 fiber [11]. The same could not be repeated in other specialty fibers. Ultra-long FBG of 20 to 50 cm in length have been demonstrated, by others and ourselves. However, very poor reproducibility was noted: very few FBG showed a theoretical spectrum for an all-in-phase grating, although ~1 out of 3 showed acceptable quality for a DFB laser (detailed in section 2.4). The reason for this low repeatability was extensively studied for this PhD as it was a limiting factor in ultra-long FBG development. The problem that was found is the *non-uniformity* in the effective refractive index of optical fibers, which is described in article 2.

It was already well known that parameters during fiber drawing are difficult to control [69]: temperature, strain on the fiber, core meander, etc. To control and minimise these problems, which affect the guided mode RI, various parameters are measured during or after the drawing process such as RI profile, eccentricity, core position, dopant concentration, defects and stress profile. However, most of these characterizations are performed at single points along the fiber or averaged over a long length (meters).

Nevertheless, various techniques have been demonstrated to get some information on the index profile or on a written FBG along the fiber length. Side-diffraction monitoring has been widely developed to measure RI modulation (Δn) in FBGs [70-73], with a resolution down to 5×10^{-6} refractive index units (RIUs) [74] and 5 pm on the measurement of the grating period [75]. Despite

their good performance, these techniques do not give any information on the effective refractive index n_{eff} itself. Fiber profiling capable of measuring absolute RI with a high resolution has been demonstrated [76], but only gives a short-length profile (mm-range) and is therefore not practical for meter lengths. Other techniques which could measure various FBG parameters were shown, but only in a relative scale with limited sensitivity such as: by heat-scan [77], time domain reflectometry [78] or acousto-optic method [79]. As mentioned in a previous section, a frequency domain reflectometry (OFDR) was proposed to measure and correct for phase errors caused by phase-mask in a FBG by Miller *et al.* [49]. However, the measurement proposed by Miller *et al.* involved a probe grating limited in length to that of the phase mask and is therefore not suitable to characterise meter-length fibers. The solution we proposed is detailed in article 2.

2.2.6 Optical Fourier domain reflectometry (OFDR) as characterisation tool

Optical Fourier domain reflectometry (OFDR) was often used as crucial characterisation and diagnostic tool for FBG fabrication. This technology was used for the characterisation method proposed in article 2 and used in article 3. Therefore, a little background on this method is necessary.

OFDR has been known for a long time [80] and uses the same principle as frequency domain optical coherence tomography (OCT): light from a wavelength swept source is injected in an interferometer where the sample lies in one branch, as shown in Figure 2.11. In the case of fiber characterisation, the sample is much longer (~10 m), which requires a high spectral resolution (Fourier transform limitation). For a single one-point reflection, we would expect to see a sine-wave (single frequency) on the detector as the wavelength is swept at a constant rate. To resolve multiple reflection points, a Fourier transform of the spectral interference would give the complete reflection profile along the fiber length. Since this is an interferometric measurement, information on phase is also available and can be accessed through the Fourier transform. The phase derivative corresponds to the wavelength at the reflection point, if said reflection point is selective in wavelength, such as a FBG. Such a technique allows for sub-mm resolution for tens of meters of length of fiber. The formalism of OFDR was described by Glombitza *et al.* [81] as well as the distributed sensing theory by Froggatt *et al.* [82]. The main challenge to achieve long lengths of measurable fiber is the coherence of the scanning laser. Froggatt *et al.* solved this issue with a

patented system using a self-monitored cheap scanning DFB diode system [83] to correct for phase variation during the scan and therefore achieved an artificially extra-long laser coherence length.

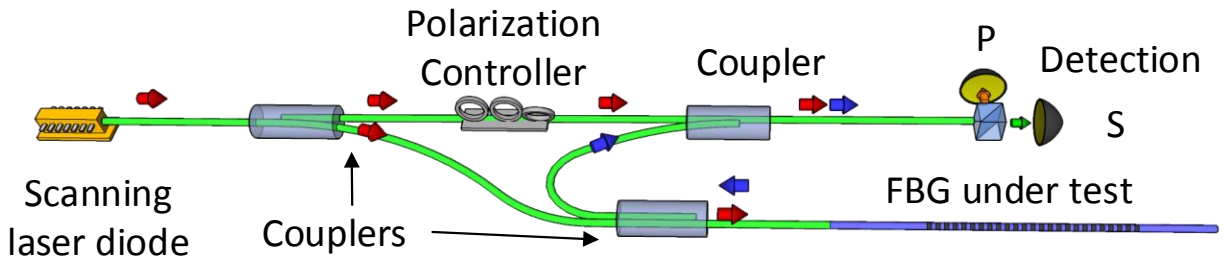

Figure 2.11: Optical circuit of an OFDR system.

2.3 Specialised applications

This section details some applications which were investigated during my PhD. Those applications are not related to those shown in the Thesis, but have been part of the investigation process which revealed flaws in our writing techniques.

2.3.1 Chirped fiber Bragg gratings

Apart from their usefulness as selective reflectors, the first advanced application of FBGs was chirped FBG (CFBG) [15] used for dispersion compensation and temporal compression/expansion. As was seen in the last section, much effort was focused on developing ultra-long FBGs specifically as linearly chirped gratings. A chirped grating has a quadratic phase variation, giving rise to a linear variation of resonance wavelength along the FBG position. Therefore, the reflection point of light will change as wavelength changes, therefore linearly varying the group delay with wavelength as shown by:

$$\tau = 2\frac{Ln_g}{c\Delta\lambda}(\lambda - \lambda_B) = D(\lambda - \lambda_B) \tag{2.39}$$

Where D is the dispersion typically given in $[\mathrm{ps/nm}]$ and inversely proportional to the chirp C given in $[\mathrm{nm/mm}]$ $(\Delta\lambda/L)$. Since a reflection occurs, the dispersion parameter D is proportional to twice the one-way propagation delay inside the fiber.

Ultra-long CFBGs have the interesting possibility for high dispersion [64-66], allowing large dispersion compensation in a single device. We have demonstrated such applications of CFBG for

the compression of giant-chirped pulses, in collaboration with Woodward *et al.* [84], in which a 400 mm FBG with a 0.8 nm bandwidth fabricated in our lab was used in the compression of giant-chirped nanosecond pulses.

It is important to note that chirped FBGs which have large delay dispersion (*D* parameter), have very low chirp (*C* parameter). The opposite, i.e. highly chirped FBGs (large *C*), was also experimented on in our research during a collaboration with an industrial partner. A technique demonstrated by Farries *et al.* [85] was used to develop very short yet high chirp (~20 nm/mm). This technique consists of using a scanning (not continuous) Talbot interferometer, as shown in Figure 2.6(a), with lenses having different focal lengths added in each branch of the interferometer. The deformed wave fronts from the lens can therefore induce a high chirp to the fringe pattern in the FBG. Such low dispersion FBGs were used to compress specific fs pulses with great success.

2.3.2 Superimposed gratings Delay enhancement

More specialised structures were also studied in our laboratory using CFBGs. We were interested in tuning cavity modes between a Fabry-Perot cavity consisting of CFBGs. By approaching the FBGs to the point where they are super-imposed, special tuning of the Fabry-Perot free-spectral range (FSR) can be achieved. Such a concept is similar to using asymmetric CFBGs in a fiber Michelson interferometer [86, 87] which is a non-resonant system, where the band-pass filter has a sinusoidal shape.

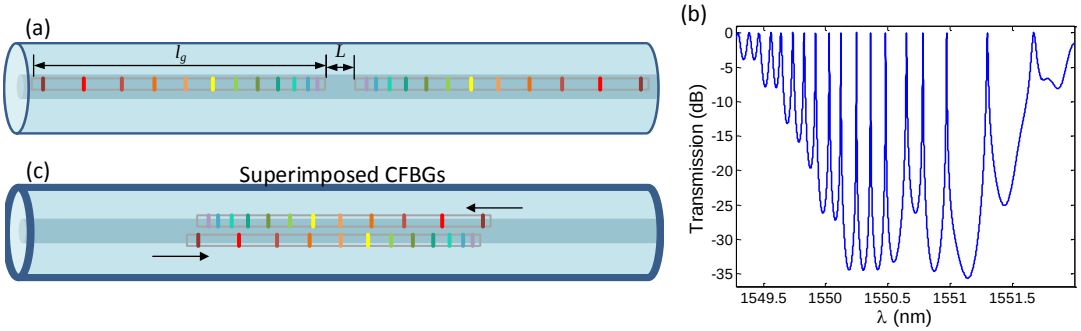

Figure 2.12: (a) Fabry-Perot structure constructed with near-by CFBGs as proposed by Dong *et al.* as a tunable FSR cavity and (b) its corresponding simulation with L=1 mm, l_g=4 mm and $\Delta\lambda$=2 nm. (c) CFBG superstructure which we have proposed and designed [88].

However, for superimposed FBGs in a Fabry-Perot configuration, the transmitted modes are resonant which implies a trap-state with a corresponding longer life-time. Such an idea of

superimposed FBGs with non-uniform phase was first proposed by Zheng et al. [89]. Using near-by CFBG was then proposed by Dong et al [90], where they showed that the FSR varies with wavelength depending on the configuration, as shown in Figure 2.12(a) and (b).

An interesting property of such a cavity, is that the FSR can be tuned towards infinity when 2 CFBGs are superimposed. When this happens, a large central resonance mode can occur. We were interested in the properties of such a large mode from which brings a delay to transmitted light. By multiplying consecutive superimposed-dual-CFBG, the resulting superstructure could result in delay enhancement over a wide bandwidth, the equivalent of a large bandwidth cavity mode. This was demonstrated experimentally for a single cavity, and Rouard's simulation was performed for the superstructure of consecutive cavity [88], as shown in Figure 2.13. However, the array of consecutive superimposed CFBG was not successfully fabricated due to uncontrollable variation in phase, and the project was put on hold. This issue is now understood as a refractive index variation, as explained in article 2.

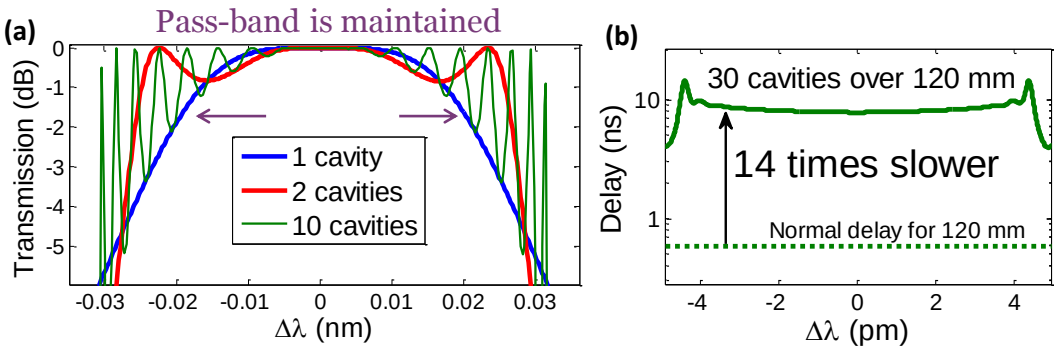

Figure 2.13: Simulation and design of broad-band superimposed CFBG cavity arrays. (a) Transmission spectrum of 1 to 10 cavities to show how the pass-band is relatively maintained. (b) Delay with wavelength of a 30 superimposed CFBG cavity array.

2.3.3 Optical scatter enhancement

FBGs are normally used in or around their stop-band, and the side-mode structure is often seen as being detrimental. This is why apodization is often a critical part of high quality FBGs. However, the side-mode structure can be of some use, particularly in sensing. This side-mode structure decreases over a wide band for non-apodized FBGs and is sensitive to high frequency variation. In an ultra-long FBG, there is an intrinsic phase noise during writing which causes the side-mode

structure to be both random and of higher reflectance, as shown in Figure 2.14. This induced random spectral structure can be seen as an analogue to Rayleigh scattering, which is also caused by a permanent random structure inside the optical fiber on a smaller scale (~nm, sub-nm).

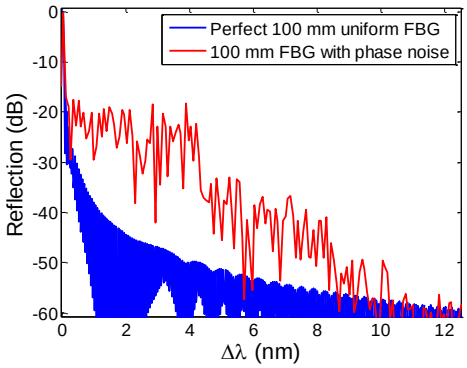

Figure 2.14: Effect of phase noise on side-mode structure of a uniform FBG. This is a simulated example for a 100 mm long FBG with a κ_{ac} of 50 m^{-1} and considering typical writing conditions.

One interesting property of FBGs is its sensitivity to strain and temperature, both of which affect the Bragg wavelength and induce a wavelength shift. This has led FBGs to be widely used as sensors [91, 92]. Such wavelength shifts also occur for the side-mode structure as well as for the Rayleigh spectral signature. This led to the development of a distributed sensing based on the Rayleigh scatter signal by optical frequency domain reflectometry (OFDR) [82, 93] as well as in the time-domain (coherent optical time domain reflectometry (COTDR)) [94, 95]. However, such techniques have always been limited due to the low level of Rayleigh scatter signal in optical fibers. Attempts have been made to enhance the signal by using weak FBG arrays [96, 97] or weak continuous FBGs [98]. However, as these methods use FBGs in the stop-band, they sacrifice the high resolution of OFDR which comes from the broad-band Rayleigh signal. For this reason, we proposed to use the side-mode structure of a strong continuous FBG as an "enhanced Rayleigh" scatter signal. To our surprise, during test writings, we discovered that the presence of a FBG was not even required to raise the Rayleigh scatter signal: simple UV exposure raised the broad-band reflectivity (+20 dB) far outside the stop-band (>10 nm) as much as a uniform FBG or an intended random-phase FBG [99], as shown in Figure 2.15. This led to a much higher sensitivity (10 mK) for a length resolution of centimeters. It was already known that UV increases the refractive index through the creation of defects, as explained in section 2.1.1, and increased loss has been measured after UV exposure [100]. The reason for this increase in Rayleigh signal from simple UV exposure

is likely due to the defects being localised spatially, therefore acting as point variation in refractive index [101]. The nature of this localisation is still under investigation.

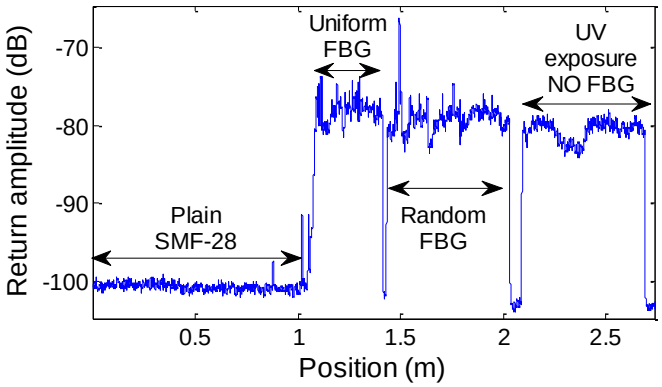

Figure 2.15: Effect of UV exposure on back-scatter return signal from a OFDR measurement.

Further enhancement is also possible (+40 dB) when moving just closer to the stop-band (<10 nm) by accepting some loss of resolution. We demonstrated this in a biomedical application for shape reconstruction where FBG writing was used for signal enhancement [102].

2.4 Distributed feedback lasers

The main focus of ultra-long FBGs application in this thesis is distributed SRS and SBS gain feedback lasers. This section reviews the literature on this technology.

2.4.1 Theory of distributed feedback fiber Bragg gratings

A distributed feedback (DFB) mode in a FBG is a resonance mode in which the feedback is distributed along the entire length of the grating, contrary to a mirror cavity where the reflecting elements are only at the far ends of the cavity. A Bragg grating has natural DFB resonance modes, which are the side-modes present around the stop-band. These are distributed resonating cavities caused by the abrupt grating ends. With sufficient gain, these modes can start lasing. By incorporating gain competition or differential quality (Q) factor between the sides modes [103], one of those modes can be set to lase, enabling single-frequency output. This has long been demonstrated in semiconductor Bragg gratings and are commonly known as DFB laser diodes [104-107].

The same can be applied to optical fibers. Uniform FBG lasers using a distributed feedback have been demonstrated as lasers in rare-earth doped fibers and predicted with Raman gain, both of which are described in the next sub-sections. However, another type of DFB configuration has been proposed [108]: π-phase-shifted DFB FBGs. These FBGs incorporate a phase defect inside its structure, which opens an allowed state in its bandgap, as shown in Figure 2.16(b), where a typical π-shifted FBG is compared with a uniform FBG, both of which can lase if gain is present. Such FBGs can be modeled as:

$$\phi = \begin{matrix} 0 & z < z_{shift} \\ \phi_{shift} & z \geq z_{shift} \end{matrix} \tag{2.40}$$

Where ϕ is the grating phase, as defined in equations (2.1), ϕ_{shift} is the phase shift and z_{shift} the position of the phase-shift. Ideally, ϕ_{shift} should be equal to π, i.e. the fringes are shifted by $\Lambda/2$ or a quarter-wavelength (inner-material wavelength, not vacuum value), while the shift position should be centered ($z_{shift} = L/2$). The ideal shift is formulated in equation (2.40) as an instantaneous shift. In practice, the shift will occur over a certain length Δz and can be modeled as a linear function or as an error function over the length Δz.

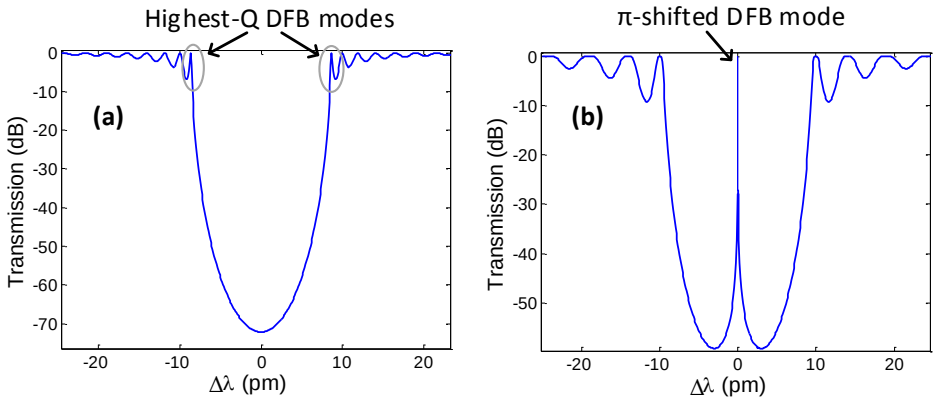

Figure 2.16: Calculated example of (a) a uniform FBG spectra and (b) a π-phase-shifted FBG. The FBG is 300 mm in length with a κ_{ac} of 30 m^{-1}. Central wavelength is 1550 nm.

The main advantage of a π-shifted DFB FBG is the extremely high Q-factor of its resonance mode, compared with a uniform DFB FBG side-modes. This Q-factor is a general figure of merit for cavities describing how long the energy can be stored within a resonator so that the inverse of the lifetime of the cavity is proportional to the frequency and defined as:

$$Q = \frac{\nu_0}{\delta\nu} = \frac{\lambda_0}{\delta\lambda} \tag{2.41}$$

As an example, for a uniform FBG of $\kappa_{ac}L = 10$ and 300 mm length, the highest Q side-mode has a Q factor of 7×10^6 (Figure 2.16(a)), while a π-shifted DFB mode in the same FBG will have a Q factor of 4×10^8 (Figure 2.16(b)). The presence of a phase-shift in the FBG also affects the surrounding side-modes, diminishing their Q-factor, since the effective length of the uniform grating has been halved. This therefore reduces competition and ensures single-frequency emission for laser operation. Linewidth of such π-shifted DFB modes have been measured down to a few KHz [109-111]. Also, such high Q cavities can be used for non-linear optical interaction, as proposed by Hu *et al.* [112] and discussed in sub-section 2.4.3.

However, DFB modes are not necessarily ideal in practice. If the shift is reduced ($\phi_{shift} < \pi$), the DFB mode will move to a higher frequency (lower λ) within the stop-band, and the opposite, if the shift is increased, as shown in Figure 2.17(a). This effectively reduces the Q-factor. If the phase-shift position z_{shift} is brought off-center, the Q factor will be reduced and the transmission spectra will show loss in the DFB mode, as shown in Figure 2.17(b). However, the shortened uniform part of the FBG becomes the preferred laser output. This can be compared to an unbalanced cavity with a higher reflectivity on one side and lower reflectivity on the desired output side. An off-center phase-shift is commonly used to control the output direction of a DFB laser.

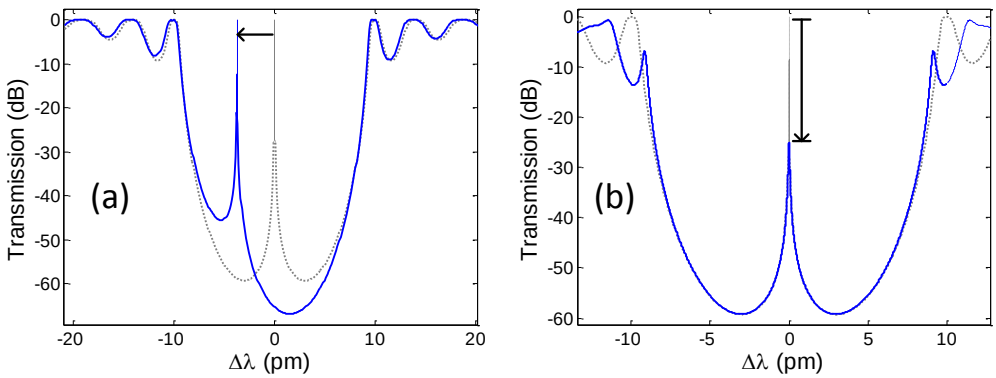

Figure 2.17: Calculated example of (a) a reduction in the phase-shift value (0.7 π , centered in FBG) and (b) a 20 % off-set from center of the π-phase-shift. Central wavelength is 1550 nm. The dotted gray line shows an ideal phase-shift.

Another possible imperfection is the width of the phase-shift. If the shift is large (non-negligible Δz compared to the FBG length), then more total phase-shift is required to have a centered DFB mode. Indeed, the DFB mode moves spectrally towards the edge of the stop-band, as it does when the phase-shift is lower than π, even if $\phi_{shift} = \pi$. Also, a slow phase-shift induces a wavelength chirp in the stop-band: since a variation in phase involves new wavelength resonance components, a slow variation induces these components near the Bragg wavelength. Indeed, if we replace the instantaneous shift in equation (2.40) by an error-function, then its derivative, i.e. the instantaneous Bragg frequency variation with position, is a Gaussian of width Δz. If this Gaussian is large, it can be compared to a quadratic chirp in the Bragg wavelength. The effect of such a chirp moves the sides-modes asymmetrically inside the stop-band and reduces the overall grating strength, as can be seen in Figure 2.18(c). Therefore, the Q-factor is reduced and a potential competition with the side-mode appears. The effect of enlarging Δz is shown in Figure 2.18 (a) and (b). The DFB mode can be brought back to the center of the FBG (maximum Q-factor) by increasing the phase-shift $\phi_{shift} > \pi$, at the cost of increasing the non-linear chirp as shown in Figure 2.18(c).

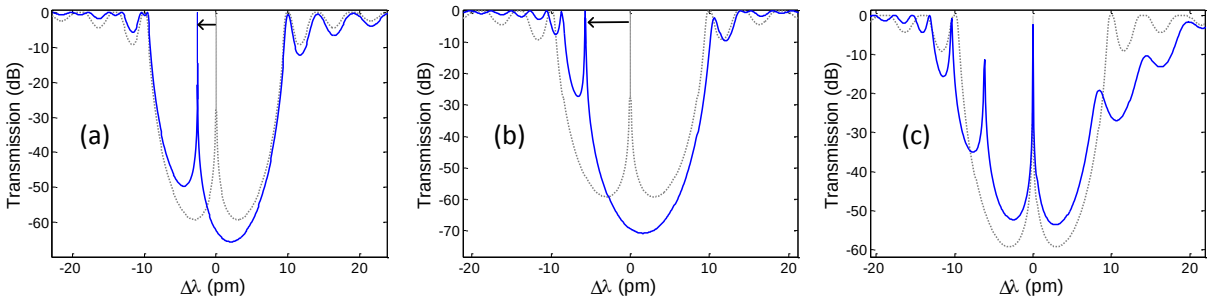

Figure 2.18: Effect of increasing the phase-shift region, using an error function model. The dotted gray line shows an ideal phase-shift. (a) Calculated example showing a 2cm wide π-phase-shift. (b) Calculated example with a 9cm wide π-phase-shift. (c) Calculated example of a 9cm wide phase-shift with an increased phase-shift value to re-center the DFB mode.

For the FBG fabrication presented in this thesis, the DFB mode position z_{shift} and width Δz were well controlled. Article 1 presents a method to have a good control on ϕ_{shift}. However, non-linear chirp did appear due to fiber non-uniformity as described in article 2, which had a similar effect, yet more random then what is shown in Figure 2.18(c). This has been a major challenge which was tackled during the PhD.

When designing a DFB grating as a laser, modeling such device becomes important. Coupled-mode theory of DFB gratings for laser operation was first proposed by Kogelnik *et al.* [113] and developed for rare-earth active medium by de Sterke *et al.*[114] and for non-linear gain by Perlin *et al.* [115]. However, the general form of the equation can be expressed as:

$$\frac{\partial A_f}{\partial z} + \frac{n_{eff}}{c}\frac{\partial A_f}{\partial t} = \left[g - \frac{\alpha}{2} + i\left(\gamma_s\left(2|A_p|^2 + |A_f|^2 + 2|A_b|^2\right)\right)\right]A_f + i\kappa_{ac}A_b \tag{2.42}$$

$$-\frac{\partial A_b}{\partial z} + \frac{n_{eff}}{c}\frac{\partial A_b}{\partial t} = \left[g - \frac{\alpha}{2} + i\left(\gamma_s\left(2|A_p|^2 + 2|A_f|^2 + |A_b|^2\right)\right)\right]A_b + i\kappa_{ac}^* A_f \tag{2.43}$$

Where A_f and A_b are the forward and backward waves inside the FBG, g is the gain term, which depends on the type of gain medium, α is the loss (scattering and absorption), γ_s the non-linear Kerr effect constant for the signal fields including self-phase modulation and cross-phase modulation and κ_{ac} is the FBG coupling constant. This term can be linked to the non-linear refractive index: $\gamma_s = 2\pi n_2/\lambda_s$. The phase-shift, when present, is normally included inside of κ_{ac} (as a complex phase), making it a spatially varying term. The relation of the pump field itself depends on the model and can be expressed as another coupled-mode equation, or by a saturable field, which is detailed in the next sub-sections. Its effect on the Kerr non-linearity is generally negligible, unless ~100 W or more are used for the pump. These equations are in the time domain and extremely difficult to solve numerically. Article 4 develops a simpler method by solving them in the frequency domain (supposing CW operation) with some approximations (only one lasing mode), which makes solving much faster.

2.4.2 Rare-earth medium DFB lasers

The first DFB fiber lasers that were proposed were in rare-earth (RE) doped medium. The first complete modeling of RE DFB, done by Yuan-Hwang and Winful [116], supposed the gain term of equations (2.42) and (2.43) to be in the form of a saturable gain and did not consider pump depletion. Also, the Kerr effect of the pump was neglected, as pump power used in RE DFB lasers is generally less than a watt. The gain term can therefore be formulated as:

$$g = \frac{g_0}{1 + \frac{|E|^2}{|E_s|^2}} \tag{2.44}$$

Where g_0 is the linear pump dependant gain, E is the total field of forward and backward waves and E_s is a saturation field which depends on the rare-earth dopant concentration and their cross-sections.

Since the work was done in the 70s and 80s on DFB theory in semi-conductors, rare-earth DFB lasers were mostly attempted in a phase-shifted configuration, the first being done by Kringlebotn *et al.* [117] for a Er/Yb codoped fiber. Following this, multiple demonstrations were made with improved performance in various RE ions: Yb [118], Er [109, 119], Tm [111]. Techniques were implemented to avoid polarisation competition in the emission, an effect caused by the intrinsic and UV photo-induced birefringence in the fiber. Ibsen *et al.* proposed the use of cross polarisation (in respect with fiber axis) to expose the photosensitive core during writing [119], a configuration known to induce birefringence, but also adding loss to one of the polarizations, therefore favoring the other one during lasing. Injection locking was also proposed [120], although such a scheme remains difficult and unstable. Finally, twisting a fiber can also control the polarisation [121, 122].

2.4.3 Raman and Brillouin gain DFB lasers

2.4.3.1 Raman gain

The performance of RE DFB fiber lasers proved to be of high interest: low threshold and single-frequency narrow linewidth emission. However, such lasers are limited to RE amplification bands, therefore cannot not be applied to any applications. Using optical non-linear gain, such as stimulated Raman scattering (SRS), to pump a fiber DFB laser was first proposed by Perlin and Winful [115] for a non-shifted (uniform) FBG configuration as a means to reach outside RE bands. This would allow DFB lasers to be operated at any wavelengths in the near infrared, as high-power Raman laser were already manufactured throughout the entire 1-2 µm band. However, the FBGs have to be very strong ($\kappa_{ac} > 100\ \mathrm{m}^{-1}$ for $L = 0.5$ m) to get a practical pump threshold (few W, or less) and single-frequency emission is not guarantied, therefore Youfang and Broderick proposed the use of phase-shifted DFB FBGs instead [112]. According to their calculations, threshold of a few watts was predicted.

The model of Raman pumped DFBs involves adding the pump field variation as an extra coupled-mode equation, since Raman gain is not saturable as is RE doped medium. Therefore, the gain term of equations (2.42) and (2.43) must be expressed as:

$$g = \frac{g_s}{2}\left|A_p\right|^2 \tag{2.45}$$

While the pump field equation has the following form:

$$\frac{dA_p(x)}{dz} + \frac{n_p}{c}\frac{\partial A_p}{\partial t} = \left[-\frac{g_p}{2}\left(\left|A_f\right|^2 + |A_b|^2\right) - \frac{\alpha}{2} + i\gamma_p\left(\left|A_p\right|^2 + 2\left|A_f\right|^2 + 2|A_b|^2\right)\right]A_p \tag{2.46}$$

Where n_p is the pump effective refractive index, g_s the Raman gain, $g_p = g_s(\lambda_s/\lambda_p)$ and $\gamma_p = \gamma_s(\lambda_s/\lambda_p)$. These 3 time-domain differential equations can be solved numerically by a method proposed by de Sterke *et al.* [114] or by time-iterative shooting/Runge-Kutta method [115].

Following this modeling, Raman DFB lasers were first demonstrated by Westbrook *et al.* in 2011 [123], but at a very high threshold (40 W) at 1584 nm. It was then shown that using a small core fiber radically improved the performance and ~watt level thresholds were achieved [124-126]. Shi *et al.* then showed in 2012 that using polarized light can increase the gain, therefore reduce the threshold to the sub-watt level [127]. Since then, there has been no new improvement in Raman DFB, until our own contributions. We have shown the lowest threshold reported until now for a single-frequency Raman laser (350 mW), as well as the highest slope efficiency single-ended-output laser (8.5%) and the first Raman DFB fiber laser shown in the 1178 nm band [128]. Such a low threshold can potentially allow for a direct diode pumping.

As further investigation into Raman ultra-long DFB FBG, Shi *et al.* studied the effect of phase noise on DFB laser performance [129]. Although such noise does degrade laser performance, it does not account for the low efficiencies observed in practice. Shi *et al.* also investigated other non-linear effects that could occur around the stop-band, such as four-wave mixing and modulation instabilities for possible new applications of ultra-long DFB FBGs [130].

2.4.3.2 Brillouin gain

Another optical non-linear gain that has been used for DFB FBG is stimulated Brillouin scattering (SBS). However, the main advantage of Raman gain, which is its potential operation in non-RE band, cannot be applied to Brillouin scattering gain, since the Brillouin Stokes shift is very small: 10.8 GHz in SMF-28, which corresponds to 86 pm in wavelength shift at 1550 nm. Nevertheless, a SBS pumped DFB fiber laser has shown some interesting properties, which has also led to a better

understanding of ultra-long and high-field DFBs. Such a DFB laser was first proposed and demonstrated by Abedin *et al*. in 2012 [131]. This laser showed a very low threshold (30 mW), due to the higher SBS gain compared to SRS. An interesting observed effect was that the SBS frequency shift, normally with a bandwidth of 20 MHz, could be tuned over 1 GHz. This was attributed to a push-broom effect [132] from the Kerr non-linearity and possible heating within the FBG: once the FBG is lasing, the non-linear induced phase change moves the DFB mode. If pump tuning is done in the right direction, this appears as a much larger bandwidth than expected. This effect if further detailed in article 1 and discussed in section 8.2.

Shortly afterwards, the dynamics of SBS laser were modeled by Winful *et al.* [133] to understand this effect. Because the life-time of the acoustic wave has an important effect on the dynamics, this wave and its corresponding coupled-mode equations must be added to the model. The gain from equations (2.42) and (2.43) then becomes:

$$gA_f = 0$$

$$gA_b = \frac{g_B}{2A_{eff}} Q_f^* A_p \tag{2.47}$$

$$2\tau_B \frac{\partial Q_f}{\partial t} + Q_f = A_p A_b^* \tag{2.48}$$

Where g_B is the Brillouin gain, A_{eff} the effective mode area, τ_B the acoustic phonon lifetime and Q_f the acoustic phonon wave amplitude in the forward direction. The pump is far from the stop-band, but may still feel the effect of the presence of the FBG nearby, which generates a backward-pump. However, in these equations, as well as the model implemented by Winful *et al.* such a backward pump is neglected in the calculation (therefore there is no generation of backward phonon waves). Because of the directionality of SBS, the gain is only applied to the backward Stokes field A_b. The pump field itself is also slightly different from equation (2.46) as:

$$\frac{dA_p(x)}{dz} + \frac{n_p}{c}\frac{\partial A_p}{\partial t} = -\frac{g_B}{2A_{eff}} Q_f A_b + \left[-\frac{\alpha}{2} + i\gamma_p\left(\left|A_p\right|^2 + 2\left|A_f\right|^2 + 2|A_b|^2\right)\right] A_p \tag{2.49}$$

Where the negative gain term depends on the pump from the relation in equation (2.48). It can be noted that the gain in equations (2.47) and (2.49) depends on the acoustic wave, which in turn

depends on the pump and amplified backward Stokes wave. The results of Winful *et al.* showed that Kerr non-linearity cannot account for the large tuning range observed by Abedin *et al.* Therefore, the main suspect appeared to be temperature, a hypothesis verified by my work on Raman DFB lasers as shown in article 4.

To demonstrate the power of ultra-long DFBs and of a new phase-shift writing technique we recently developed, we published the realisation of ultra-long DFB FBGs (50 cm) Brillouin laser in standard fiber, the first Brillouin laser to operate in SMF-28 optical fiber. We observed the same large tuning bandwidth as shown by Abedin *et al.*, which was studied for different FBG strengths. This is the subject of article 1.

CHAPTER 3 GENERAL METHODOLOGY AND ORGANISATION

This chapter describes the methodology employed during the course of the research and the organisation of the articles presented in the next chapters. The articles and the link between each is clearly described.

3.1 Methodology of the overall research

Fabrication of new types of FBGs is an iterative process. First, a new idea must be formulated into a FBG design through simulation: the optimal value of all relevant parameters for fabrication must be found. Then, the FBG is fabricated according to those parameters. Finally, the FBG is characterised and if satisfactory, tested in its intended application. If the results are as predicted, different designs can be attempted until sufficient data is collected for a conclusive optimisation. Most of the time, however, the FBG is not perfect or the results in the application tests are not satisfactory. In such a case, a combination of simulation, personal experience and mind scratching is used to find the problem and attempt a solution for a second iteration, and so on.

During the PhD, however, this process was not always linear as described above, since problems were not known before-hand. When we thought we had fully understood the limitations, new problems emerged and we had to back-track through the process to identify it.

As described above, the general methodology for FBG design used during this thesis includes 3 main processes: simulation, fabrication and characterisation. The last one includes operating the FBG in its intended application. These will be described below in the following sub-sections.

3.1.1 Design and simulation

3.1.1.1 FBG simulation

Simulations for the results presented in this thesis were done using the transfer matrix method, as described in Chapter 2, section 2.1.2. This method is well suited to analyzing ultra-long FBGs, studied in this thesis. In the simulation, the FBG is divided into M sections each of Δz in length. Typical matrix sections, Δz are in the order of ~1 mm, which is much longer then the grating period, therefore there is little need to ensure an integer number of period in each section. Each of these

sections represents a uniform FBG to which the solution is known (equation (2.13)), which is then represented in a matrix form (equations (2.18) to (2.22)). This operation is repeated for every wavelength of interest to arrive at the spectral response. In this thesis, FBGs can have a custom chirp (resonance wavelength variation), phase or amplitude profile of the grating and potential noise. To include these parameters, the calculated matrix for each section, Δz is represented by:

$$T_{\Delta z} = [\mathrm{T_{FBG}}(\lambda, \lambda_B, \kappa_{ac}, \kappa_{dc})] \begin{bmatrix} \exp(-i\,\Delta\phi/2 + \alpha\Delta z/2) & 0 \\ 0 & \exp(i\,\Delta\phi/2 - \alpha\Delta z/2) \end{bmatrix} \quad (3.1)$$

Where $\mathrm{T_{FBG}}$ is the transfer matrix as defined by equations (2.18) to (2.22), which is calculated for a particular scanned wavelength λ, and in which parameters of resonance (λ_B), apodization (κ_{ac}) and DC refractive index change (κ_{dc}) can be changed for each section Δz. The phase variation between this section and the previous one ($\Delta\phi$) as well as loss (α) is included in a separate matrix. Gain can be represented as negative loss. Each section can then be combined (matrix multiplication) to form a general transfer matrix, described by equation (2.24). From this matrix, transmission and reflection solutions ($R(L)$ and $S(0)$ respectively) can be found based on boundary conditions ($R(0) = 1,\ S(L) = 0$). Knowing the exact field at the boundaries for both waves, the internal field can be calculated as follow:

$$\begin{bmatrix} R(L - m\Delta z) \\ S(L - m\Delta z) \end{bmatrix} = T_{\Delta z_{M-m+1}} \begin{bmatrix} R(L - (m-1)\Delta z) \\ R(L - (m-1)\Delta z) \end{bmatrix}, m = 1, 2, \dots, M \quad (3.2)$$

Where $L = M\Delta z$ is the total grating length. As can be seen, this technique is very versatile, fast and allows a recovery of both phase and amplitude of the fields. Other techniques (thin-film and Rouard's) were used on occasion, mostly as diagnostic tools or in other projects involving short FBGs. However, any simulation involving the work presented in this thesis was done performed using the transfer matrix method.

3.1.1.2 DFB laser simulation

Another important simulation method that was developed during the thesis is related to the 3rd objective: model and simulate SRS gain phase-shifted DFB FBGs. As was shown by the coupled-mode equations (2.42), (2.43), (2.45) and (2.46), the problem is not simple, due to the time-domain nature and the boundary conditions (being incomplete on each side). To resolve this, a shooting method coupled with Runge-Kutta-4 (RK4) is normally used for each time step, which is a very heavy burden and can take hours to find a single solution with an ordinary computer. Since we

wish to vary many parameters to understand the Raman DFB fiber laser's behavior and its limitations, this method was not acceptable.

To decrease the burden of simulation, a few approximations were made. First off, we supposed continuous wave (CW) operation. Although, some authors observed instabilities in the time domain in some very restricted simulations [112], our proposed method neglects this. Fortunately, such instabilities were never observed experimentally. For such an approximation, the coupled-mode equations (2.42), (2.43), (2.45) and (2.46) can be re-written in the frequency domain, where the frequency is substituted by λ for simplification:

$$\begin{aligned}
\frac{dA_p(x)}{dx} &= \left[-\frac{g_p}{2}\left(\left|A_f\right|^2 + |A_b|^2\right) - \frac{\alpha}{2} + i\gamma_p\left(\left|A_p\right|^2 + 2\left|A_f\right|^2 + 2|A_b|^2\right)\right]A_p \\
\frac{dA_f(x,\lambda)}{dx} &= \left[\frac{g_s}{2}\left|A_p\right|^2 - \frac{\alpha}{2} + i\left(\gamma_s\left(2\left|A_p\right|^2 + \left|A_f\right|^2 + 2|A_b|^2\right) + \frac{\Delta\beta}{2} - \frac{1}{2}\frac{d\phi}{dx}\right)\right]A_f + i\kappa_{ac}A_b \\
-\frac{dA_b(x,\lambda)}{dx} &= \left[\frac{g_s}{2}\left|A_p\right|^2 - \frac{\alpha}{2} + i\left(\gamma_s\left(2\left|A_p\right|^2 + 2\left|A_f\right|^2 + |A_b|^2\right) + \frac{\Delta\beta}{2} - \frac{1}{2}\frac{d\phi}{dx}\right)\right]A_b + i\kappa_{ac}A_f
\end{aligned} \tag{3.3}$$

Where $\Delta\beta = 2\pi n_{eff}/\lambda$. It can be noted that the last two equations highly resemble the FBG coupled-mode equation (2.11). Although κ_{dc} was neglected by previous authors in analysing Raman gain DFBs, it can be added to equation (3.3) as it simply shifts the overall FBG position. Considering this resemblance, if the first equation of the pump can be treated independently, then equation (3.3) can be resolved using the transfer matrix method with the known solution to FBGs. Such a method involves a wavelength scan and selecting a specific wavelength to calculate the field, i.e. the lasing wavelength. This simulation method leads to a second approximation: the laser emission is considered as single-frequency, as only one lasing wavelength can be evaluated. This approximation is valid as long as only one mode remains with a high Q-factor in the stop-band. This is also observed experimentally: for low-power operation, DFB fiber lasers have single-frequency emission.

Considering this, we proceed by supposing an initial guess for A_p, A_f and A_b, which is used to find the pump field in the first equation of (3.3) using the standard RK4 method. This calculated pump field, as well as the initial guess for A_f and A_b are then used for the intensities $\left|A_p\right|^2$, $\left|A_f\right|^2$ and $|A_b|^2$ in the last two coupled-mode equations. These last two equations are then treated separately by solving the FBG transfer matrix. The gain, loss and non-linear Kerr effect are included in the

κ_{dc} term of the FBG coupled-mode equation (2.11). The field solution is found at the DFB mode wavelength. This resonance wavelength must be found at each iteration, as the non-linear Kerr effect "moves" the DFB mode according to the intensity of the internal fields. This solution can then be compared with the initial guess, which can be corrected accordingly.

The method proved very successful, as will be described in Article 4. Both FBG or Raman gain DFB laser simulation are used to design the proper FBG and find the appropriate parameters. Once that is done, we can then proceed to the fabrication step.

3.1.2 Fiber Bragg grating writing system

FBGs were fabricated during my PhD using the Fabulas installations. This installation mainly includes a FBG writing station as well as a 3D optical micro-machining/wave-guide writing station, as shown in Figure 3.1. This thesis will not detail the latter, as it was not the subject of the research presented here. The Fabulas lab includes many lasers, two of which are used with the FBG writing station: a 266 nm wavelength, 4th harmonic of a Nd:YBO laser, and a 213 nm wavelength, the 5th harmonic of another Nd:YBO laser. The 266 nm is a 2nd harmonic through a BBO crystal of a 532 nm Spectra-Physics Navigator laser. Typically, this laser output in the UV is 150 mW, but powers of 300-400 mW can be achieved by using the maximum pump output. However, since such power tends to damage the optics in the long term, powers above 200 mW are usually avoided. The 213 nm laser is a commercial Xiton laser, which can provide an output up to ~100 mW. Although the 213 nm yields much stronger FBGs, as the photosensitivity at that wavelength is much higher, it is the 266 nm laser which was used for many of the results presented in this thesis due to compatibility issues described below.

The FBG writing system has a 1 m long air-bearing stage from Aerotech. The stage is equipped with an optical Fabry-Perot encoder to allow a closed-loop positioning stability down to a few nm. However, when moving, this error does increase significantly depending on the speed, leading to phase noise. The noise reduces at lower stage speeds and is better averaged out over the length on the illuminated fiber area. However, ultra-long FBGs require writing speeds in the order of ~100 µm/s for the fabrication time to be reasonable.

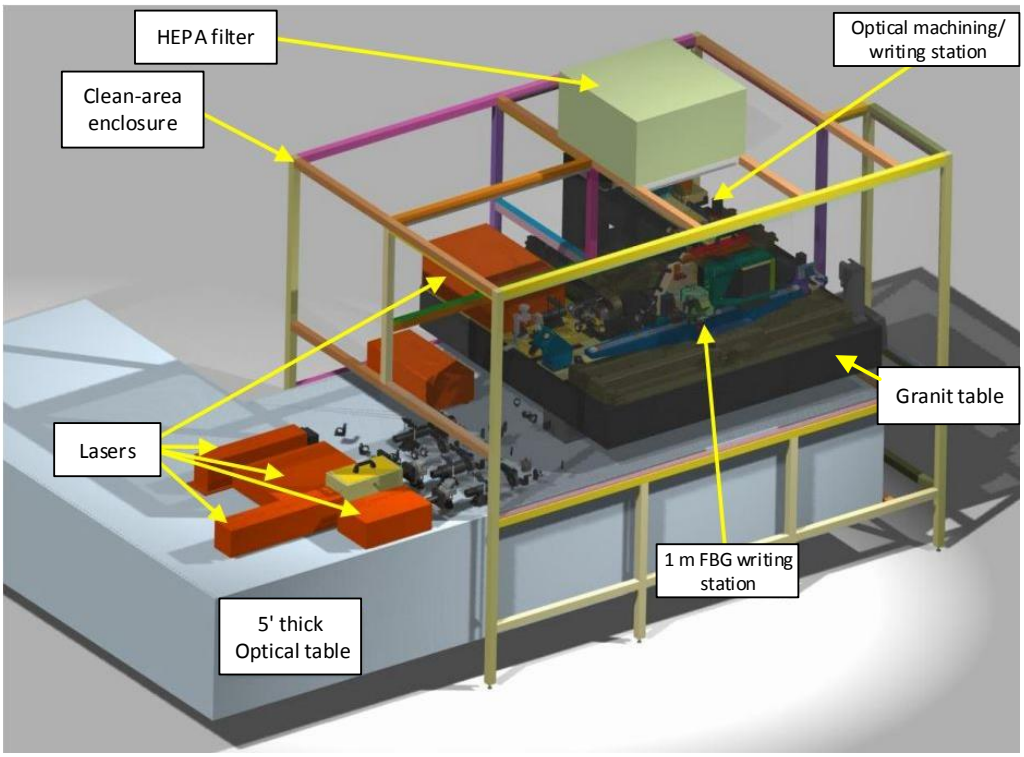

Figure 3.1: 3D design of the Fabulas station used for this thesis.

The writing system used throughout this thesis consists in an electro-optic modulated (EOM) Talbot interferometer, as shown in Figure 3.2. Unfortunately, the available EOMs are not compatible with 213 nm wavelength laser emission, therefore only the 266 nm laser could be used with such system. This is however not a problem for ultra-long FBGs, as the required κ_{ac} is very low, even for strong gratings. A cylindrical lens is used to focus the light perpendicular to the fiber axis, to maximise the UV light exposure of the core. The other axis (fiber axis) is also slightly focused to control the spot size. On our system, the typical illumination spot size was 100 to 150 µm in length, represented by Δz in Figure 3.2. The beam is separated into 2 branches by a phase mask, and then recombined at a controlled angle θ by kinematic adjustable mirrors. This angle defines the fringe pattern's period as described by equation (2.32). Inverted phase modulators in each branch are used to change the phase of the fringes, hence "move" the pattern on the fiber. To do so, a saw-tooth wave, called the *fold* wave, is sent to the modulators, in which the phase jump corresponds to an integer number of periods.

The Bragg wavelength is then defined by the drive frequency and the fiber speed, as given by equation (2.37). As mentioned in the previous chapter, this frequency and speed that adjusts the

Bragg wavelength must be within a certain bandwidth of the Bragg wavelength as defined by the fringe pattern, i.e. ±4 nm for our spot size around 1550 nm.

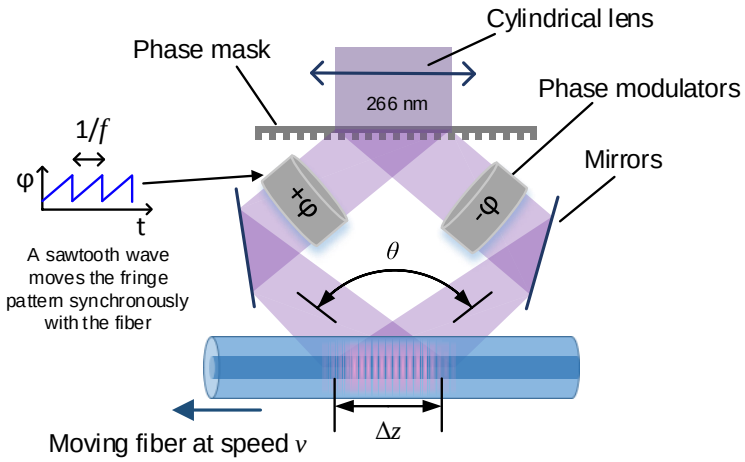

Figure 3.2: Schematic view of the Talbot interferometer used to write continuous FBGs.

Such a system allows tunability of all FBG parameters along fiber length in the following way:

- The Bragg wavelength λ_B can be changed along the FBG to induce a customized chirp. This can be done by changing the fold frequency (for linear chirp only) or by changing the moving speed of the stage (custom chirp).
- The coupling constant κ_{ac} can be controlled through apodization. By adding a linear scrambling wave (saw-tooth or triangular) to the fold wave, the written fringes can be erased. A 100% apodization ($\kappa_{ac} = 0$) corresponds to when this scrambling wave's amplitude equals 2π. The scrambling frequency must be different and ideally much higher than the fold frequency.
- The phase ϕ can be changed by applying a DC voltage to the modulators. However, it was found that this method is not ideal; due to the lack of feedback on the induced optical phase by the modulators, this phase may change over time because of varying environmental conditions (including any effect the DC voltage may have on the crystals). Another method to control the phase of the grating was proposed and demonstrated by changing the Bragg wavelength (λ_B). Indeed, phase is the integral of the grating period $\Lambda(z)$. A Gaussian or square shaped Bragg wavelength increase (ex: +100 pm over 1 mm) can be implemented

to induce a phase shift. Since our stage offers a very precise control of its speed, tuning the speed of the stage has proven to be the best way to customize the phase of a FBG for the EOM system.

- The dc coupling constant κ_{dc} can also be customized by tuning the laser power. However, to maintain a constant κ_{ac}, an inversed-apodization is required to compensate for the change in the effective index of the mode. Alternatively, the DC level can be raised during second passage on a previously written FBG, while deactivating the fold wave: in such a case, no fringes will be inscribed (they will erase themselves) and the refractive index will be raised according to the laser power. Tuning the κ_{dc} can be useful to induce a slight chirp, but since the exact amplitude of change is difficult to control, this method was not used.

Compared with a piezo-driven system, a EOM-based Talbot interferometer generates less vibrations (less phase noise) and can allow much higher driving frequencies. A piezo driven system has a low cut-off frequency due to mechanical inertia: any speed over 10 µm/s will see a degradation in the saw-tooth wave sent to the piezo due to the higher required frequency. This also limits apodization: a perfect apodization requires a high-frequency scrambling wave to erase the period linearly. A piezo driven system can be also apodized, but at a frequency similar to the driving one, which leads to a non-linear apodization when it nears 100 % ($\kappa_{ac} \rightarrow 0$). An EOM does not have these disadvantages. The comparison of both systems is shown in Figure 3.3, for a writing speed of 30 µm/s. While the EOM system can implement single-period jumps, the piezo requires a jump of 4 periods to remain within an acceptable frequency (<20 Hz) to avoid serious degradation of the saw-tooth wave shape. An example of a good apodization function at high frequency (with EOM) is compared to a non-ideal apodization at low frequency (with piezo) in Figure 3.3.

Considering that a EOM driven Talbot interferometer yields higher quality gratings and can go to higher speeds, it is therefore better suited for ultra-long FBG fabrication. However, the current system was limited (until recently) at around the S-C-L bands only (1480 to 1650 nm). Therefore, to make ultra-long gratings at other wavelength, as it was done with our collaborator MPB Communications Inc. [128], the piezo-driven phase mask system must be used. This is why all results presented in this thesis are from FBGs made in the C-L bands (1530 to 1620 nm).

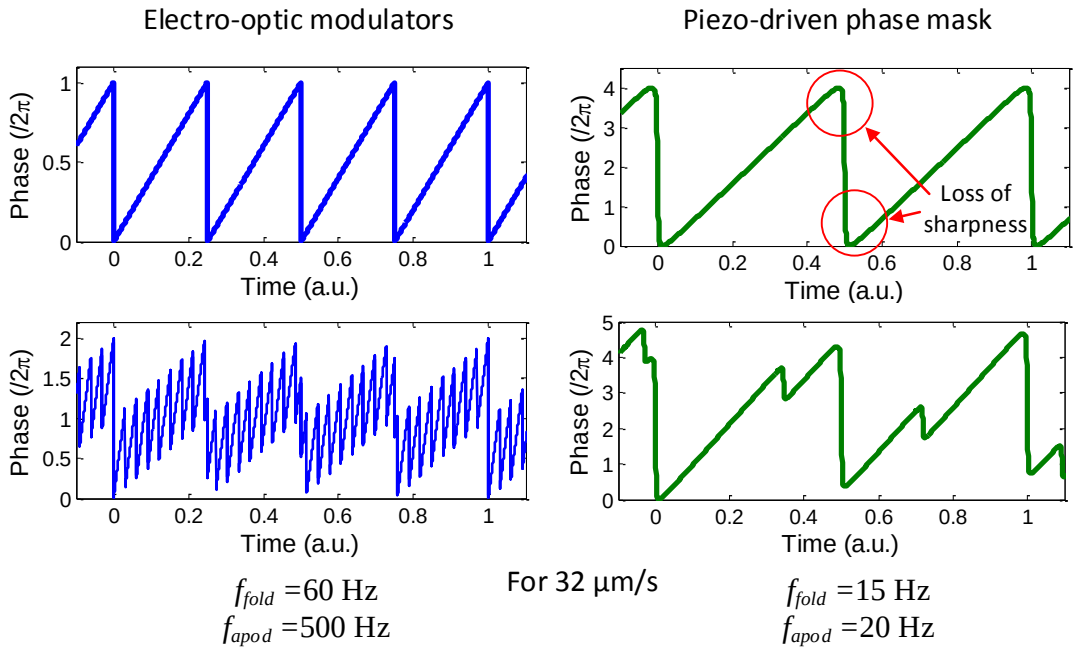

Figure 3.3: Comparison of the modulator and piezo performance for a speed of 32 µm/s. The 2 lower graphs show the case of apodization. To maintain an acceptable quality in the saw-tooth wave, the piezo must be used below 20 Hz.

3.1.3 Characterisation

During or after the FBGs are fabricated, characterising them is crucial to the understanding of potential problems. The most important characterisation system used here is an optical back-reflectometer (OBR) by Luna. This system uses optical frequency domain reflectometry to analyse the fiber, or in our case, the FBG. The principle, as explained in the previous chapter, is a scanning laser source which measures the reflected light from a sample placed in an interferometer, as shown in the upper part of Figure 3.4. By performing a Fourier transform on the obtained interferometric spectra, a reflected amplitude and phase profile can be found. An inverse Fourier transform on a specific section of that profile can uncover that portion's reflected spectra (and phase). The system by Luna uses a patented technology [83] in which the phase of the laser is monitored as the laser is scanned, as shown in the lower part of Figure 3.4. From this measurement, a correction is numerically applied to the detected signal of the fiber under test (FUT). This system is simple and allows the use of a cheap laser source, while giving a resolution of ~0.1 pm. However, the Luna OBR can be used only in the C-L bands (1530 to 1620 nm).

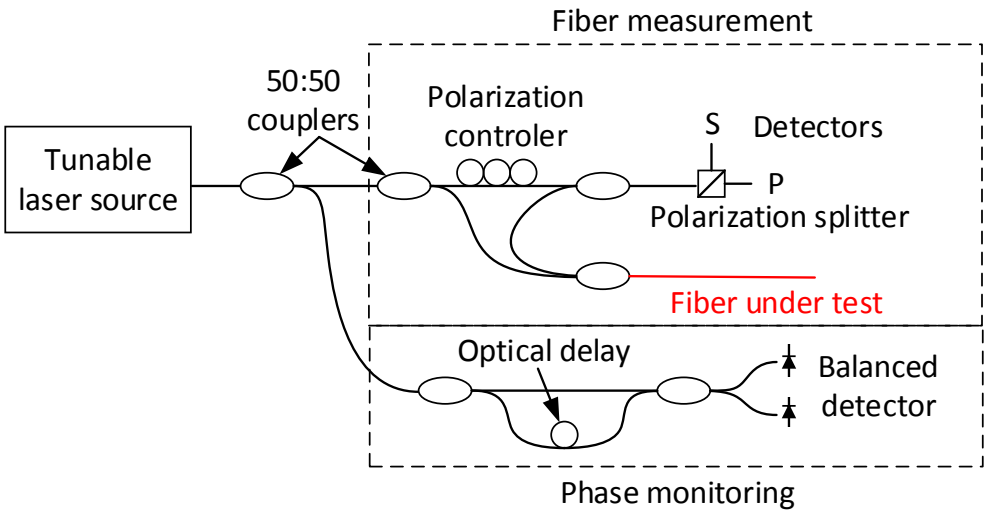

Figure 3.4: Optical circuit of the Luna OBR system. The top section represents the typical OFDR measurement interferometer, while the bottom section represents the patented Luna phase monitoring system to enable the use of low-coherence diode laser.

This OBR system was very useful to monitor a fiber during the writing process and hence diagnose problems. It was also used to calibrate the Talbot interferometer's angles as multiple FBG can be written in the same fiber and measured individually, even at the same wavelength.

Once fabricated, an important characterisation is the measurement of the transmission and reflection spectra. The measurement methods used was either the scanning tunable laser source method, or using the Luna OBR. In all cases, the resolution is defined by the precision of the tunable laser, which is 3 pm for our JDS tunable external cavity laser system, 0.16 pm for our Apex DFB diode tunable source and ~0.1 pm for the Luna OBR. The Apex and Luna system were mostly used, but the former is limited to the C band (1530 to 1565 nm).

When using a standard tunable laser source (not the OBR), transmission spectra is acquired directly (without any components), while reflection is acquired using a circulator or a 3dB coupler, as shown in Figure 3.5(a). As for the OBR, reflection spectrum is quite straightforward, as this is the primary function of such a system. For transmission, this can also be done by using a circulator, as shown in Figure 3.5(b). However, the OBR adds interference noise at maximum resolution, which is why the Apex tunable laser source is better suited when scanning in the C-band. For the Raman gain DFB lasers studied, the FBGs were made at 1578 nm, for which the OBR had to be used for characterisation.

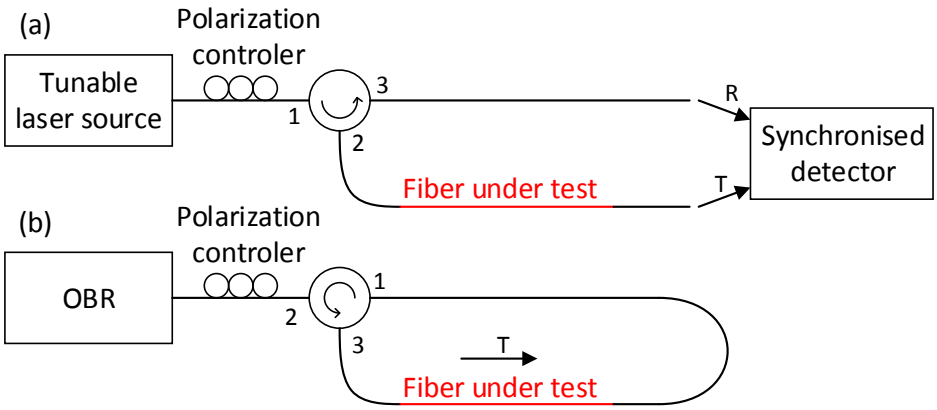

Figure 3.5: Measurement method

Group delay can be measured with the Luna OBR as well. Since this OFDR systems gives information on phase, this can be used to calculate group delay. The system calculates the phase derivative of the time domain (thus the spatial) reflection profile, which corresponds effectively to the reflected wavelength along this profile. From this profile, group delay can be recovered. When studying a narrow-band FBG (such as a weak grating), the phase derivatives gives the FBG central wavelength along the fiber length. Such information has been used to measure frequency deviation along the FBG position during or after writing and is used for the refractive index characterisation in articles 2 and 3.

3.1.4 DFB Laser operation

The tools described in the last sub-section are for characterising the FBG itself. Since one of the objective of this thesis is to implement and optimize functional DFB fiber lasers, a test bench had to be used to test and measure the performance of such devices. This test bench is described in Figure 3.6. The pump is a 20W Raman laser operating at a wavelength of 1480 nm. The Raman gain peak in the FBGs with this pump wavelength is at 1578 nm. The pump is injected into a SMF-28 (~80% efficiency) which then passes through a WDM coupler to separate the backward 1578 nm signal and the partially reflected pump. The forward signal is also separated (1480 nm pump/1578 nm signal) through a WDM coupler at the output. Isolators are used to ensure no back reflection from terminal connectors influences the DFB laser. An important limitation were the splices. As the fiber used for Raman gain is a small-core fiber (~4 µm MFD, 0.25-0.3 NA), the mode-mismatch is large when spliced to a standard fiber (10µm MFD, 0.13 NA) leading to a loss

of ~5 dB. The splices were therefore optimised by tapering and with long arc times (to expand the core), which allowed us to reach a transmission of 80-90%. Including the loss from other components, we have a total injection efficiency into the FBG of 60-65%, or 50-60% at the pump monitoring point (due to the output splice). The maximum injected power inside the FBG is therefore ~12 W. The phase shift was placed towards the backward-output, as this is the typical configuration of such lasers, since the counter-propagating signal is easier to separate from the pump.

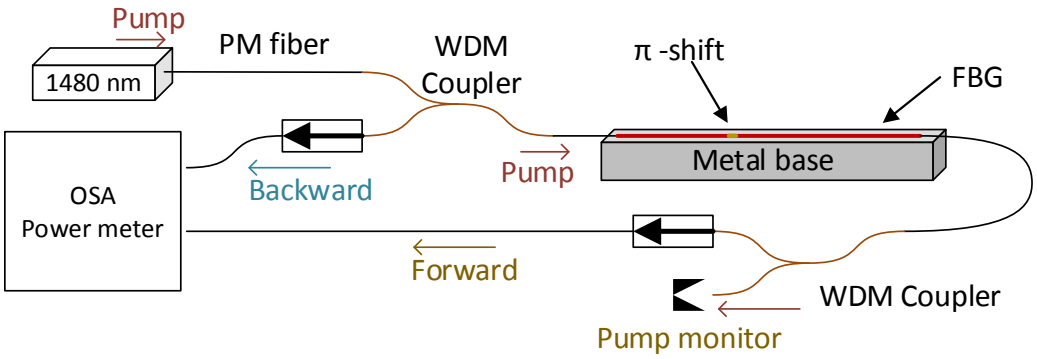

Figure 3.6: Experimental setup of the DFB laser test bench.

The FBG support was a tricky issue. Since any temperature gradient induces a chirp in the FBG, which can be detrimental to laser operation, the base must be thermally conductive to ensure uniform temperature distribution along the fiber. Also, any heat generated by the fiber itself has a greater chance of dissipating with a conducting base. The support which yielded the best results was a thick aluminium plate with a 2 x 2 mm square groove on the top surface. The fiber was placed in this groove which was filled with glycerol, to ensure maximum thermal contact with the fiber. The whole plate was isolated in foam to avoid environmental influence, and a thermo-electric cooler (TEC) was used underneath to cool the plate to 10 °C. Having a cooler environment around the fiber increases the thermal dissipation from any heat generated inside the core.

The forward and backward waves were measured by a power meter, OSA and ESA for different pump levels. A variant of the system used a polarised Raman pump laser: a free-space polarizer was added as well as fiber polarization controllers, although this reduced the available pump power down to 5-6 W. It was found that a polarised pump increases the gain by a factor of ~2.

3.2 Organisation of the articles

The thesis is structured in 4 articles, which describe in detail the work I performed during my PhD on ultra-long FBGs. The work led to the first article on DFB structures. However, even though ultra-long FBG in standard fiber (SMF-28) had been successfully fabricated, the implementation of a phase-shift was difficult with the EOM Talbot system. By investigating this issue, we found that it was most likely the lack of feedback on the modulators which caused the problem. After further investigation, a solution was found: the phase shift was implemented through a wavelength variation through speed variation using our precise 1-m long stage. This proved to be very effective: ultra-long π-shifted DFB FBGs are now highly reproducible. To test such ultra-long devices, Raman gain was used to implement FBG lasers. Unfortunately, Raman gain did not lead to lasing in SMF-28 fiber. Brillouin gain, on the other hand, did lead to lasing, which is the subject of the first article.

Article 1 [134] is entitled **"Stimulated Brillouin scattering in ultra-long distributed feedback Bragg gratings in standard optical fiber"** and published in Optics Letters. This article addresses 3 of the objectives in this thesis: to find and understand the limitation of ultra-long writing (phase-shifts in EOM Talbot system), to find and describe a solution, and to demonstrate a DFB fiber laser using non-linear gain, SBS in this case. The article presents the new writing technique for phase-shifted DFBs (by implementing a brief wavelength increase through speed variation) and presents characterisation results on two SBS DFB fiber lasers, one with a strong FBG and another with a weaker one. This article provided important insights on a problem with strong DFB fiber lasers which helped in the subsequent modeling of Raman laser: the thermally induced non-linear chirp induced by the high intensity of the internal oscillating mode.

As mentioned earlier, Raman gain did not lead to lasing in the SMF-28 based DBF FBG with the 12W of available pump. This is likely due to the low effective gain in standard fiber (large mode area) which competes with the intrinsic loss induced by the UV exposure. Therefore, small-core fibers were used instead to demonstrate a Raman DFB fiber laser. After several attempts, a few successful lasers were demonstrated, yet reproducibility and quality of FBGs were noted to be poor. Large non-linear chirp was often observed in the FBGs. Initially, environmental fluctuations and bad-luck were thought to be the cause, but these reasons could not explain the large discrepancies

constantly observed. A new problem had arisen and after a long and agonising investigation, the source was found: *spatially, optical fibers are intrinsically non-uniform*.

This conclusion, as well a new measurement method to prove it, is the subject of **Article 2 [135]**, entitled "**Are optical fibers really uniform? Measurement of refractive index on a centimeter scale**" published in Optics Letters. This letter directly addresses the first objective of the thesis: finding and understanding the limitations of writing ultra-long FBGs. This discovery was indeed highlighted as a serious limitation. The article showed that OFDR (our commercial Luna OBR) measurements on probe FBGs allows a measurement of spatially resolved effective refractive index (RI) with an absolute precision of 10^{-4} RIU and a relative precision of 10^{-6} RIU. With this very high relative precision, a frequency deviation of the FBG resonance could be observed indicating a variation in the RI in the order of 10^{-5} RIU, which is catastrophic for ultra-long FBGs.

The first solution in mind was to find a better fiber. After an investigation of half-dozen fibers from multiple manufacturers, the problem seemed to be universal, except for SMF-28 in which the variations could be considered within an acceptable margin. Fortunately, a solution was eventually found: we simply needed to compensate for this measurable and intrinsic fiber defect using our tunable system.

Article 3 [136], entitled "**Reproducible Ultra-Long FBGs in Phase Corrected Non-Uniform Fibers**" published in Optica, demonstrates this solution and shows the first high quality ultra-long (~1 m) FBGs in *any* fiber. This directly addresses the second objective in this thesis: developing the writing of *perfect* (or as near as possible) ultra-long FBGs.

With this new writing technique, reproducible Raman gain DFB fiber laser could now be made in series with controllable varying parameters. Parallel to the work done in **articles 2 and 3**, a new simulation method was developed and used to simulate Raman gain DFB fiber lasers.

Article 4 [137], entitled "**Optimization and Realization of phase-shifted Distributed Feedback Fiber Bragg Grating Raman lasers**", submitted to Optica, is the combination of simulations and experimental results. For instance, the thermal gradient induced by the internal field was modeled and experimentally validated. This paper addresses the last two objectives in this thesis: developing a simulation method and model for Raman gain DFB fiber laser and demonstrate and optimise operation of such lasers.

The following chapter will present the article, after which their results will be discussed.

CHAPTER 4 ARTICLE 1: STIMULATED BRILLOUIN SCATTERING IN ULTRA-LONG DISTRIBUTED FEEDBACK BRAGG GRATINGS IN STANDARD OPTICAL FIBER

Authors: Sébastien Loranger, Victor Lambin-Iezzi, Mamoun Wahbeh, Raman Kashyap

Published in: Optics Letters

Distributed feedback (DFB) fiber Bragg gratings (FBG) are widely used as narrow-band filters and single-mode cavities for lasers. Recently non-linear generation has been shown in 10-20 cm DFB gratings in highly non-linear fiber. Firstly, we show in this paper a novel fabrication technique of ultra-long DFBs in standard fiber (SMF-28). Secondly, we demonstrate non-linear generation in such gratings. A particular inscription technique was used to fabricate all-in-phase ultra-long FBG and to implement reproducible phase-shift to form a DFB mode. We demonstrate stimulated Brillouin scattering (SBS) emission from this DFB mode and characterize the resulting laser. It seems that such a SBS based DFB laser stabilizes a pump's jittering and reduces its linewidth.

4.1 Introduction

Distributed feedback (DFB) fiber Bragg grating (FBG) technology has been developed to offer very narrow-band filters [15]. A better wavelength control, associated with high stability of this passive wavelength selective element can enhance performance in many modern applications. For instance, tunable and stable microwave signals can be generated using dual-wavelength DFB fiber lasers [138]. Also, long narrow-band DFB gratings may be important for sensor systems [3]. DFB gratings are simple FBGs in which a phase shift is included at a certain location within the periodic structure to allow a resonating mode in the stop-band. As such, it could be considered as a Fabry-Perot interferometer with a quarter wave phase shift cavity. The mode has a high quality factor, therefore can be used for lasers when they are inscribed in active fiber [139]. Since the quality factor of strong DFB gratings can be very large, such resonators can be used for optical non-linear generation, such as stimulated Raman scattering [124] and stimulated Brillouin scattering (SBS) lasers [131].

Most of these DFB FBGs have been fabricated using a technique that limits the FBG length to a maximum of ~10-20 cm. Some stitching techniques have been used to produce longer FBG [140], but the phase is then difficult to maintain and multiple DFB modes may appear. For rare-earth doped fiber based devices, 5-20 cm FBG are more than sufficient for lasing. Raman and Brillouin DFB lasers have been recently demonstrated [124, 131] and modelled [112, 133] using highly non-linear fiber which have a high NA (high confinement) and small-core. However, for non-linear generation, this length is highly limiting for low effective-nonlinearity fiber and is not considered to be practical in standard fiber for typical DFB FBG lengths.

We demonstrate here the fabrication of repeatable and high quality ultra-long DFB FBG (50 cm) using a novel technique in standard single-mode fiber (SMF-28). These DFB gratings are tested and characterized for non-linear generation. The advantage of using standard fiber instead of highly non-linear fiber is that there is no problem of mode mismatch, hence reducing the necessity of difficult splicing. Also, SMF-28 is amongst the best fiber in terms of quality, uniformity and losses, making such a DFB of the highest quality possible. We have successfully demonstrated SBS generation using such ultra-long DFBs. However, Raman generation was not observed.

4.2 Method

The DFB FBGs were fabricated by a direct writing scheme using a Talbot interferometer as reported by Gagné *et al.* [11]. This scheme, shown in Figure 4.1(a), uses phase modulators in the interferometer to move a fringe pattern synchronously on a moving fiber. The fringe pattern's movement is controlled by a sawtooth wave and is hence synchronized with the speed of the moving fiber. The corresponding Bragg wavelength is determined by:

$$\lambda_B = \frac{2n_{eff}v}{f} \tag{4.1}$$

Where *f* is the sawtooth wave frequency, *v* the fiber speed and n_{eff} the effective refractive index of the guided mode. The amplitude of the sawtooth wave is set to correspond to 1 period of fringe displacement. The fiber is moved using an Aerotech air-bearing stage with a precision of ~1 nm, allowing the inscription of ultra-long all-in-phase FBGs [11].

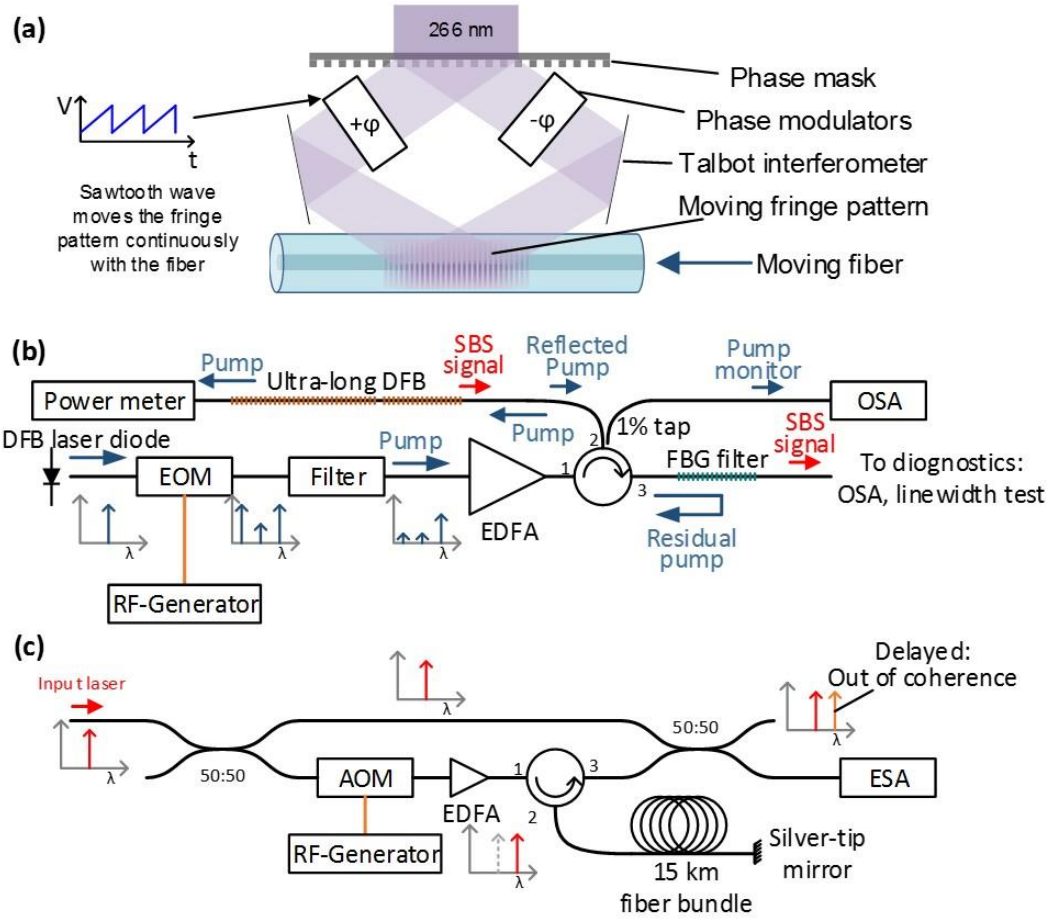

Figure 4.1: Experimental setup for: (a) FBG fabrication using Talbot interferometer and moving fiber, (b) SBS laser implementation with tuning pump and (c) linewidth characterization of pump and SBS emission. The beat note of linewidth characterization is measured with a fast photodiode and electrical spectrum analyser (ESA).

Reproducible DFBs were produced by a novel technique consisting of generating a phase shift by a small change in Bragg wavelength. Indeed, since the spatial frequency (where $K(x)$ is the local spatial frequency, and $\Lambda(x)$ is the local period of the FBG) is proportional to the derivative of the phase:

$$\frac{d\phi}{dx} = K(x) = \frac{2\pi}{\Lambda(x)} \tag{4.2}$$

The phase change $\Delta\phi$ along the length of fiber can itself be written as:

$$\Delta\phi_{shift} = \int_{x_0-\frac{\Delta x}{2}}^{x_0+\frac{\Delta x}{2}} \frac{2\pi}{\Lambda(x)} dx = \int_{x_0-\frac{\Delta x}{2}}^{x_0+\frac{\Delta x}{2}} \frac{4\pi n_{eff}}{\lambda_B(x)} dx \quad (4.3)$$

Where $\Delta\phi$ is the phase shift in the region Δx centered at x_0, where the shift takes place. This change in wavelength is implemented by changing the speed of the fiber, as shown in Eq. (4.1), a characteristic that we know is precise through feedback. Hence by introducing a small Gaussian-shaped local increase in the Bragg wavelength, a very precise and reproducible phase shift is generated since the phase is the integration of the Bragg wavelength along the fiber length. For a 4-mm full width at half maximum (FWHM) Gaussian chirp, the wavelength increase required for a pi-phase shift is 107 pm at 1550 nm, while in the case of a 2-mm FWHM Gaussian wavelength chirp, the increase is 214 pm, and so on. A wavelength increment of 107 pm corresponds to a local increase of 0.006% in the speed of the moving fiber, a variation that our high precision linear stage can easily accommodate. Such a small variation in speed has a negligible effect on the variation in the refractive index. The FBGs were written at a speed of 100 and 75 μm/s with UV optical power of 120 and 170 mW for DFB 1 and 2, respectively.

This fabrication technique was characterized on small FBGs with great success. However, when scaling up to ultra-long FBGs, the DFB mode position within the stop-band is not always centered due to the inherent random non-linear chirp introduced in ultra-long FBG from environmental changes during fabrication. Indeed, such ultra-long gratings are extremely sensitive to environmental changes which can cause a small chirp in the order of ~5 pm. We noticed a tendency towards a 3-5 pm concave chirp, and therefore could implement a correction during fabrication of the FBG. But an additional 3-5 pm non-linear and random chirp is often observed, possibly due to slight random temperature or laser power variations during writing. This chirp can be observed in the ultra-long DFB FBGs, shown in Figure 4.2, which was characterized for non-linear optical generation.

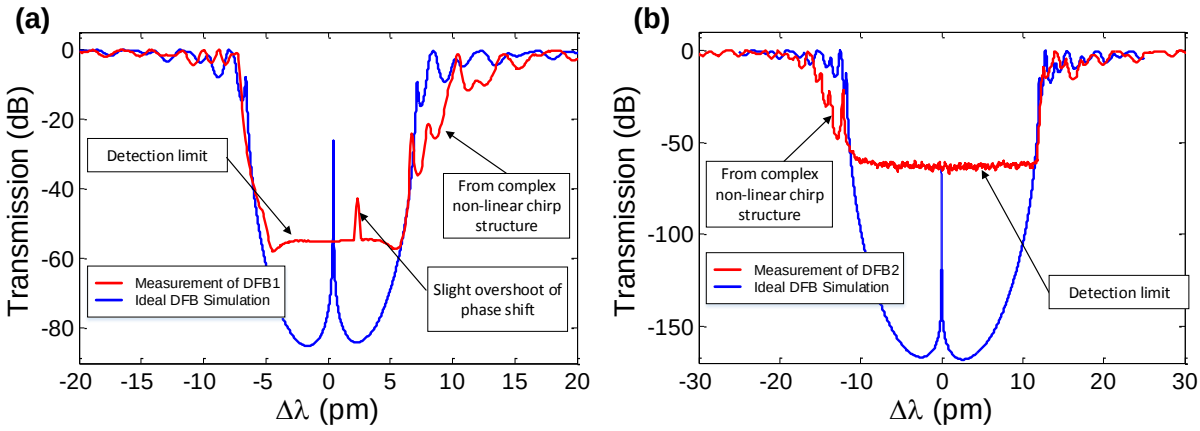

Figure 4.2 : Spectrum of 500 mm DFB FBG under test with 0.16-pm resolution. (a) DFB1 was fabricated to be the weak grating with a κ_{ac} of 24 m-1, while (b) DFB2 is stronger with a κ_{ac} of 45 m-1. The simulated transmission of the DFB mode with no gain is -26 dB and -63 dB for DFB 1 and 2, respectively (due to non-centered phase-shift). The Bragg wavelength of both FBGs is around 1549.5 nm. The resolution of simulated structure is 2 attometers.

In a weaker version (DFB1, in Figure 4.2(a)), the DFB mode can be seen to be not centered. A higher phase shift (120 pm) was intended to compensate for the chirp, but an overshoot was observed. In the stronger version (DFB2, in Figure 4.2(b)), the DFB mode could not be seen because of the limited resolution and dynamic range of our 0.16 pm resolution Apex optical spectrum analyser (OSA). However, the observation of SBS generation proves the presence of this mode as described below.

4.3 Results and discussion

Ultra-long DFB FBGs were then tested for non-linear generation. Raman generation, although predicted in our simulations, was not observed, even for ultra-strong DFB FBG (tested on gratings other than DFB 1 and DFB 2, centered at 1576 nm and pumped at 1480 nm with <-200 dB in transmission). SBS, on the other hand, could be generated easily. To characterize this, we used the experimental setup, shown in Figure 4.1(b). To generate SBS and measure the Brillouin emission, the pi-shift was placed at 175 mm in the 500 mm FBG in SMF-28 fiber in order to ensure emission mainly on the reflection side of the FBG. The Brillouin pump was a side-band of an electro-optically modulated (EOM) narrow-band 1550 nm laser. This side-band, isolated through filtering, was amplified and injected into the pass-band of the FBG, at 10.8 GHz above the DFB mode

frequency (SBS frequency in SMF-28) [141]. A 1% optical tap was used to monitor the pump and ensure that only the required side-band remained, while the injected portion within the FBG was monitored by a power-meter at the output. The pump frequency was tuned using the EOM's modulation frequency with an RF generator.

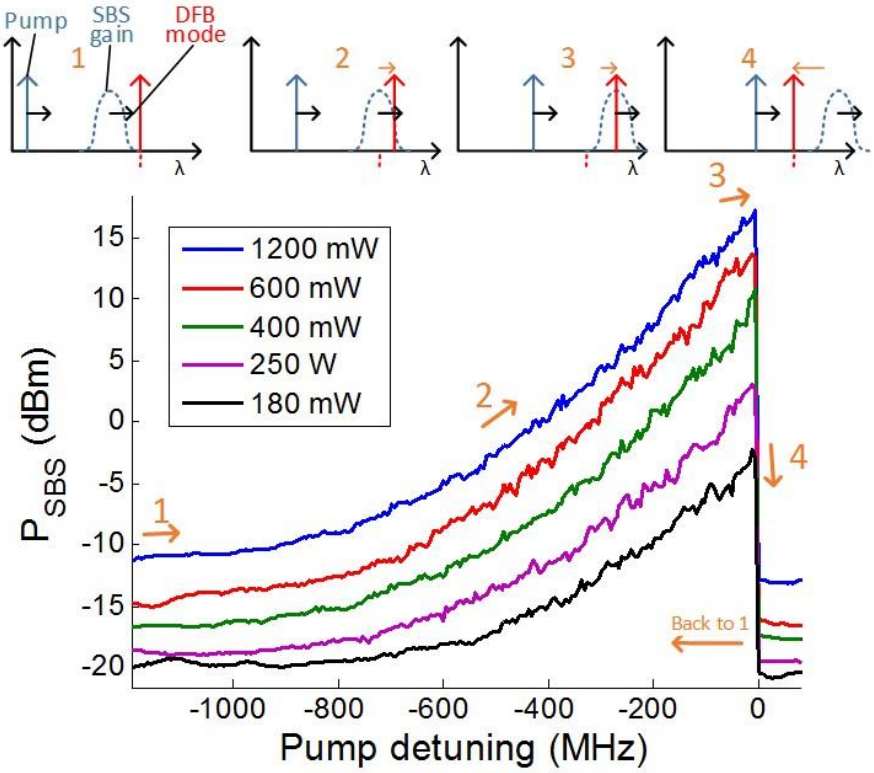

Figure 4.3: SBS generated power as a function of pump detuning and power. The pump is detuned as shown in the upper inset (by approaching the DFB mode from shorter wavelengths). The SBS gain, moving with the pump, pushes the DFB mode (state 1, 2) until the maximum is reached (state 3). The mode then "recoils" back to its original position once the maximum gain is exceeded. To recover SBS, the pump must be detuned to a shorter wavelength (state 1) to re-initiate SBS generation.

Results of pump tuning can be seen in Figure 4.3, which shows a hysteresis behavior similar to what was observed by Abedin *et al.* [131] on a shorter Brillouin DFB fiber laser using highly non-linear fiber. This behavior comes from a non-linear heating of the FBG, as proposed by Winful *et al.* [133], which occurs at the phase-shift position owing to the field accumulation within the high-Q resonator. When the DFB mode enters the SBS gain curve, Brillouin is generated. However, the accumulated energy causes a non-linear chirp which slightly de-tunes the mode to a longer

wavelength until an equilibrium is reached. As the pump is tuned towards the DFB mode, the SBS gain curves “pushes” the DFB mode until the maximum of the SBS gain is reached. As soon as the DFB mode experiences a drop in the SBS gain, the equilibrium is lost and the DFB mode “recoils” back to its original position. To recover lasing, the SBS gain must be tuned back to the short-wavelength side of the DFB mode. “pushing” effect acts as feedback to lock the lasing mode’s wavelength position on the edge of the SBS gain, which is jittering.

While the 3dB bandwidth of this detuning remains constant for different pump powers, the total detuning range increases with the pump power as it further heats the DFB mode. For steady state operation, the pump should be detuned below its maximum gain to avoid “losing” the mode.

We observed that the SBS emission from the weaker DFB1 was highly unstable, showing an on-off behavior in the order of tens of milliseconds. Although it showed the same patterns for DFB2, shown in Figure 4.3, it was also observed that the tuning bandwidth of DFB1 was much smaller, i.e. of 20-30 MHz at 3 dB, while it is 60-70 MHz for the stronger DFB2. We believe this smaller tuning bandwidth is due to a weaker “pushing” effect since the field is less intense in DFB 1 due to a weaker Q factor. Since the “pushing” effect acts as a feedback to stabilize the SBS emission, DFB1 suffers from instability as the jitter from the pump can bring the DFB mode beyond the maximum SBS gain (state 3 in Figure 4.3) and thus cause the extinction of emission. Jitter eventually brings the DFB back into a lasing state as the required “reset” frequency is quite low.

On the other hand, as can be seen in Figure 4.3, DFB2 has a wider bandwidth, hence a stronger “pushing” effect. Since DFB2 has a much stronger Q factor, its accumulated field is higher than that of DFB1 and therefore, its lasing mode is detuned further by a field-induced non-linear chirp. This makes such a laser more stable as the stronger The SBS output power was measured for both DFBs under test as shown in Figure 4.4(a). The large errors evaluated experimentally are due to 3 reasons: polarisation fluctuation causing a change in the side-band ratio at the output of the modulator, thermal effects in the FBG and in the modulator, and the interaction of the pump with the grating due to the jitter in the pump wavelength. Indeed, since the FBG was not apodized, a side-band structure was present at 10 GHz away from the DFB mode which showed a fine-structure in the reflectivity from 0% to 15 %. As can be seen from Figure 4.4(a), the strong DFB is 5x more efficient (5.6 % slope efficiency) compared to the weaker one (1.1 % slope efficiency) and we were

able to achieve a 50 mW output power in the SBS line with a pump power of 1.1 W. It can be noted that no higher order Stokes wave, such as the second order, were observed in the output spectrum.

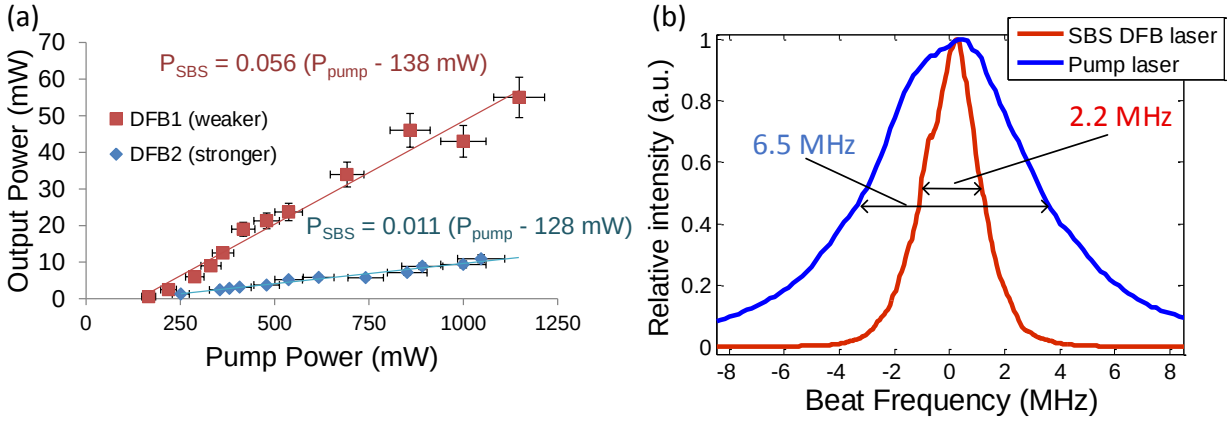

Figure 4.4: SBS laser characterization. (a) Output power of DFB 1 and 2 with their respective efficiencies and threshold. (b) Linewidth of DFB 2, the most efficient and stable SBS DFB demonstrated here, measured from self-heterodyne technique at 100 MHz, with a decoherence delay time of 150 µs. The SBS emission is compared with the linewidth of the pump. Note that any jitter within this time will cause an increase of the linewidth.

In previous work, Abedin's short highly non-linear fiber DFB [131] showed a higher efficiency (27% slope efficiency) and a 3 dB tuning bandwidth of nearly 300 MHz, which is much more than our measured tuning range. Their higher slope efficiency is expected in comparison, since we are pushing the limits of SMF 28 fiber which has a very small non-linear coefficient (30x less). The larger bandwidth, can be explained by the higher field confinement for similar lasing threshold (similar Q-factor) in a shorter DFB. The resulting higher peak field cause a larger non-linear chirp changing the phase-shift and hence amplify the "pushing" effect. In this case, the SBS emission's wavelength will follow the pump's variation precisely, giving rise to a very small beat frequency linewidth between pump and Stokes waves as observed by Abedin et al [131]. However, any jitter suffered from the pump will be also transmitted to the Stokes as well.

In the case of our ultra-long DBF, which exhibits a weaker "pushing" effect, we suppose that the DFB mode is more anchored to its original wavelength, as it does not follow the pump's jitter as much as in the short DFB case of [131]. This would result in a reduction in the linewidth of the strong DFB2 compared to its pump. In our case, the pump was a thermally stabilized DFB diode laser with a long-term stability of 15-20 MHz (slow frequency drift) and of instantaneous linewidth

of ~500 kHz. This linewidth measurement was performed with a self-heterodyne technique (shown in Figure 4.1(c)) using an acousto-optic modulator to shift the wavelength and a long delay line to render one side of an interferometer incoherent with the other.

The result is shown in Figure 4.4(b), where a decrease in the linewidth compared to the pump is observed. The linewidths observed here are larger than the minimum expected instantaneous linewidths for both pump (~500 kHz) and FBG DFB lasers (<100 kHz), as they include jitter within the 150 μs delay time of the self-heterodyne interferometric measurement. Increasing the delay much further would have approached the bandwidth of the long-term frequency drift. Interestingly, the DFB SBS fiber laser seems to stabilize the jitter bandwidth by a factor of 2, thus acting as a stabilizer. This can be further observed, in Figure 4.5, by the beat frequency of pump and SBS emission, including total jitter. Indeed, the large bandwidth observed here (17 MHz) is caused by a desynchronization of jitter between SBS emission and pump. In other words, it shows that the SBS emission does not follow all of the pump's movement, most likely due to a large thermal delay.

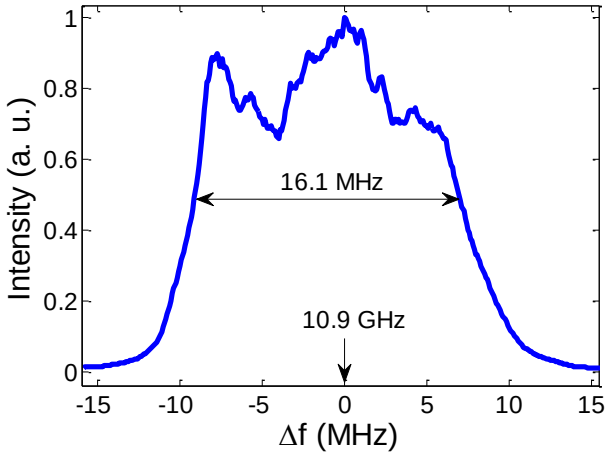

Figure 4.5: Pump-Stokes beat frequency around 10.9 GHz observed directly at the output (SBS signal output) without the pump FBG filter. Measurement done with fast photodiode and ESA.

4.4 Conclusion

In conclusion, we have demonstrated here for the first time the fabrication of ultra-long DFB in standard optical fiber without resorting to stitching techniques. These ultra-long DFBs have been used to generate SBS, although SRS has not yet been observed in our fibers. Generation of SBS in

standard fiber (SMF-28) ultra-long DFBs has a similar behavior to what was observed in short highly non-linear fiber DFBs [131], but with a few differences. First the performance was a little poorer and less stable, as can be expected from SMF-28's small non-linear coefficient. Secondly, its interaction with the pump shows a lower detuning pushing effect. Although this can be detrimental to laser stability, it opens other interesting application, as the DFB mode in such ultra-long gratings is more anchored (its frequency moves less), therefore less of the pump jitter is transferred to the lasing mode. Also, the overall pushing effect of both short and long DFBs can have interesting application in switching, as the hysteresis forces the user to detune the pump off-band (higher frequency, lower wavelength) to reset the SBS lasing process. Those ultra-long DFBs can potentially be optimized by taking into account Kerr effect [112, 142] and non-linear thermal chirp to further stabilize the generated Stokes. Further investigation is in progress to see how SRS may be generated in these ultra-long structures.

4.5 Acknowledgement

RK acknowledges Canada Research Chair program of the Govt. of Canada, SL, the Vanier scholarship program and, VL, the National Science and Engineering Research Council program.

CHAPTER 5 ARTICLE 2: ARE OPTICAL FIBERS REALLY UNIFORM? MEASUREMENT OF REFRACTIVE INDEX ON A CENTIMETER SCALE

Authors: Sébastien Loranger, Raman Kashyap

Published in: Optics Letters

Many applications of optical fiber, such as specialized fiber Bragg gratings (FBG) require high uniformity of a fiber's refractive index (RI) along its length. We show here that the mode effective index of most fibers is not constant even on a short length scale. To help improve fiber manufacturing and selection, we demonstrate a technique for characterizing meter length single-mode optical fiber's effective RI over a cm-scale with a precision of 3×10^{-6} RI units (RIU) and an absolute accuracy of 2×10^{-4} RIU. By writing several weak probe fiber Bragg gratings (FBGs) as frequency references and then measuring the frequency deviation of these probe FBGs along the length of the fiber with an optical frequency domain reflectometer, the RI distribution of the effective mode index may be found. We validate our measurements on reference and fibers under test with theoretical simulations.

5.1 Introduction

Recent development of all-optical fiber devices has made the requirements for the characteristics of specialty optical fiber more demanding. Distributed sensing, fiber interferometers, polarization monitoring and ultra-long fiber Bragg gratings (FBGs) are all applications which require precise characteristics of optical fiber for achieving high performance repeatability.

The optical fiber fabrication process has been well optimized over the years to ensure purity (low absorption loss), minimal scattering and uniformity. The challenges in the drawing process are well known [69] and some parameters are measured during or after the drawing process, such as refractive index (RI) profile, eccentricity, dopant concentration, defects, stress profile. However, most of these characterizations are performed at single points along the fiber (test samples) or averaged over a substantial length (meters).

An important parameter required in most devices is the effective refractive index of the guided mode (n_{eff}), as well as the effective group index (n_g). Therefore, controlling these parameters and

ensuring their uniformity over the device length is of vital importance for the quality of the fabricated devices. Side-diffraction monitoring has been widely developed to measure RI modulation (Δn) in FBGs [70-73], giving rise to a resolution of 5×10^{-6} refractive index units (RIU) on the grating RI modulation index [74] and 5 pm on the grating period (Λ) [75]. However, these techniques give no information on the variation of the actual $n_{eff}(z)$ within the fiber (only the UV induced modulation). Full-Fiber profiling has been demonstrated on mm-length [76], but such technique cannot be extended in m-scale. A heat-scan technique has been demonstrated [77] to get spatial relative variation in FBG parameters and time domain techniques were demonstrated using Bragg gratings [78] or acousto-optic method [79] to measure variation in the $n_{eff}(z)$ along a grating, but not its absolute value. An optical frequency domain reflectometry (OFDR) technique has been proposed to correct for phase errors of FBGs [49], but cannot be used for fiber characterization, as it is used behind-the-mask, making the measured phase errors dependent not only on the fiber, but on the mask as well as well as being limited to short lengths (~10 cm).

We propose here a new method to measure the distributed RI along the fiber with unprecedented sensitivity. The proposed method allows a precision in the RI variation along the fiber of 3×10^{-6} RIU. The maximum measurement length is ~0.8 m. In this paper, the method is described, referenced and validated. Several fibers are also characterized as examples of this application. Fibers from different sources are used and compared for their uniformity.

5.2 Method

In this technique, a long weak probe FBG is first written in the entire region of interest. This weak FBG is then measured by OFDR [81] using a commercial LUNA system [82]. This OFDR instrument is a wavelength scanning interferometer which can determine the position of a reflected wavelength. Therefore, such an instrument can measure the reflected wavelength of a FBG as a function of position (z) along the fiber. For a constant written period (Λ) inside the fiber, the Bragg reflection wavelength (λ_B) will depend on n_{eff}:

$$\lambda_B = 2n_{eff}\Lambda \tag{5.1}$$

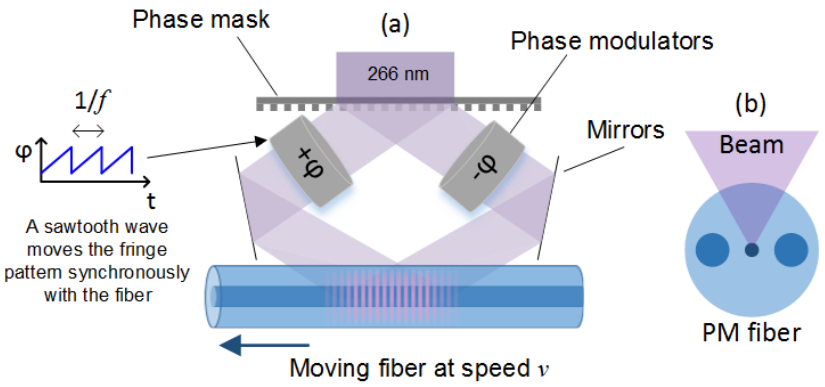

Figure 5.1: (a) Direct writing scheme using a Talbot interferometer for inscribing probe FBGs. (b) Position of fiber in respect with beam all along writing length for PM fibers.

The challenge in this characterization method is writing a constant and controlled period grating. To do so, we use a direct writing scheme as shown in Figure 5.1 which utilizes a 1m long air-bearing stage to move the fiber precisely without vibration [11, 134]. In each of our measurements, a 20 cm length of the test region of the of fiber was first exposed (apodized, no FBG written) prior to the test, to pre-heat the writing region and optical modulators to bring them into thermal equilibrium. In this scheme, the written period is uniquely defined, in the first order, by the speed of the fiber (v) and the frequency (f) of the waveform moving the fringe pattern:

$$\Lambda = \frac{v}{f} \quad \rightarrow \quad \lambda_B = \frac{2n_{eff}v}{f} \tag{5.2}$$

The spot size, i.e. the number of periods of the fringe pattern, will determine the tuning bandwidth around the fringe pattern's natural period determined by the interferometer. Our current spot size (around 100 µm) gives a 7 nm FWHM tuning bandwidth in the C-band. Higher order effects from temperature, air current and vibration, can also change the Bragg wavelength randomly. The speed is monitored precisely with a free-space Fabry-Perot interferometer. However, we can suppose that small random speed variations can occur and random (undetectable) phase drift of our function generator is also possible. The UV exposure power is extremely low, thus yielding a weak FBG (κ_{ac} ~ 1-10 m^{-1}) with a RI modulation in the order of 1×10^{-6} RIU. Each test was done at constant speed and the power was actively stabilized to avoid time-dependent variations in the exposure. To avoid confusion with RI modulation (Δn) and $n_{eff}(z)$ variation, we define:

$$\Delta n_{eff}(z) = n_{eff}(z) - n_0 \tag{5.3}$$

Where n_0 is a reference refractive index.

To avoid alignment errors along the fiber, which could affect λ_B through a higher order effect, the fiber's position is mapped using cross-positioned cameras. The fiber holders are then adjusted to allow a position variation of less than 10 µm along the 1 m stage. Considering the beam is 100 µm wide, such variation in core position does not influence the measurement. This was verified through writing tests.

Since the only error expected in Eq. (5.2) are random fluctuations, we can therefore correct for such an effect by performing several subsequent measurements at different wavelengths on the same fiber sample on a fixed section. This can be done by simply changing the frequency as shown in Eq. (5.2). In our demonstration, for each subsequent test, the grating was detuned by 1 nm. Since the bandwidth of such long FBGs is in the order of tens of pm, the FBGs are considered independent of each other, unless $\Delta n_{eff}(z)$ is in the order of 10^{-3}, which would be catastrophically large for any fiber.

5.3 Results and discussion

A reference test was performed in the best fiber available - SMF-28, well-known for its uniformity, and which is expected to have the smallest $\Delta n_{eff}(z)$ along its length. This reference, shown in Figure 5.2(a), shows little correlation in fluctuations between the 3 independent measurements at varying wavelengths, which would indicate a $\Delta n_{eff}(z)$ of less than the observed noise; noise which likely comes from environmental fluctuations. From the RMS noise in the measurement, we can define a precision for $\Delta n_{eff}(z)$ of 3×10^{-6} RIU. The flatness of this measurement also indicates no recurring errors from our stage, which validates our assumption of the constancy of speed and frequency.

As for the validation in the calculated $\Delta n_{eff}(z)$ from our OFDR measurement, this was done by measuring the reflection spectrum of the weak FBG. As expected from our measurement of SMF-28, the corresponding spectrum of the 250 mm long was a near perfect FBG, shown in Figure 5.2(b), to which a theoretical curve was fitted. Such FBGs in SMF-28 up to a length of 1000 mm, were reported previously using this exact same writing scheme by Gagne et al. [11].

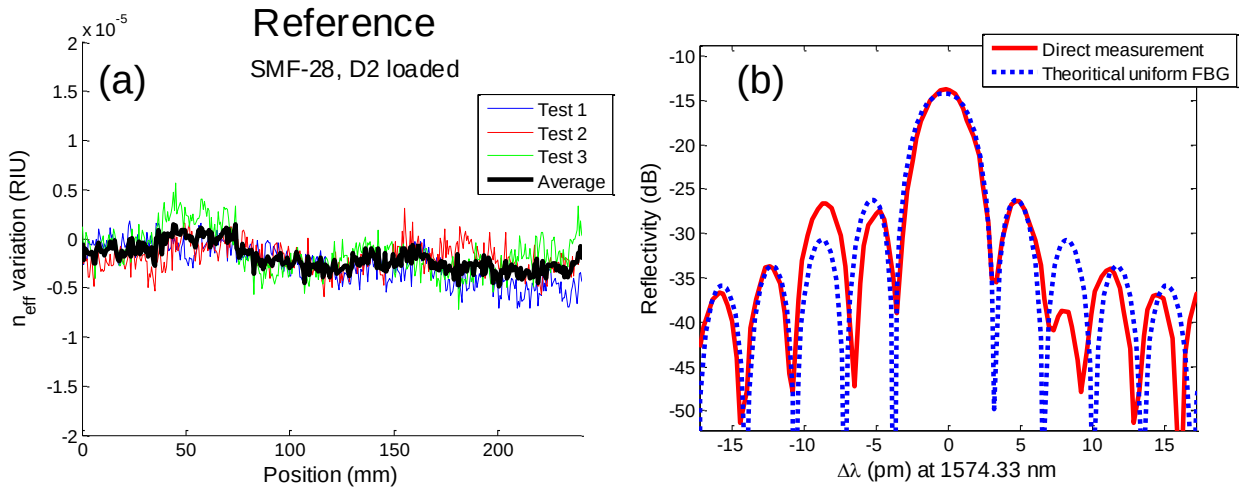

Figure 5.2 : Reference characterization performed in SMF-28, which is expected to be the highest quality fiber available (most uniform $n_{eff}(z)$). (a) Refractive index characterization (around n_{eff} = 1.4478), where the thin lines show 3 independent measurements and the thick line shows the average of the 3. (b) Measured and simulated (dashed line) reflectivity spectrum of this 250 mm FBG shows little apparent chirp and near perfect structure.

Further characterization and validation was also performed in a less perfect fiber. A small-core, high NA (high Ge concentration), polarization maintaining (PM) panda-style fiber (called PM1) was characterized in Figure 5.3(a)-(b). The PM's rod axis was aligned perpendicular to the beam, as shown in Figure 5.1(b), all along the 30 cm test length to avoid fluctuation in the exposure due to rotation of stress rod. The polarisation of the injected OFDR laser was aligned to one of the polarisation axes of the PM by eliminating the other polarisation Bragg resonance. This ensures that the probing laser will remain constant and will rotate along the fiber if the rods are to rotate, therefore eliminating polarisation artefact in the measurement. As can be observed, large variations in $n_{eff}(z)$ were observed. To ensure that such variations do not come from repeated errors of our test bench or from an exceptionally defective fiber piece, 2 samples of fiber were tested. Each sample was measured 3 times (3 different λ_B) to compensate for environmental fluctuation.

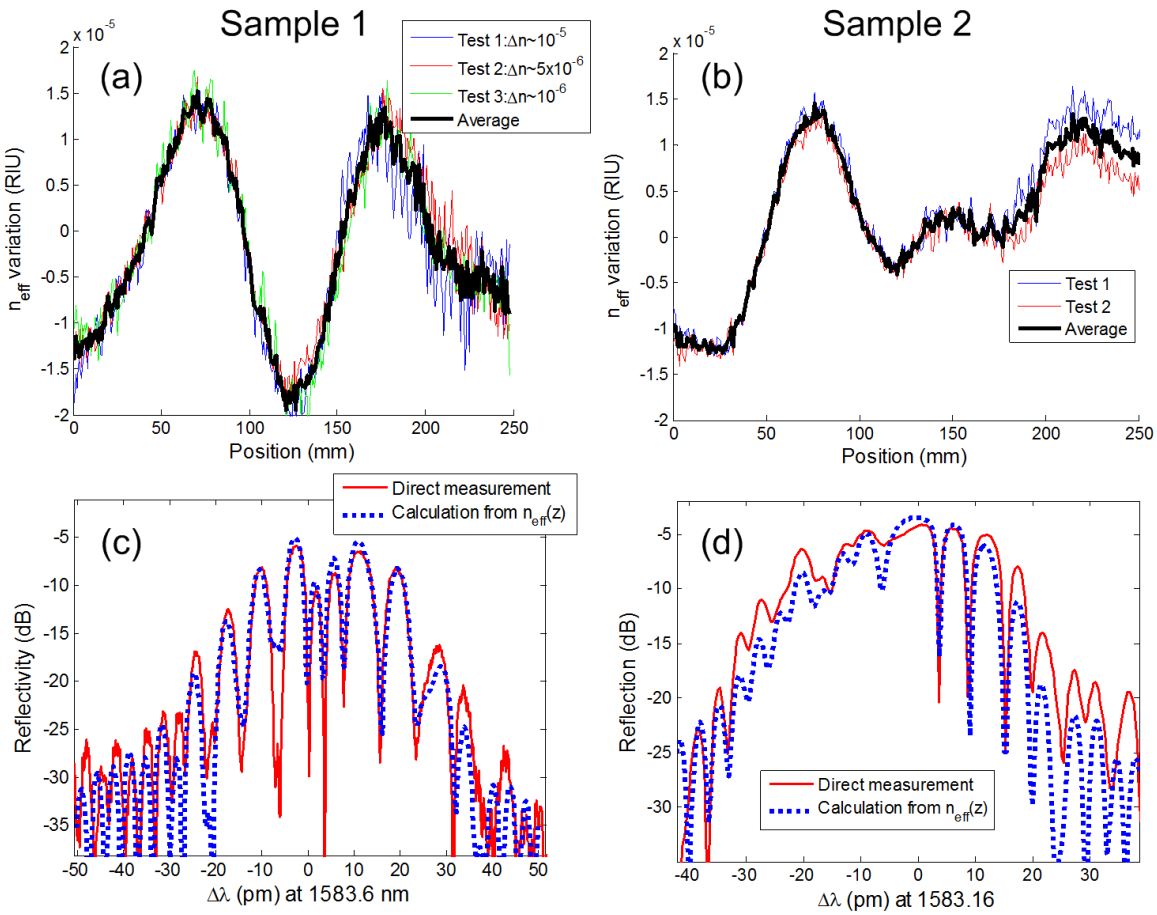

Figure 5.3: Characterization of a small-core (4 µm MFD, 0.3 NA), PM fiber (PM1). (a) and (b) show two different fiber samples. Several independent tests are shown with their average. The exposure (therefore Δn) was varied in (a). The reflectivity spectrum of both samples is measured in (c) and (d) respectively and the spectra compared with a calculated spectrum using the measured refractive index variation in (a) and (b).

To validate our OFDR measurement of $\Delta n_{eff}(z)$, the reflection spectra were once again taken and compared with a calculated FBG considering the measured $n_{eff}(z)$ variation. As can be seen in Figure 5.3(c)-(d), both samples match quite well in terms of chirp and mode position. Since there is no apparent correlation in the shape of the measured $\Delta n_{eff}(z)$ distributions (Figure 5.2 to Figure 5.5), we can assume the absence of inherent errors that could come from the stage or misalignment, making random fluctuation the main concern.

Further possible errors or misinterpretations have also been considered. Firstly, the exposure and appearance of a probe FBG will change the refractive index. Our tests were made with minimal

exposure to minimize this potential problem ($\Delta n \sim 10^{-6}$), but higher exposure was tested to see if it would impact the RI distribution measurement. In Figure 5.3(a), the first sample of this PM fiber was exceptionally tested with 3 different UV intensities, the strongest one leading to a $\Delta n \sim 10^{-5}$ and the lowest one for our standard exposure led to $\Delta n \sim 10^{-6}$. As can be seen, all 3 cases showed the same distribution in variation, which is expected as the power increases the RI evenly along the fiber. A larger noise is observed at the end as less signal is collected from the reflectometry measurement due to the presence of a stronger FBG. Therefore, weak FBGs are preferable for probing the fiber.

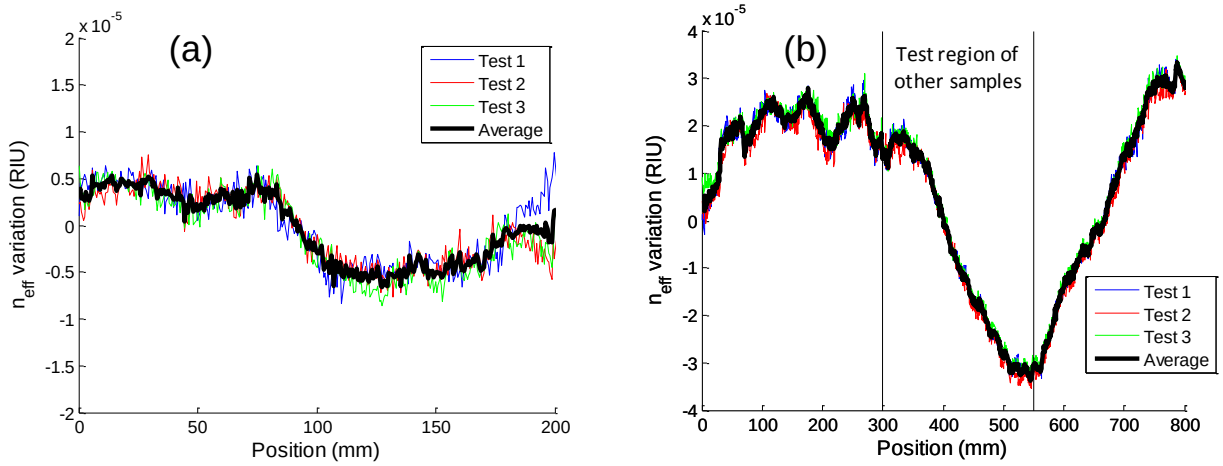

Figure 5.4: Characterization of a small-core, high NA fiber and non-PM fiber (SM2). (a) and (b) show two different fiber samples, (b) of long length. The thin lines are the 3 tests, while the tick like is the average of the 3. Note, the scale of Δn_{eff} in (b) is twice the scale of other figures.

A possible cause for observing a frequency shift in the FBG wavelength could come from a variation in exposure caused by core position variation inside the fiber. Core-meander is a known phenomenon in the drawing process and determines the quality of the fiber. However, such variation in UV exposure of the core does not involve a n_{eff} variation, therefore bringing a possible misinterpretation of our measurement. To verify this possible error, we deliberately varied the beam position by 10 µm in amplitude in random patterns on a scale of ~50 mm in variation period. This was done in one of the measurements shown in Figure 5.5(b). As can be observed, moving the beam does add noise to the measurement, but the main underlying variation is still clearly visible. It can be expected that a larger displacement of ±10 µm of the beam with respect to the core could become problematic for the RI distribution measurement, however this would be

considered catastrophic for any decent fiber manufacturing. It is important to note that core meandering and rod displacement can affect the n_{eff}, as this parameter depends both on material and spatial environment of the mode. Such meandering is a fiber drawing problem and could be the cause of the observed Δn_{eff}.

The PM fiber in Figure 5.3 showed a large variation in the RI distribution, which causes major non-uniform chirp to appear in the transmission spectrum of a grating. For many narrow-band applications, such variation is unacceptable, especially for FBGs longer than a few cm.

Fallowing this, a non-PM small-core high NA (high germanium concentration) fiber was tested (SM2). The results are shown in Figure 5.4 for two different samples. The first sample shows a relatively small variation in RI distribution. Despite this, such variation was sufficient to split in half the spectra within the central resonance lobe. The second longer sample (800mm) shows a major variation of the RI of ~ $\pm 5 \times 10^{-5}$ RIU over a length of 35 cm. Hence, the spectrum of such a FBG was not of the highest quality. It remains to be said that this fiber with a similar core as PM1 has generally less variation in n_{eff}.

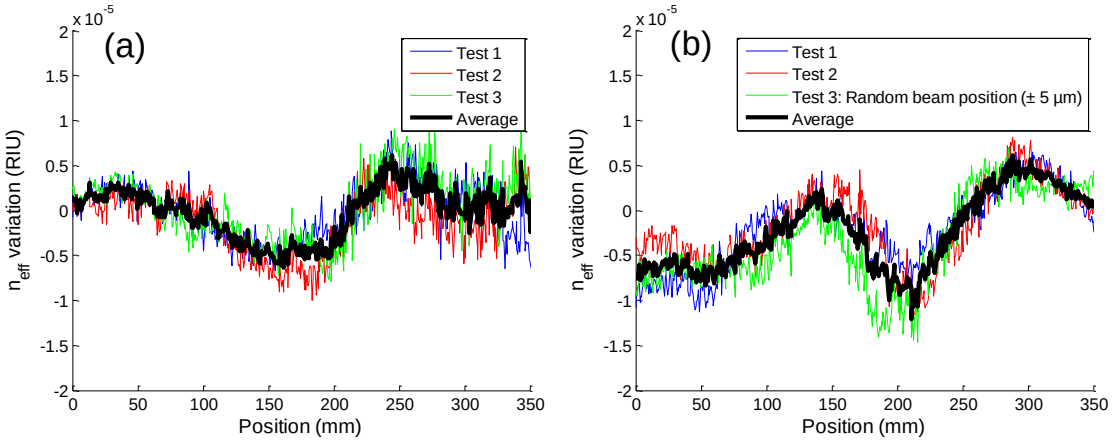

Figure 5.5: Characterization of a 6µm mode field diameter PM fiber (PM2). (a) and (b) show two different fiber samples. 3 tests are shown with the average. The 3rd test in (b) was done by including ± 5 µm random displacement in the beam over ~5 cm range.

Another PM fiber with a larger core was also tested. This fiber (PM2) has a 6 µm MFD, a 0.16 NA and Panda style stress rods. The RI characterization for two samples of the same fiber is shown in Figure 5.5. The same typical variations as observed in PM1 are also observed in PM2, but with

half the amplitude. Since the core is large, such fiber is perhaps less sensitive to core displacement within the stress-field, leading to better performance.

5.4 Conclusion

In conclusion, we have shown a new method to characterize a fiber's n_{eff} along its length. This method uses the fabrication of a weak probe FBG, followed by an OFDR characterization. By finding the distributed reflected wavelength along the fiber, one can correlate any subsequent wavelength shift to a refractive index shift. This is only possible in a continuous writing scheme where the fiber is moving and where the grating period is strictly related to speed and frequency of the waveform set on the phase-modulators. Noise from environmental fluctuation can be compensated for by performing multiple measurements at various wavelengths by changing the writing modulation frequency. A rougher setup for cheaper industrial characterization can also be considered, but such a system would have to be characterized with a reference fiber such as SMF-28 to correct for systematic errors from misalignment, and more tests would be required to properly average out the noise.

It is surprising to observe large refractive index variations on such a small length scale since the short-range fluctuations in the preform translate to very slow variations in the pulled fiber. Our analysis has shown a noise floor of $\Delta n_{eff}(z)$ at 3×10^{-6} RIU. Such noise can be further reduced by further averaging to compensate for environmental fluctuation. The absolute accuracy of measurement of $n_{eff}(z)$ is $\pm 2 \times 10^{-4}$ RIU, calculated from maximum deviation of the written λ_B from the aimed value in our tests, as alignment, temperature and strain may vary from one sample to another when they are placed on the test bench. This technique should allow the writing of long corrected FBGs with unprecedented quality.

5.5 Funding

The authors are grateful for funding of the research by Canada's NSERC's strategic research and the Discovery grants, and Canada Research Chairs programs.

CHAPTER 6 ARTICLE 3: REPRODUCIBLE ULTRA-LONG FBGS IN PHASE CORRECTED NON-UNIFORM FIBERS

Authors: Sébastien Loranger, Victor Lambin-Iezzi, Raman Kashyap

Published in: Optica

Ultra-long fiber Bragg gratings (FBGs), i.e. FBGs of several tens of cm in length, have attracted much attention in the last decades for their potential applications in advanced devices. Although numerous fabrication methods as well as ultra-long functionalized FBGs have been proposed and demonstrated successfully, such devices are difficult to reproduce. We have recently found that specialty optical fibers of the type required for these applications is highly non-uniform on a short length scale, severely affecting the characteristics of ultra-long FBG. We propose here a new production technique that can be adapted to any non-uniform fiber for ultra-long FBG fabrication. This technique involves a fiber characterization prior to FBG inscription followed by the writing of a phase corrected ultra-long FBG. This technique has no limitations in terms of correction amplitude or FBG length. The results are quite astonishing as near perfect 1 m length scale FBGs are possible in fibers in which it was impossible to write uniform period gratings prior to phase-correction.

6.1 Introduction

Fiber Bragg gratings (FBGs) have been used widely in numerous applications, from filters in telecommunications to sensors in many areas of photonics. Ultra-long FBGs, which we define as being longer than the length of commonly available phase-masks, i.e. ~> 15 cm, have been studied over the last decades leading to numerous demonstrations in various applications such as lasers, dispersion compensation and in nonlinear optics. Stitched FBGs were first proposed, but those typically included phase errors [62, 64]. Continuous writing scheme were then proposed to avoid such errors [15, 65-68]. However, random phase errors were still frequently observed, which led to applications in random gratings [143]. Ultra-long distributed feedback FBGs (DFB-FBGs) have been also successfully used as Raman lasers [125]. Despite these numerous attempts and demonstrations, our own considerable experience has shown unequivocally that such ultra-long FBGs are not reproducible as they often show significant phase errors if examined at higher spectral

resolution and only the few “best-typical” results are normally seen in publications. For ultra-long FBGs to become widely deployable, the reasons for their lack of reproducibility need to be addressed.

A reproducible method has been shown recently in standard fiber (SMF-28) for up to 1 m long FBGs [11], the longest all-in-phase FBGs ever produced with good reliability. This fabrication method was used to produce a 50 cm long Brillouin DFB laser in SMF-28 [134]. Although ultra-long FBGs in SMF-28 do seem reproducible, such reproducibility is very hard to demonstrate in other types of fibers. We have recently demonstrated that the fibers themselves are not uniform over even short lengths in the order of cms (variation in the effective mode index) and cause large fluctuations in the FBG’s instantaneous Bragg wavelength along the fiber [144]. This random and unpredictable chirp effectively reduces the stop-band strength, enlarges the bandwidth and causes unwanted mode-resonances to appear within the stop-band. Various techniques have been developed to characterise FBGs spatially: the refractive index modulation (coupling constant) can be determined by side-diffraction [71, 72], while all parameters can be determined by optical Fourier domain reflectometry (OFDR) [49], thermal iterative chirping [145] or inverse reconstruction [73]. These techniques can allow the observation of repetitive phase defects in the FBG during a specific writing cycle, which can be subsequently corrected, as shown by Miller *et al.* [49, 146]. However, the latter method is limited in terms of FBG length and phase correction to variations in the order of 2π. We have seen in our investigations that in many fibers, the observed phase-shift can be 20π radians or greater along ~ 10 cm, making this technique impossible to apply for correcting ultra-long FBGs.

We have implemented a modified correction scheme based on the one reported by Miller *et al.* and applied it to ultra-long FBG fabrication in our continuous direct writing technique, overcoming the limits in phase-correction. Hence, in this paper we demonstrate ultra-long phase corrected FBGs. The final phase-corrected FBGs show near theoretically perfect spectra, overcoming the problems of reproducibility. The method will be described followed by a demonstration of a few phase-corrected FBGs to highlight the power of this technique.

6.2 Method

A continuous direct writing scheme was used [11], as shown in Figure 6.1(a), based on a Q-switched 266 nm wavelength laser, a Talbot interferometer and phase modulators to synchronise the fringe movement with the moving fiber. An air-bearing stage stabilised by a laser interferometer moves the fiber. The phase modulators are driven with a saw-tooth wave function, the frequency of which determines the Bragg wavelength so long as the wavelength is within a certain bandwidth of the fringe pattern determined by the Talbot interferometer and spot size. The DFB FBGs demonstrated here include a π-shift near the middle of the FBG through a speed variation [134]. The relationship between the Bragg wavelength λ_B and writing parameters is as follows [15]:

$$\lambda_B = \frac{2n_{eff}v}{f} \tag{6.1}$$

Where n_{eff} is the effective refractive index of the mode (around 1.45, dependent on fiber), v the speed of the moving fiber (typ. 100 μm/s) and f the frequency of the saw-tooth wave function on the modulators (selected for the target λ_B). Here, $n_{eff}(z)$ needs to be corrected and v is used to correct it.

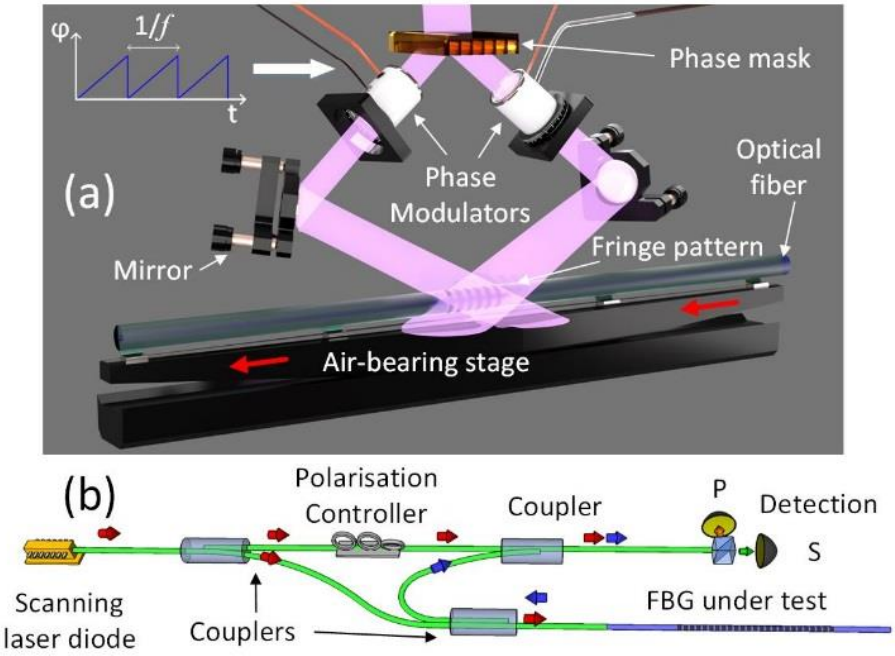

Figure 6.1: (a) Experimental setup for FBG writing. The system is a continuous direct writing scheme. The fiber moves at speed, v while the phase modulator moves the fringe pattern using a

saw-tooth function with a frequency, *f*. (b) A commercial OFDR characterization system is used to find the frequency deviation along the fiber.

The required correction was measured by probe FBGs using OFDR, as shown in Figure 6.1(b), prior to the target FBG being written. Three weak probe FBGs were written at the same location as the final target FBG with Bragg wavelengths separated by 1 nm each and outside of the target bandwidth of the desired FBG. The wavelengths of the probe FBGs were set using the saw-tooth wave frequency *f*. As the probe FBGs are very weak (<-10 dB in transmission, $\kappa_{ac}L$<0.3) and lie outside of the target FBGs bandwidth, their spectra do not interfere with the latter. The frequency shift along fiber position (phase derivative measured by OFDR) was then averaged for the 3 probe FBGs and a correction profile was derived. The FBGs' strength can be altered by the UV exposure (speed of writing and UV power) and apodization. A combination of these adjustments was used for the probe gratings depending on the FBG type and fabrication time needed for each grating.

Using more than a single probe FBG for characterisation is essential, as environmental fluctuation can easily mask the spectra through noise of a few pm (slow varying), as well as measurement errors causing peaks to appear in the OFDR phase derivative. Having several probe FBGs and comparing their respective frequency deviations ensures that the correction is valid and truly represents defects in the fiber.

6.3 Results

To demonstrate the ultra-long FBG writing technique, 3 high-NA fibers were tested, including one that was polarisation maintaining. Such fibers have several applications in non-linear optics, but were found to be highly non-uniform even over short lengths [144], which pose serious issues for ultra-long FBGs. Of the three fibers, HNA1 is a high NA (0.25), germanium-boron co-doped and cladding mode suppressed fiber. HNA2 is a highly nonlinear fiber with a large NA (0.3) and small core (3 μm diameter). PMHNA is a polarisation maintaining (PM) fiber with a small core (3 μm diameter) and large NA (0.3).

For the first demonstration of phase-correction, a 95 cm long FBG was written in HNA1. The frequency deviation (difference from the target λ_B) resulting from a spatial variation in the refractive index of the fiber, were first measured using the 3 probe FBGs. The average of these measurements is shown in Figure 6.2(a). A required correction was then applied to the desired

stronger FBG. The resulting change is shown in Figure 6.2(b), in which the reflection spectrum of one of the 3 probe FBGs (all 3 probe FBGs had near identical spectra) is seen with the dramatically narrower spectrum of the corrected FBG in the background. The latter is shown in greater detail where it is compared to a theoretical fit yielding a κ_{ac} of 3.9 m^{-1} ($\kappa_{ac}L$ = 3.42) in Figure 6.2(c). Theoretical calculation was performed using the transfer matrix method [15].

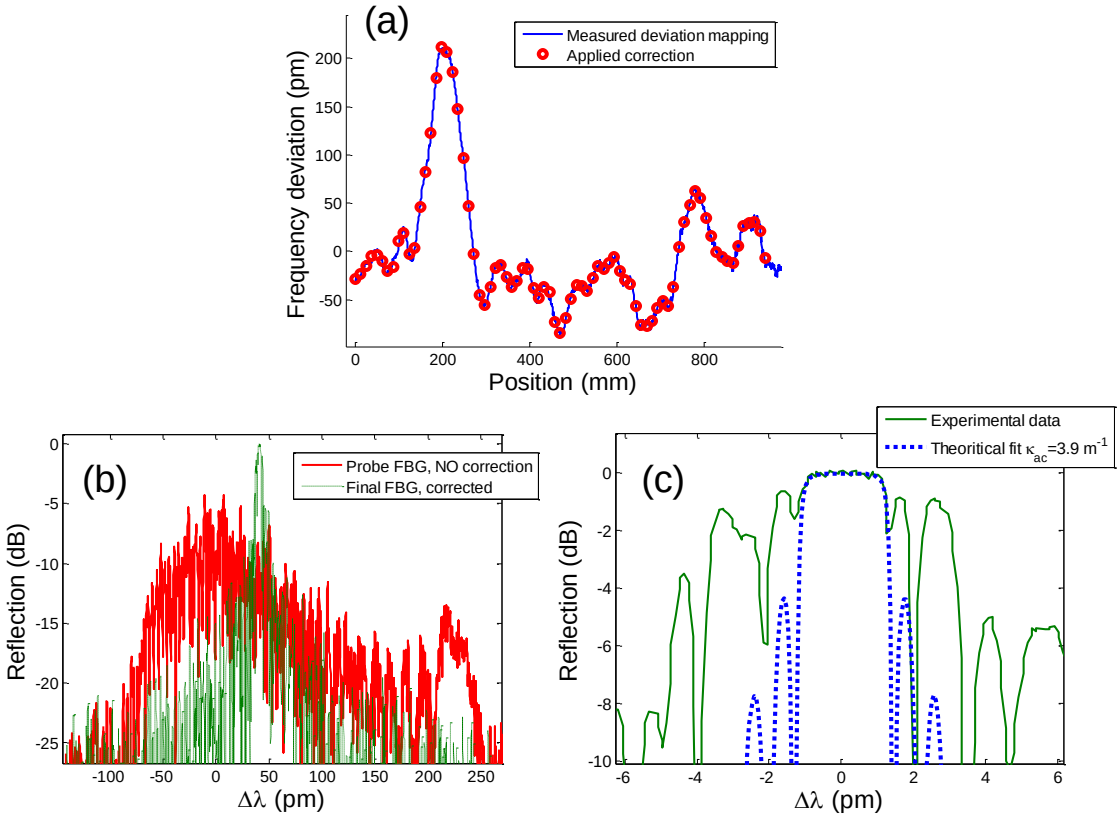

Figure 6.2 : Corrected 95 cm long uniform FBG fabricated in HNA1 fiber at 1555.3 nm. (a) Measured frequency deviation by OFDR from the average of the probe FBGs. (b) Comparison of one of the un-corrected probe FBG spectra with the corrected required FBG, a zoom of which is reproduced (c), along with the theoretically designed spectra.

High Ge content fibers typically have a weak birefringence, intrinsic to fabrication or induced by UV writing, which generates two Bragg resonances separated by ~5 pm for this fiber. Since the dual spectra could not be observed in the probe FBGs, as their bandwidths are >100 pm, the testing laser's polarisation could not be aligned with one of the axis during the frequency deviation characterisation. We believe this is the reason why the correction was not quite perfect and generated stronger side-lobes.

To achieve better results, a PM fiber was used. As in the first case, a 95 cm corrected FBG was written. This time, however, the polarisation of the OFDR laser was aligned along one of the axes of the PM fiber, as the resonances of the two polarisations could be easily distinguished in the probe FBGs' spectra. The average of the frequency deviation along the length as measured by the OFDR of the 3 probe FBGs is shown in Figure 6.3(a). The corresponding spectra of one of the probe FBGs is shown in Figure 6.3(b). As can be observed once again, the probe FBG spectra is of poor quality. By correcting the frequency deviation, we obtained the FBG shown in Figure 6.3(b) (in the background), a close-up of which is shown in Figure 6.3(c). As can be seen, this FBG is very close to a perfect theoretical FBG of 95 cm length over the full stop-band and the first side-lobes.

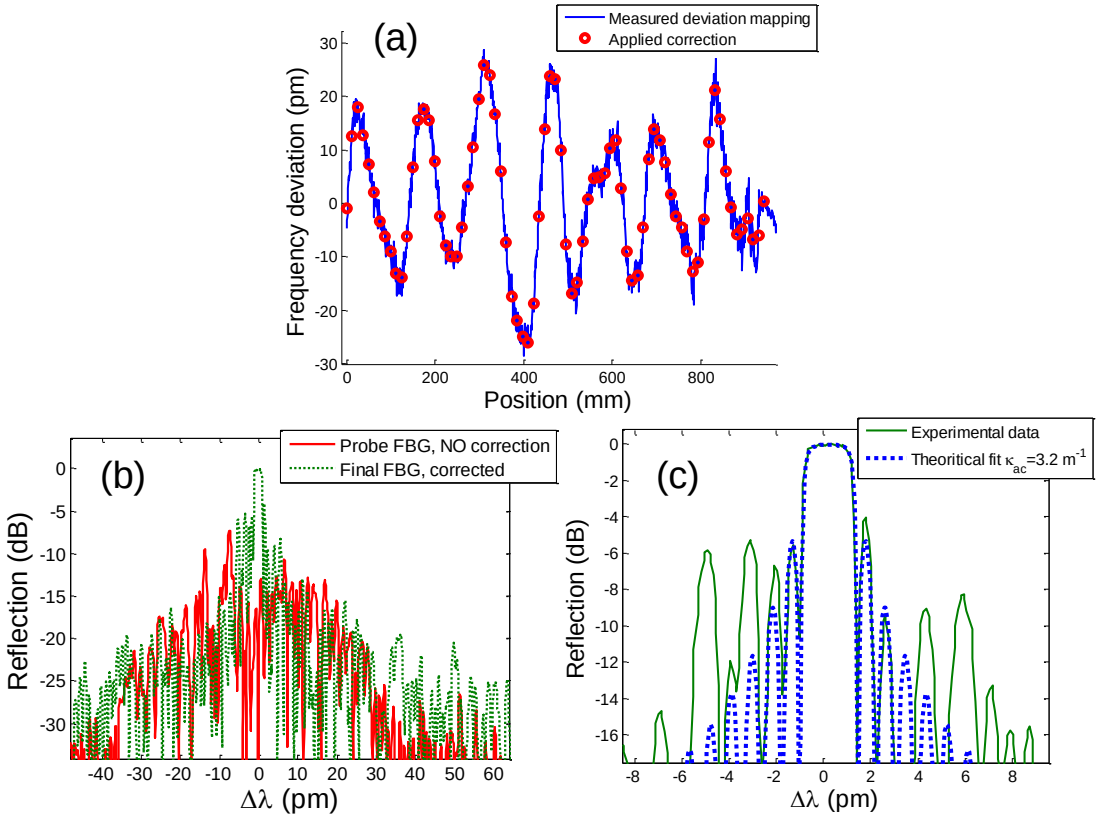

Figure 6.3: Corrected 95 cm long uniform FBG fabricated in PMHNA fiber at 1559.7 nm. (a) Measured frequency deviation by OFDR derived from the average of spectra of the 3 probe FBGs. (b) Comparison of one of the un-corrected probe FBG with the final corrected FBG which is reproduced and zoomed in (c) where it is compared with the theoretical spectra of a 95 cm long FBG.

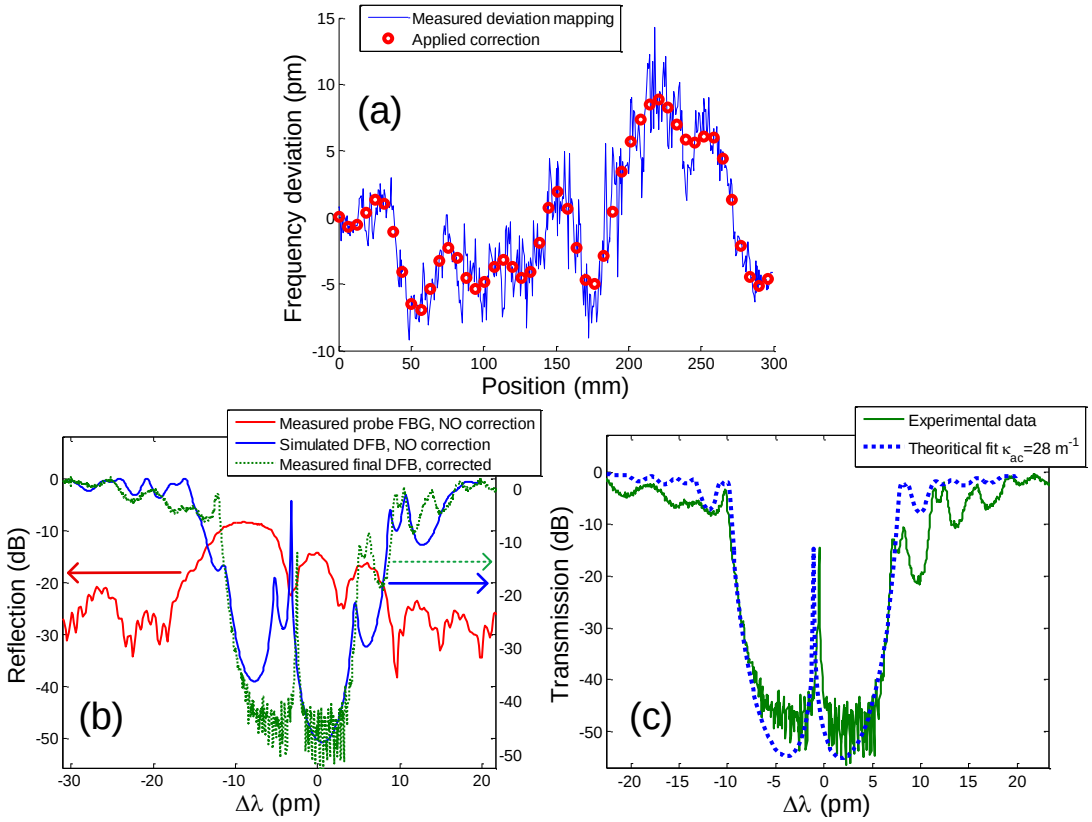

Figure 6.4: Corrected DFB FBG of 30 cm fabricated in HNA2 fiber at 1578.1 nm. (a) Measured frequency deviation with OBR from 3 probe FBG average. (b) Comparison of one of the un-corrected probe FBGs (in reflection) with the final corrected DFB (in transmission). A simulated DFB with its final κ_{ac} strength was calculated with the frequency deviation in (a) to show what the DFB would have looked like in transmission if not corrected. The final corrected DFB is reproduced in (c) where it is compared with a theoretically perfect DFB.

As near-perfect ultra-long uniform FBGs have been demonstrated with good reproducibility in difficult fibers, we now try to functionalize the FBG by adding a π-phase shift near the middle of the grating. The DFB-FBG tested here were shorter because they were designed according to our Raman generation test bench, which limited the length. Stronger versions (< -80 dB in transmission) required for lasers, not shown here as the features cannot be resolved due to lack of spectral resolution, showed significant improvement in single-mode performance at 1578 nm when pumped at 1480 nm, details of which will be published elsewhere in a near future. A weaker DFB (-55 dB in transmission) is shown in Figure 6.4 to demonstrate the effect of the correction on the

quality of the FBG. Figure 6.4(a) shows the measured frequency deviation of 3 probe FBGs and Figure 6.4(b) shows the corresponding reflection spectra of one the probe FBGs. Since we are interested here in a DFB grating for a laser application and since such FBGs are quite strong, transmission spectra are shown of the resulting corrected FBG in Figure 6.4(b)-(c). To appreciate the difference between un-corrected and corrected FBGs, a simulated transmission spectra of an un-corrected FBG is shown in Figure 6.4(b). This simulation is based on the frequency deviation measured in Figure 6.4(a). This simulated un-corrected DFB grating looses stop-band strength due to non-linearity and has multiple internal modes, which interfere with the desired π-shifted DFB mode. In contrast, the correction yields a theoretically near perfect DFB FBG, with a slight non-linear chirp generating asymmetric side-lobes, which do not compromise the functionality of this DFB.

6.4 Discussion

Despite the significant observed gain in FBG quality, we do still observe some imperfections, manifesting mainly in the appearance of side-lobes. This is likely due to noise and errors in the characterisation, as well as influence from environmental fluctuations during the final writing process. As birefringence is typical of any high Ge photosensitive non-PM fibers, a better characterisation of the frequency deviation performed along one of the UV induced, or intrinsic, principal axes is necessary, especially for FBG of length > 50 cm. A solution would be to make a second iteration in the characterisation using corrected probe FBGs aligned with the principal axis, after the initial coarse correction. The characterisation of the newly corrected probe FBGs will allow a finer correction for the final targeted FBG.

Typical FBGs of ~10 cm or less are not significantly affected by the fiber's n_{eff} fluctuations. For 20-30 cm FBGs the defects are not necessarily critical, but they do affect the reproducibility of high quality FBG's affecting overall yield. However, for 30 cm to 1 m ultra-long FBGs, these defects are quite critical, as shown in Figure 6.2(b) and Figure 6.3(b), as each fluctuation generates internal resonances and significantly enlarges the bandwidth.

It should be noted that ultra-long FBGs are extremely sensitive to the environment. Indeed, the spectrum can radically change (chirped, resonance modes) with the slightest bend or temperature gradient. Therefore, if the conditions change between the fiber characterisation and the application,

then the applied correction may not be adapted to the application and the FBG spectrum may be of poorer quality. To avoid this, the OFDR characterisation should take place with the probe FBGs in the operating conditions of the future desired FBG.

6.5 Conclusion

From our results, we can see a significant improvement in the spectral characteristics of ultra-long FBGs after correcting for intrinsic fiber non-uniformity. As can be seen from the frequency deviation measurements and from our previously reported measurements [144], optical fibers, especially specialty optical fibers, are surprisingly non-uniform, which makes it impossible to generate or replicate perfect ultra-long FBG without correction. This phase correction technique can be applied to any continuous writing scheme for ultra-long FBG, including femtosecond laser writing. The ultimate limitation of the corrected gratings length is currently seen to be from the temperature gradient across the grating during testing and fabrication. Although the correction does place an overhead on production since a prior characterisation must be performed, all the results of our correcting scheme show excellent reproducibility. The advantages of a near 100% yield in FBG production, perhaps outweighs this overhead. This solution therefore allows high quality functionalised long and ultra-long FBGs to be highly reproducible and therefore commercially viable. Also, instead of directly correcting FBG frequency, this technique could also be used to flatten fiber refractive index by controlled exposure.

6.6 Acknowledgement

The authors are grateful for funding of the research by Canada’s NSERC’s strategic research and the Discovery grants, and the Canada Research Chairs programs.

CHAPTER 7 ARTICLE 4: OPTIMIZATION AND REALIZATION OF PHASE-SHIFTED DISTRIBUTED FEEDBACK FIBER BRAGG GRATING RAMAN LASER

Authors: Sébastien Loranger, Amirhossein Tehranchi, Herbert Winful, Raman Kashyap

Submitted to: Optica

Single frequency laser sources have found a great number of applications, but are difficult to implement and suffer from poor robustness, quality (linewidth and stability) and are generally expensive to fabricate. One solution for a cheaper and simpler single-frequency source is a π-phase-shifted distributed feedback (DFB) fiber Bragg grating (FBG) based laser. Typically, such a laser usually uses a fiber with rare-earth dopants as an active medium to produce gain. However, its operating wavelength is limited to the emission bandwidth of the rare-earth-dopant in the fiber. A proposed solution to overcome this limitation is to use Raman gain. Raman DFB fiber lasers have been successfully demonstrated and a few simulations have been undertaken and reported. However, a thorough study of parameters and careful optimization has not been reported due to the long computation time and difficultly in the fabrication of long FBGs with known parameters. We demonstrate here, with the aid of a fast, but exact method, a detailed optimization study on phase-shifted Raman DFB fiber lasers. These theoretical results are compared with the experimental operation of many fabricated FBGs thanks to a newly developed fabrication technique for the replication of FBGs. We show that fabricated lasers have poor performance compared to simulations of ideal lasers. We also show that the difference in performance is due to the high internal optical intensity induced nonlinear thermal gradient along the FBG.

7.1 Introduction

Single frequency (SF) laser sources are in high demand for many applications, e.g., in coherent detection, interferometric systems, metrology, optical characterization systems, and so on. Typical SF solutions include amplified semiconductor DFB diodes lasers, which exhibit a relatively large linewidth, or costly and bulky external cavity lasers. The π-phase-shifted (PS) distributed feedback (DFB) fiber Bragg grating (FBG) has been known as a reliable single frequency laser (SF) source [117, 118]. However, the operation of π-PS-DFB fiber lasers has been mostly limited to the spectral

bands of rare-earth dopants. Access to any wavelength outside the rare-earth dopant's band, is possible using Raman gain in DFB fiber lasers, first proposed and simulated for uniform FBGs by Perlin and Winful [115]. π-PS DFBs were then proposed by Hu et. al., [112] where optimization was conducted in a small core photonic crystal fiber for long FBGs (20 cm). The first functional DFB using the Raman gain in fiber but with a very high threshold (40 W) at 1584 nm was realized by Westbrook *et. al.* [123] . It was then shown that small-core, high NA fiber was much better and could yield Watt-level thresholds [124, 125]. Shi *et. al.* demonstrated that using polarized pump and an ultra-long FBG (30 cm) a sub-Watt threshold could be achieved [127], at a lasing wavelength of 1120 nm. We have also recently demonstrated even lower thresholds at 1120 nm and 1178 nm [128]. Despite these developments, the performance in terms of slope efficiency has curiously remained poor (1% to 7% for single-sided output) compared to the expected simulated efficiencies (40-50%). Several hypotheses have been studied, such as phase noise [129] and other non-linear processes [130], without any completely successful explanation for the poor performance.

Whilst there are a few experimental works on such lasers [123-127], there is still a lack of investigation on the design of the phase-shift position and value, to optimize the laser performance and to explain the weak efficiency obtained in practice. This problem needs a rigorous solution of the coupled mode equations for Raman DFBs which is very demanding in calculation time, especially when solved in the time domain which may be why no profound study on Raman DFBs has been reported. Hence, we solved this problem by developing a fast method based on an approximation and iterative solution search, to accelerate the calculation and enable the study of many cases. The steady-state power distribution using the fast method agrees well with a more standard method and thus is used for a full study of all optimizable parameters in an ideal case. By modeling a thermal gradient, the prime suspect for the degraded slope efficiency, a full comparison of simulation is made with experimental data for the first time to the best of our knowledge. Thanks to the improvement in fabrication techniques, we have been able to produce a number of ultra-long PS-DFB-FBGs, with near perfect characteristics, thus enabling a good agreement between the experiment and theory.

7.2 Theory and simulation of ideal PS-DFB-FBGs

7.2.1 Simulation method

The coupled-mode equations that need to be solved in a PS-DFB-FBG system have been previously described in the time domain [112, 115]. To simplify calculations, we first consider the system to operate as continuous waves (CW) and in the steady-state, therefore any instability in simulation as observed in references [115] and [112] are neglected here. Such instabilities need to be verified experimentally, which we have not observed in our experiments. Using such an approximation, we can re-write the coupled-mode equations in the frequency domain, converting frequency (ω) to wavelength (λ) for calculation simplicity as:

$$\frac{dA_p(x)}{dx} = -\frac{g_p}{2}\left(\left|A_f\right|^2 + |A_b|^2\right)A_p - \frac{\alpha}{2}A_p + i\gamma_p\left(\left|A_p\right|^2 + 2\left|A_f\right|^2 + 2|A_b|^2\right)A_p \tag{7.1}$$

$$\frac{dA_f(x,\lambda)}{dx} = \frac{g_s}{2}\left|A_p\right|^2 A_f - \frac{\alpha}{2}A_f + i\kappa_{ac}A_b + i\left(\gamma_s\left(2\left|A_p\right|^2 + \left|A_f\right|^2 + 2|A_b|^2\right) + \frac{\Delta\beta}{2} - \frac{1}{2}\frac{d\phi}{dx}\right)A_f \tag{7.2}$$

$$-\frac{dA_b(x,\lambda)}{dx} = \frac{g_s}{2}\left|A_p\right|^2 A_f - \frac{\alpha}{2}A_f + i\kappa_{ac}A_b + i\left(\gamma_s\left(2\left|A_p\right|^2 + 2\left|A_f\right|^2 + |A_b|^2\right) + \frac{\Delta\beta}{2} - \frac{1}{2}\frac{d\phi}{dx}\right)A_f \tag{7.3}$$

where A_p, A_f and A_b are the pump, forward and backward field amplitudes, respectively, along the propagating x-axis and the latter two are functions of wavelength, λ. In this case, $\Delta\beta = 4\pi n/\lambda - 2\pi/\Lambda$, which represents the detuning from the Bragg wavelength, where Λ is the period of the FBG. g_p and g_s are the Raman gain coefficients for the pump and signal, respectively, and assumed as $g_s = g_p(\lambda_p/\lambda_s) = 0.7 \times 10\text{-}13$ m/W. γ_p and γ_s are the Kerr non-linearities also for the pump and signal, respectively, and considered as $\gamma_s = \gamma_p(\lambda_p/\lambda_s) = 2\pi n_2/\lambda_s$, with n2 = 3.2 × 10-20 m2/W. Power (in W) of pump and signals can be expressed as $P_i = |A_i|^2 A_{eff}$, where A_{eff} is the effective mode area estimated to be 12 μm^2 for small core (~4 μm mode field diameter) fibers. The loss, α, unless otherwise specified, is taken to be 0.03 dB/m as a conservative, yet realistic value for this

type of fiber in which an FBG is written. The coupling constant, κ_{ac} is varied during our optimization. The phase profile, $\phi(x)$ which is the phase of the periodic structure within the FBG, defines the PS-DFB nature of the FBG:

$$\phi(x) = \begin{cases} 0 & x < x_{shift} \\ \phi_{shift} & x \geq x_{shift} \end{cases} \tag{7.4}$$

where x_{shift} and ϕ_{shift} are the position and value of the phase shift, respectively. A standard PS-DFB would have $\phi_{shift} = \pi$. Later, we study the role of changing this value and show that it has a similar effect as enlarging the phase shifting region considered in a previous numerical study [112]. Both position and value parameters, as well as the coupling constant and grating length are investigated and optimized. The solved problem and relevant variables are schematized in Figure 7.1.

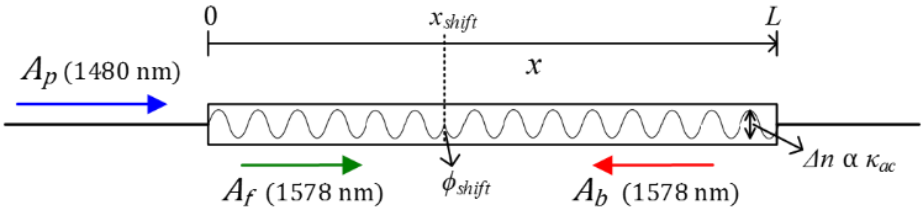

Figure 7.1: Schematic of a PS-DFB-FBG including the system variables.

The coupled-mode equations (7.1) to (7.3) were solved by an approximate iterative approach, which we will refer to as iterative approximated field fit (IAFF) for simplicity. Approximations of the signal fields A_f and A_b are used to solve the pump equation. Then, the pump as well as the approximations of signal fields are used to find a solution for the signal fields by the transfer matrix method, typically used in FBG simulation [15]. The initial approximation is then compared with the solution and a correction applied until a convergence is found. At each iteration, the transmission spectra $A_f(x = L, \lambda)/A_f(x = 0, \lambda)$ is calculated and the field solution is computed at the resonance mode, which moves in frequency due to non-linear effects. This IAFF method has the downside of only considering one lasing mode. At higher pump power, other lasing modes which may appear due to non-linearity, can start lasing as has been observed experimentally.

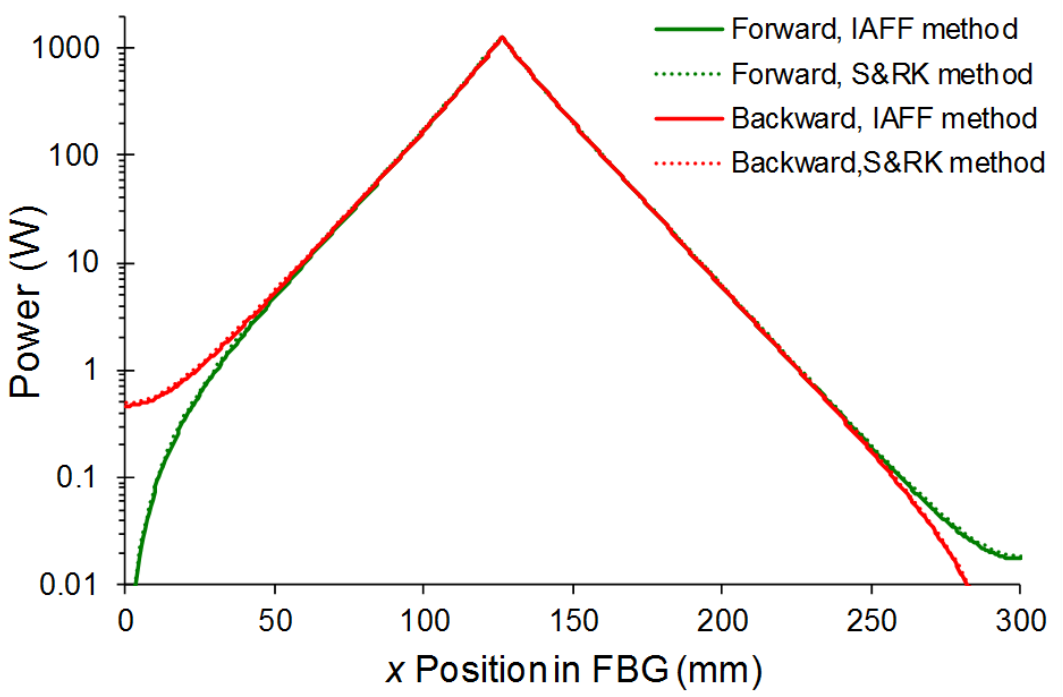

Figure 7.2: Power distributions along the PS-DFB-FBG for comparison of field calculation using two methods: iterative approximated field fit (IAFF) used in this paper as a fast method, and a differential equation solution based on shooting and Runge-Kutta (S & RK) algorithm as a standard method. The simulated grating is 300 mm long, with a κ_{ac} of 40 m^{-1}, a loss of 0.03 dB/m and a π-phase-shift at 126 mm (-24 mm off-center). The pump power is 3W.

To justify the use of the IAFF method, power distributions in a π-PS-DFB calculated by it as well as by a fully resolved method utilizing both shooting and Runge-Kutta (S & RK) algorithms are compared as shown in Figure 7.2. As can be seen, the solutions for both methods match within the error criteria chosen for convergence. This IAFF method allows a solution to be found in a few minutes on a standard computer, the limiting step being the spectral (λ) scan to find the DFB mode at each iteration. By parallel processing, the IAFF method allows for a complete study on a single parameter (e.g., 10 cases of x_{shift}, each with 20 solutions at different pumps from 0.1 to 10 W) in ~2 hours, whilst the S & RK method requires ~ 2 weeks of continuous computing.

7.2.2 Optimization results of ideal PS-DFB-FBGs

Using this approximated approach, we have optimized the design of an ideal PS-DFB-FBG. During optimization, the two figures of merit to observe are threshold pump power and slope efficiency.

The threshold power is the most variable parameter and the most limiting for applications, while the weak efficiency can be compensated for by amplification if higher power is needed. When optimizing the threshold, the most limiting characteristic of the FBG is its overall strength, i.e., the product of the coupling constant and length, $\kappa_{ac}L$. The threshold is known to increase exponentially with a reduction in this product. Long (L > 100 mm) and ultra-long (L > 200 mm, above the typical length limit of phase masks) FBGs have two advantages: the requirements of κ_{ac} is reduced and the longer lengths increase the time-of-flight of photons, (and thus the lifetime), lowering the threshold for a constant $\kappa_{ac}L$, as can be seen in Figure 7.3(a) for different losses.

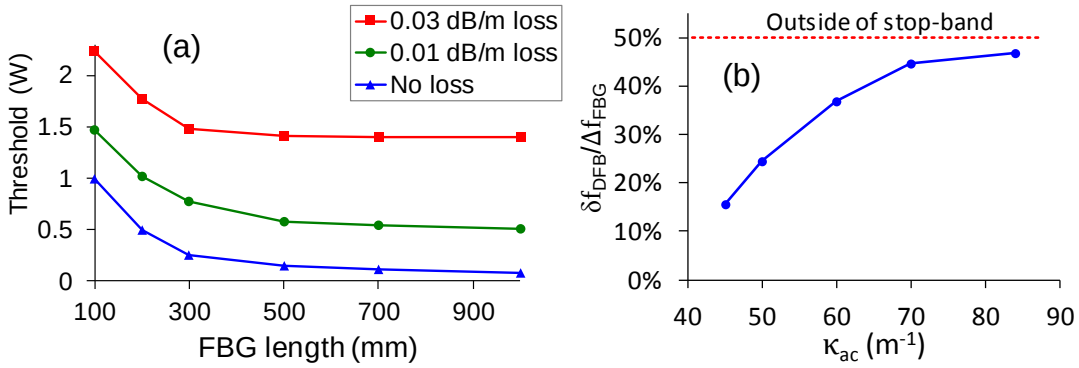

Figure 7.3: Justification for the choice of PS-DFB-FBG length and strength. (a) The threshold power is shown versus FBG length for a constant $\kappa_{ac}L = 12$. (b) A limitation from non-linearity is shown as the strength of FBG is increased for a constant pump power (8.8 W): the DFB mode displacement (δf_{DFB}) is tuned towards the outside of the stop-band bandwidth (Δf_{DFB}). All FBGs simulated here have a π-phase-shift at -5% of the length away from the center. The FBGs in (b) are 200 mm long.

However, there are limitations in terms of length and overall FBG strength. Firstly, FBGs over 500 mm are difficult to fabricate while maintaining the quality and reproducibility needed due to their sensitivity to environmental fluctuations. Secondly, if such FBGs are fabricated, their operation is difficult for the same reasons: they must be maintained perfectly uniform in temperature and in strain along their entire length. The third reason is the Kerr non-linearity due to the high optical intensity within the PS-DFB-FBG: the induced non-linear phase-shift detunes the DFB mode towards outside of the stop-band, as shown in Figure 7.3(b). When the mode approaches the side of the FBG stop-band, it may become unstable or other modes from higher order chirp will start lasing as was observed experimentally [128]. Considering these limitations and the fact that there

is little advantage in increasing the length beyond 500 mm, as shown in Figure 7.3(a), especially for typical fiber losses, an optimal length of Raman DFB-FBG would be around 300-400 mm. From our simulation, we have found that an optimal $\kappa_{ac}L$ product is between 10 and 15, beyond which there is little advantage in terms of threshold, while potential non-linear complications may occur.

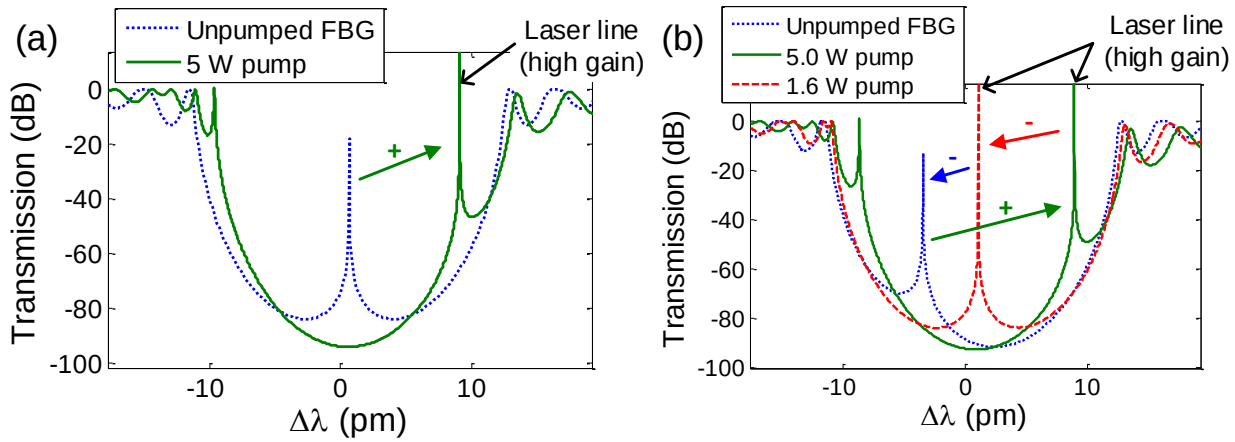

Figure 7.4: The effect of non-linearity on the DFB mode. The DFB mode is detuned (red-shifted) toward the edge of the stop band as power inside the FBG is increased. Case of (a) a π-PS FBG and (b) a 0.75π-PS FBG. The lasing lines are represented by high gain lines (gain as seen by the input seed). The arrows with + and – signs on top show a red- and blue-shift of the lines with increase and decrease of power, respectively. FBGs are 300 mm long with a centered phase shift. κ_{ac} is 40 m^{-1} and the loss is 0.03 dB/m.

The non-linear mode detuning mentioned earlier is an important effect in Raman DFBs which has many consequences on its operation. This detuning is shown in Figure 7.4. As can be seen in the simple π-PS case in Figure 7.4(a), for a 5-W pump power, the spatially non-uniform Stokes field generates a non-linear phase shift resulting from the γ terms in eqs. (7.2)-(7.3). This phase shift effectively pushes the mode outside of the stop-band, thus the quality factor of the cavity is reduced, and in turn the threshold increases until an equilibrium is reached (typically known as push-broom effect [132]). However, the non-linear chirp caused by this phase variation also enables higher-order side-band modes to appear in the stop-band from the other side, which we believe is the source of multi-mode operation at high pump powers. To get an idea of the Kerr nonlinearity induced phase change inside the FBG in this case, the peak of the fields (shaped as shown in Figure 7.2) would yield an equivalent refractive index change of 1×10^{-5} refractive index units

(RIU), or equivalent to ~1.1 °C increase in temperature (values at the peak of the variation, which is located at the phase shift, considering a thermo-optic coefficient of 9×10^{-6} RIU/°C [15]).

To compensate for this non-linear phase detuning, we propose to reduce the initial phase-shift written in the FBG. This effectively detunes the DFB mode to shorter wavelengths inside the stop-band, as shown in Figure 7.4(b). Although this increases the threshold as the initial Q-factor of the cavity is reduced, once the DFB is lasing, the output power is increased by a small amount. An interesting effect of this configuration is the appearance of hysteresis between the activation and shut-down state, as the mode will stop lasing only when it reaches the center of the stop band and the push-pull effect is no longer in equilibrium. The figures of merit of a PS-DFB-FBG versus a reduced inscribed phase shift is shown in Figure 7.5(a). As expected from such a design, the efficiency is increased, but at the cost of a higher activation threshold. However, the shut-down threshold remains quite stable, hence the appearance of a hysteresis. An example of this activation/shut-down hysteresis is illustrated in Figure 7.5(b) where one can find a 1.75 W difference between the two thresholds. In this simulation, when increasing power, the initial field approximation at each power level was taken as low intensity (then increases until solution is reached). When decreasing power (from 5W), the initial field approximation was rather taken as high intensity (decreased slowly towards the solution).

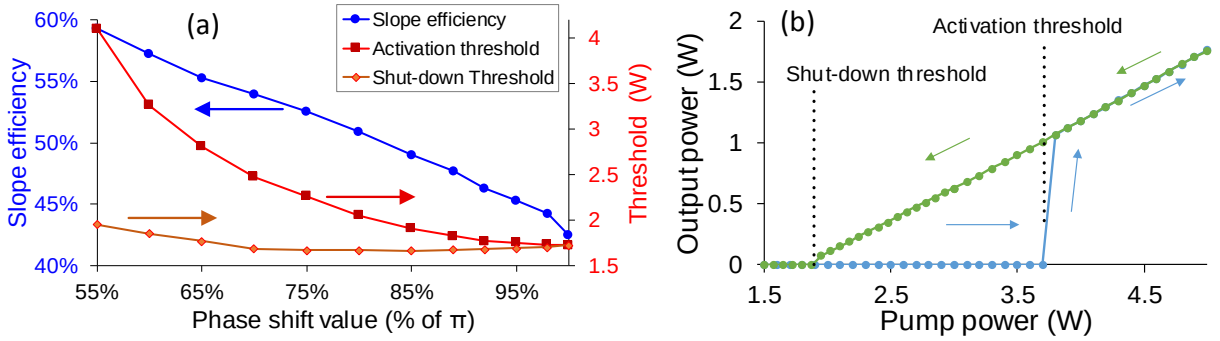

Figure 7.5: Effect of phase-shift value. (a) The activation threshold (when increasing the pump from 0 W initially), shut-down threshold (when decreasing the pump after achieving lasing state) and slope efficiency are shown with varying phase-shift values (b) An example of activation/shut-down hysteresis is shown with a phase shift of 0.6π. FBGs are 300 mm long with a phase shift at -8% from center. κ_{ac} is 40 m-1 and the loss is 0.03 dB/m.

From this result, an optimized value of phase shift can be considered depending on the available pump power to start-up the laser. Such optimization is shown in Figure 7.6(a), where an increase of 32 % in output power is calculated by reducing the phase shift to 0.6π for a pump power of 3.5 W.

Another parameter to be optimized is the position of the phase shift. It is well known that to have a preferential output direction (co- or counter-propagating to the pump), the phase shift should be displaced from the center towards the intended output port. Typically, an output counter-propagating to the pump is preferred as it is easier to separate pump and signal. Displacing the phase-shift from the center increases this preferential output's slope efficiency. However, since this effectively reduces the reflection on one side of the DFB defect (reduced length), this reduces the Q-factor, and therefore increases the threshold. From these two competing effects, an optimal phase-shift position can be calculated depending on the pump power and the FBG strength, as shown in Figure 7.6(b). Although the length and FBG strength can be easily chosen by the above criteria, the optimal design of the phase shift is a function of the available pump power.

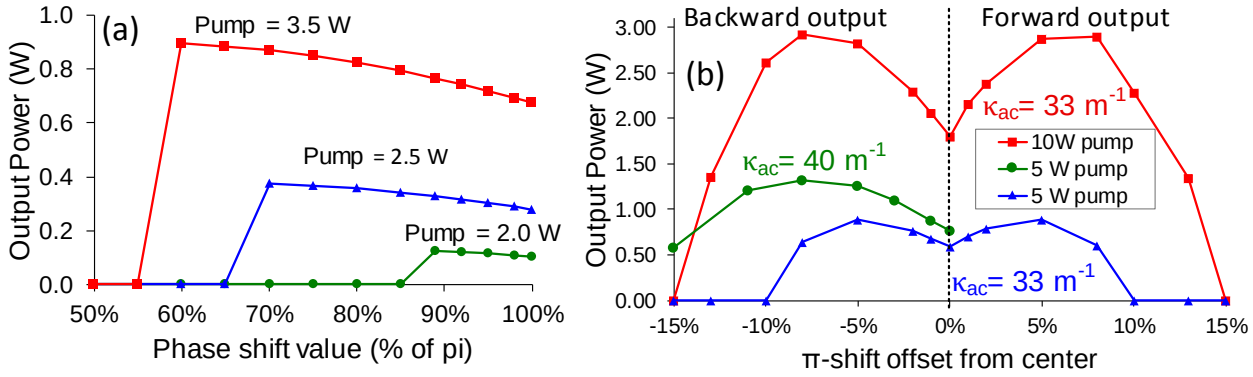

Figure 7.6: Optimization of phase shift (a) values and (b) positions at different pump levels. The optimization in (a) considers activation threshold. FBGs are 300 mm long. Phase shift is at -8% from center and κ_{ac} is 40 m-1 in (a). The loss is 0.03 dB/m.

7.3 Fabrication and characterization

While this optimization study has led to a better understanding of Raman DFB fiber lasers, it remains that the experimental results on such lasers generally show poor slope efficiency. To further understand their behavior, we have fabricated many PS DFB-FBGs to compare the experimental data with the theoretical results. The FBGs were fabricated using a continuous writing

scheme with a Talbot interferometer and phase modulators as described by Gagne et al. [11], as shown in Figure 7.7(a). For the UV exposure, a 4th harmonic Q-switched Nd:YAG laser operating at a wavelength of 266 nm was used and the fibers were deuterium loaded to reduce the required power and avoid local heating during writing. The fiber used was a high Ge SM1500 high NA (0.3) from Fibercore, with a small core (4 µm mode field diameter). After writing, the fiber was heated at 70°C for 3 days for outgassing. A phase correction technique [136] was used to correct for fiber non-uniformities [144] and ensure reproducibility of the FBGs. FBGs were written for a Bragg wavelength of 1578 nm and pumped at 1480 nm.

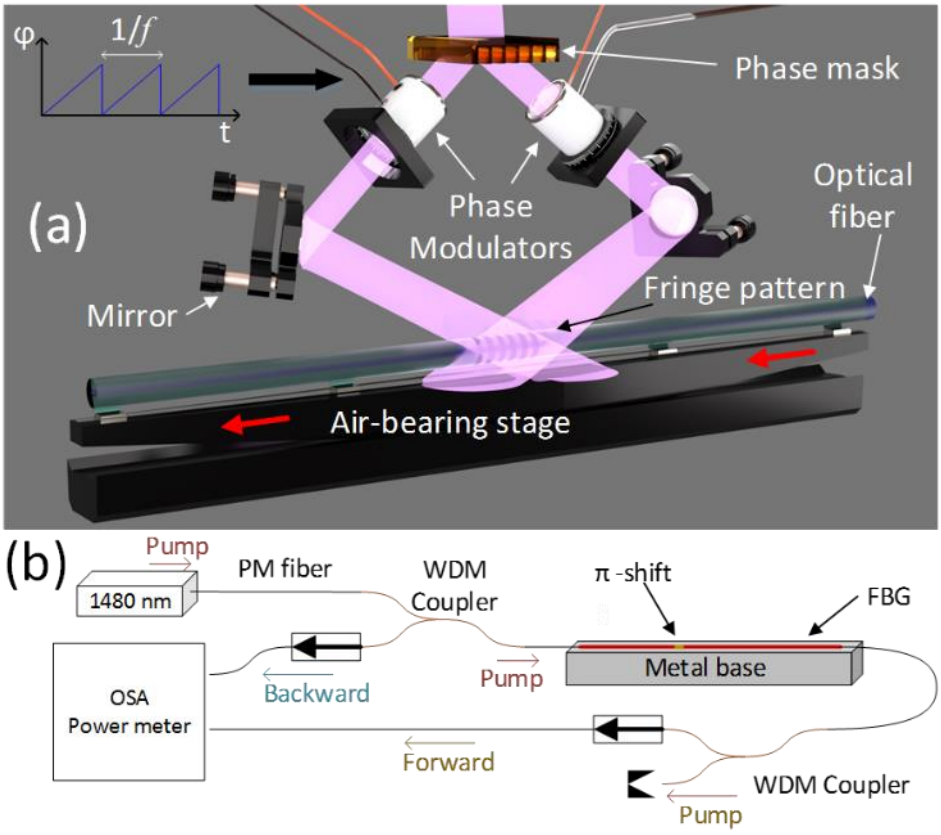

Figure 7.7 : (a) Schematic of the fabrication system using a Talbot interferometer and moving fiber, (b) PS-DFB-FBG laser implementation with a 1480 nm pump. The FBG is placed on a cooled-down metal groove immersed in glycerin.

To ensure thermal uniformity during operation, the DFB lasers were placed in a 270 mm long glycerin groove in a thick aluminum base. The base was cooled and isolated from ambient air. Because of the limited length of our current base, the tested FBGs were 250 mm long. The experimental setup for laser operation is shown in Figure 7.7(b).

Despite the effort to stabilize the FBGs, a low slope efficiency was measured for all lasers comparable to those reported in the literature, as shown in Figure 7.8(a). The prime suspect for this is the thermal gradient induced by part absorption of the high optical power at the PS, proposed by Abedin et al. [131] and the authors [134], in the study of DFB FBG Brillouin fiber lasers. To explore this phenomenon, the FBGs were placed on different bases with different thermal conductivities. A radical decrease in the efficiency was observed when using less thermally conducting bases, confirming the suspicion. Despite the lower efficiency, the threshold does not change.

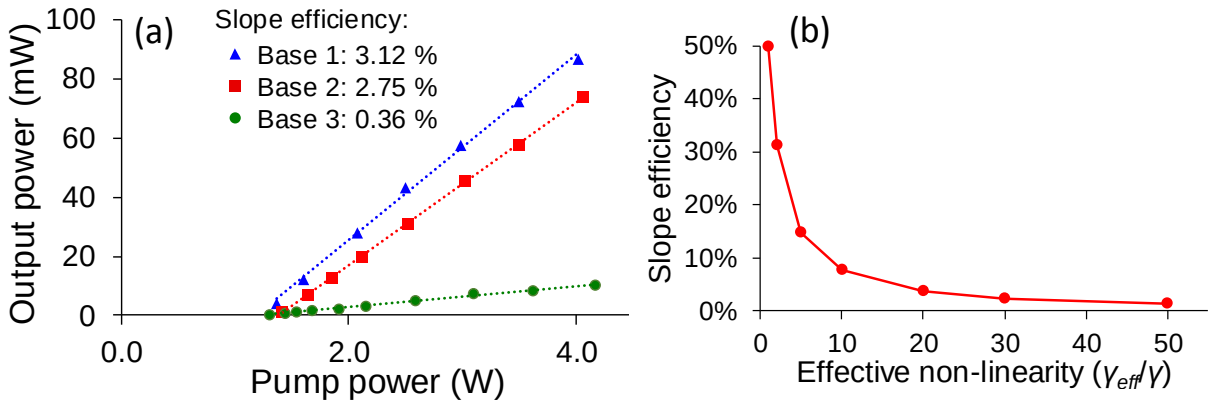

Figure 7.8: Output power characterization of a 250 mm long π-PS fabricated FBG considering different bases for thermal management. Base 1 is a thick metal cooled plate (at 10°C) in which the fiber is placed in a 1 mm wide grove covered in glycerin. Base 2 is a thin metal plate in which the fiber is placed bare on the surface (no grove or glycerin). Base 3 is a thin plastic base in which the fiber is also placed bare on the surface. (b) Simulation of efficiency versus effective non-linearity ratio due to thermal gradient from non-uniform field for 300 mm, π-PS at -8% from center and 40 m-1 FBGs.

We, therefore modeled the thermal gradient, considering that a temperature variation will lead to an increase in refractive index (as is the case in silica fiber), thus a linear increase in phase. By approximating heating as being linear with local intensity, and by neglecting the difference between self-phase and cross-phase modulation in Eqs. (7.2)-(7.3), we increased the non-linear term by a certain factor to represent the contribution due to heating as:

$$\gamma \rightarrow \gamma_{eff} = \gamma + \frac{\partial \beta}{\partial T}\frac{\partial T}{\partial I} \tag{7.5}$$

where β is the propagation constant, T the temperature and $I = |A|^2$, the optical intensity of the lasing mode. The effect of an increased non-linear term is calculated and shown in Figure 7.8(b). As can be seen, an increase in non-linearity can decrease the slope efficiency by an order of magnitude. Based on our observed slope efficiencies, we estimate an effective non-linear term to be ~35 times that of the Kerr coefficient. Considering the known thermo-optic coefficient (9×10^{-6} RIU/°C [15]), this would give a temperature increase of ~10 mK/W. Considering that in such highly non-linear FBGs the internal total peak power is reduced to 100-300 W, then the peak temperature rise at the fiber core would be in the order of 1-2°C. The heating, due to absorption loss from the high intensity within the DFB cavity, the heat generated through the quantum defect and the limit in the thermal conductivity making this gradient uniform, is therefore the main cause limiting the operation of the Raman DFB fiber laser. Figure 7.9 is an observed example of hysteresis with a reduced phase shift, as predicted by theory. It shows activation/shut-down thresholds of 1.5/3.6 W and a slope efficiency of 2.75% by decreasing the pump power toward the shutdown.

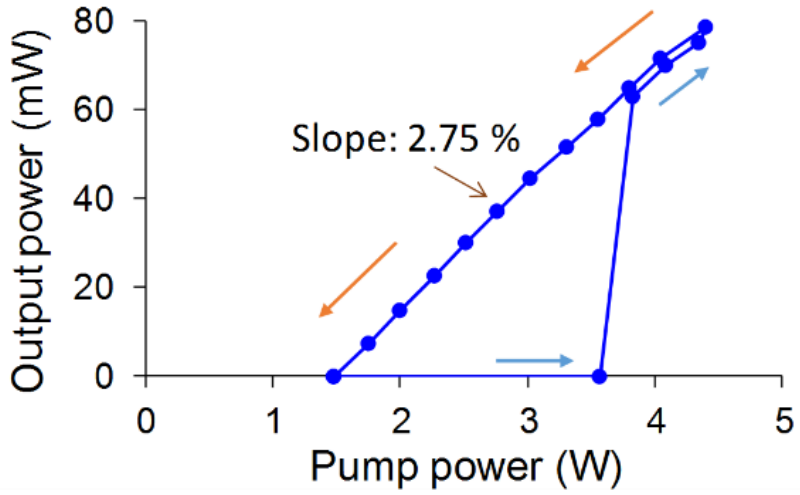

Figure 7.9: A 0.7π phase-shifted FBG on base 1 where the output power shows hysteresis of activation/shutdown. This 250 mm long FBG has its phase shift placed at -20 mm from center with a κ_{ac} of ~ 70 m-1.

Further study of parameters was therefore undertaken and the experimental results are compared to the simulation with the higher non-linearity induced from heating. Figure 7.10 illustrate the experimental and theoretical results including variation in the threshold and slope efficiency,

respectively by moving the phase shift position off-center by up to 20% of the FBG length. It can be noted that the coupling constant of the fabricated FBGs is higher than the optimally targeted value. We have tried multiple strength levels (κ_{ac}) and this one allowed the FBGs to operate within the power available from our pump laser. We believe this is due to high loss in our fibers, as no effort (avoiding deuterium loading and optimizing annealing) was yet made to reduce it. Despite this, we see a good fit of our theoretical results to the experimental values.

The saturation of the threshold in Figure 7.10(a) is due to the large $\kappa_{ac}L$ of our fabricated grating. Normally, as predicted by theory, the threshold should increase as the phase shift is moved off center, due to the reduction in the effective $\kappa_{ac}L$ on the shorter side of the phase-shift. However, for our fabricated FBGs at high κ_{ac}, the threshold is mainly limited by loss, and not much from FBG strength $\kappa_{ac}L$, hence why there is little change in the threshold in Figure 7.10(a). Interestingly, as can be seen in Figure 7.10(b), the slope efficiency seems to saturate when the phase shift position is off-center. This was also observed in other simulations with a more optimal $\kappa_{ac}L$ value of 12, therefore this saturation seems to be an effect of the high effective non-linearity. This would indicate that phase shift position optimization is of little use when a high non-linearity is present.

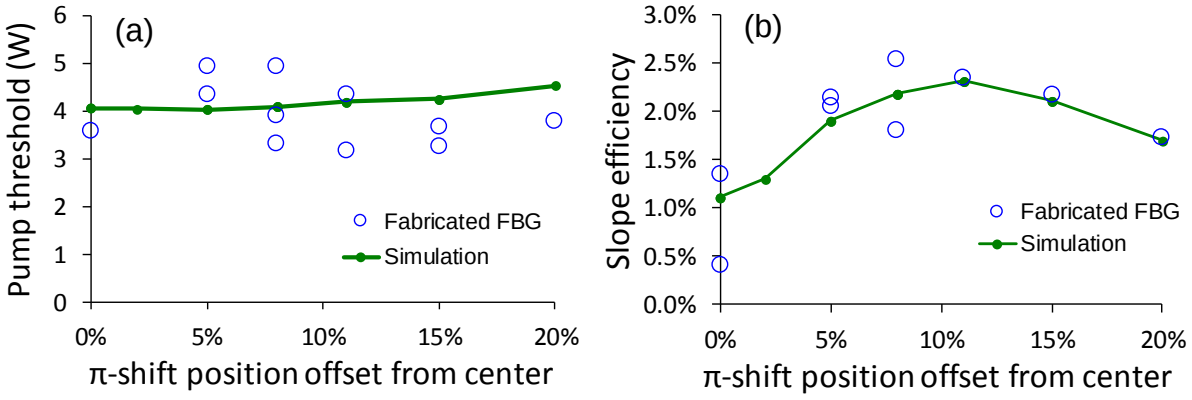

Figure 7.10: Comparison of measurement and simulation results for series of fabricated FBGs using a large γ_{eff} (=35γ). (a) Pump power threshold and (b) slope efficiency of output power with phase-shift position. The theoretical results are fitted to the experimental data using a loss of 0.1 dB/m and a coupling constant of 70 m-1. All FBGs are 250 mm, the current length limit of our temperature controlled base.

7.4 Conclusion

We have demonstrated a fast method for resolving the mode in Raman DFB fiber lasers which has allowed a vast optimization study of all relevant parameters when supposing single-mode operation. We conclude that such a laser should have an optimal length of 300 to 400 mm for threshold minimization, as longer lengths make fabrication and handling more complicated. $\kappa_{ac}L$ should be above 10, to ensure < 5 W threshold, but should not exceed a value of 15, as there is little improvement in threshold above this level (it is rather limited by loss) and non-linear effects become more important. Sub-watt threshold are possible for low-loss fiber and $\kappa_{ac}L{\sim}12$ or higher. The phase shift value can be reduced to pre-compensate the Kerr effect phase shift and slightly increase the output power at the expense of a higher activation threshold. For a given available pump power, there is an optimal phase shift value. The same applies for the phase shift position: moving it towards one end of the FBG increases the single-sided output slope efficiency, but increases the threshold. Hence, for a given pump, there is an optimal phase shift position.

The optimization was performed for the ideal case in which there is no thermal gradient in the FBG. We have shown experimentally and confirmed by the simulation, that a thermal gradient is likely the main cause for low slope efficiencies in fabricated Raman DFB fiber lasers. As this heating is due to absorption of the intense optical intensity of the non-uniform fields in the FBG, an effect analogous to the Kerr non-linearity, an increase of the non-linear term allows the theoretical results to be fitted quite well with the experimental data. The quantum defect also has an important heating effect, analog to absorption losses, which cannot be minimized as it is material dependent (the Raman Stokes shift). Due to the thermal effect, our fabricated series of FBGs could not demonstrate the optimization of the ideal case, but did show a reasonable fit with the model when using a high “effective” non-linearity to include the thermal term, and good agreement with the experimental data. We therefore conclude that in order to achieve ideal operation with an optimized FBG design, the thermal gradient must be managed efficiently. This can be done by reducing absorption loss and by increasing the thermal conductivity along the FBG length. An alternative would be to engineer glass to achieve a low-negative thermal coefficient to compensate for the Kerr and thermally induced phase increase

7.5 Acknowledgement

We acknowledge Canada's Research Chair program of the Govt. of Canada, as well as the National Science and Engineering Research Council scholarship and Strategic grants programs.

CHAPTER 8 GENERAL DISCUSSION

In this chapter, the overall results of this thesis are discussed in two parts: first one will concentrate on FBG writing, identifying all the problems found during my PhD (first objective) and laying out the proposed solutions that were found (second objective). The second part, focuses on the discussion on Brillouin and Raman gain DFB lasers (Brillouin and Raman pump), which address the 3rd and 4th objectives in this thesis.

8.1 Optimizing ultra-long FBG writing

Ultra-long FBGs are notoriously difficult to fabricate. The main reason why this is the case is that a simple imperfection in the order of half micron can render an entire 1-m long FBG useless. Ultra-long FBGs have the particular characteristic of an ultra-narrow bandwidth, as shown in Figure 8.1, an attractive feature for many applications. However, this feature also makes them very sensitive to imperfection. Indeed, refractive index variation, as described in article 2, causes wavelength deviation in the order of tens of pm in the C-band. Also, temperature is known to shift the Bragg wavelength at a rate of ~10 pm/°C in the C-band. A few grams force on a meter of fiber can induce several μ-strain units, inducing a few-picometer shift in the Bragg wavelength. Table 8.1 shows a summary of all the problems found during the course of this study, to which various solutions were implemented. Each will be discussed in this section.

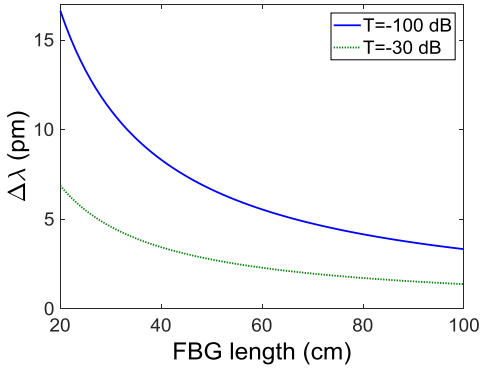

Figure 8.1: Bandwidth (between first zeros) of a uniform FBG along with length

Considering these limitations, a very good control on the fabrication method is required to avoid any defects. There are 3 types of defects which can affect the FBG: phase-shifts, low frequency phase variation (non-linear chirp), high frequency phase noise. The first two will mostly affect the

stop-band by deforming it and/or adding internal oscillating modes. High-frequency noise will mostly affect the side-modes, limiting apodization.

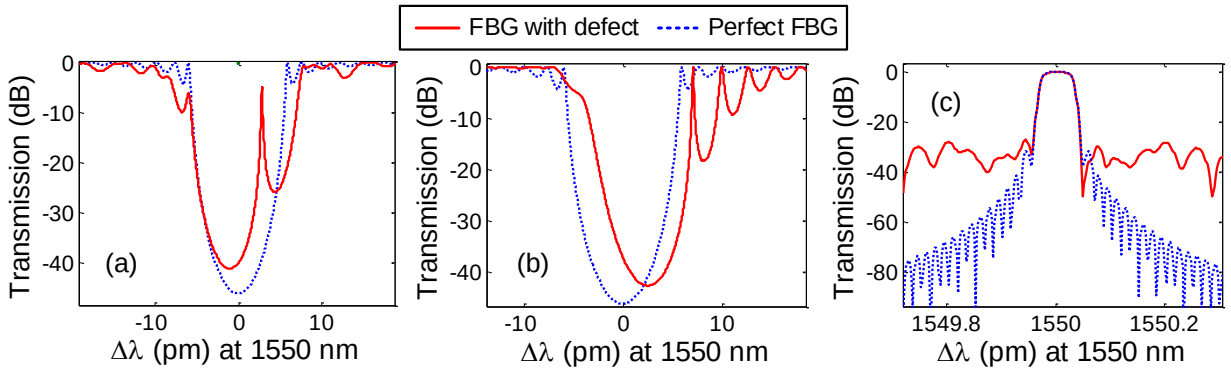

Figure 8.2: Example of the 3 main defects in FBGs: (a) phase shifts (0.6 and -2 rad at 2 locations in a 300 mm FBG), (b) slow wavelength variation (10 pm quadratic chirp on a 300 mm FBG) and (c) high frequency random phase noise (0.3 rad amplitude, 100 µm spatial variation, on a 10 mm cosine squared apodized FBG.

The first type of defect is caused by position error on the stage or phase error from the Talbot driving system (modulator or piezo). Such phase-shift errors cause modes to appear in the stop-band and would most likely render the intended FBG useless, as shown in Figure 8.2(a) and represented by the notation (a) in Table 8.1. The second type of defect is cause by a slow variation in the phase (cm-scale), inducing (by a derivative) a slow variation in wavelength. If that wavelength variation is of the order of the FBG bandwidth, it will significantly deform the stop-band, enlarging it and/or add internal modes, as shown in Figure 8.2(b) and represented by the notation (b) in Table 8.1. Any external factor which can affect the wavelength can be a cause for this, including fiber non-uniformity or temperature. The third defect is high frequency phase noise, appearing on the scale of mm or below. Such high frequency noise generates Bragg resonance component far away from the main resonance of the stop-band, and therefore affects the side-lobes. For a uniform FBG, phase noise will have little effect apart from randomizing slightly the position of side-lobes. However, for an apodized FBG, these high-frequency components become the noise floor for the side-lobes, as shown in Figure 8.2(c) and represented by the notation (c) in Table 8.1. The cause of each of these defects is described in the following paragraphs. Apart from fabrication defects, there are also equipment/experimental limitation from which the ideal FBG construction model is not met, which are represented by the notation (d) in Table 8.1.

Table 8.1: Summary of all issues found for continuous writing and their found/proposed solutions. The defects formed are (a) phase-shifts, (b) high frequency phase noise and (c) non-linear chirp (low frequency phase variation) and (d) represent limitations of the system.

Type of system	**Problem**	**Cause**	**Solution (or partial solution)**
Piezo	High phase noise (b)	Limited driving frequency	None (intrinsic to the use of a piezo)
	Non-linear apodization (d)		
	Limited speed (d)		
Modulator	Uncertain phase-shifts (a)	No closed-loop feedback on phase	λ_B shifts from speed variation
	Sensitive to temperature variation (c)		Install feedback system (direct or indirect) Fast writing, limit temperature variation
Both	Phase error from stage (momentary loss of feedback) (a)	Shock on table	Avoid vibrations on optical tables
	Phase noise from external vibration, power fluctuation, air current and stage feedback (b)	Equipment/ environment limitations	Faster power stabilisation feedback loop (for power) Enlarge beam size (compromise with below)
	Fiber position variation (c)		Ensure flatness over entire meter (fine adjustment) and put under strain
	Alignment variation from temperature variation (c)		Fast writing, limit temperature variation
	Strain variation from fiber slipping in clamps (c)		Use high retention clamps
	n_{eff} variation (non-uniformity) (c)	Fiber imperfection	OFDR measurement of probe FBGs and phase compensation for final FBG
	Limited tuning range (d)	Physical limitation	Reduce beam size (compromise with above)

Let us first compare the advantages and problem related to the use of electro-optic modulators or piezoelectric element to drive the fringe pattern's position. A few experimental limitations can be stated for a piezo driven system: limitation in speed (not practical for ultra-long FBG) and

imperfect apodization. These issues, as discussed in previous chapters, are caused by mechanical inertia of the piezoelectric element limiting the driving frequency. Also, due to the mechanically induced vibration from the piezo as well as the imperfect folding saw-tooth function, the written FBG has a large amplitude of high frequency phase noise, which limits the potential side-lobe reduction from apodization. This difference in phase noise can be observed in Figure 8.3 where apodized FBGs are compared using the piezo and modulator systems. Such limitations are resolved by using phase modulators instead to enable high-frequency drive and eliminate any additional source of vibration.

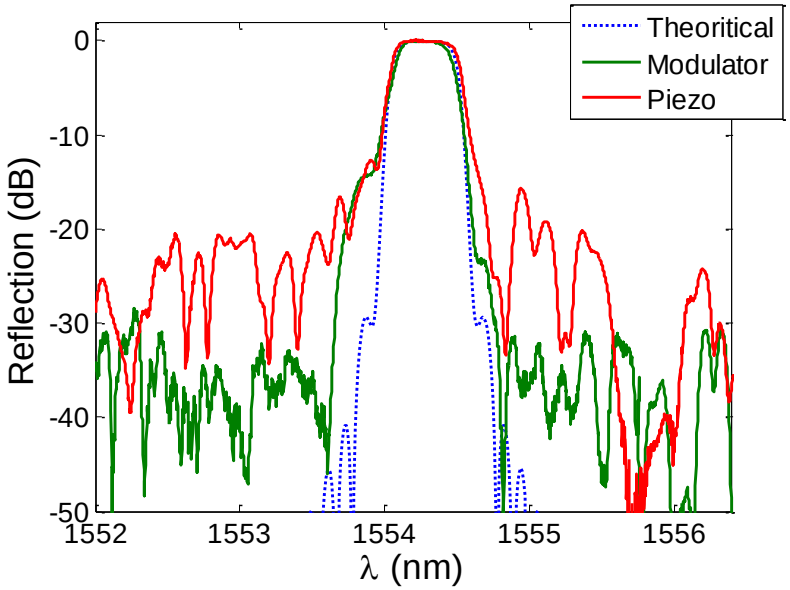

Figure 8.3: Fully apodized FBG spectra (cosine square, 7 mm) for a piezo written and a modulator written FBG.

However, modulators also have some issues of their own, which were discovered during this research. Those limitations have a common technical cause: the absence of feedback on the phase. Indeed, for a fixed applied voltage, the actual phase change induced by the Pockels cell may change. The total phase variation between the two branches of the Talbot interferometer, if two inverted phase modulators are used, can be described by the following equation:

$$\Delta\phi = 2\frac{\pi LV}{\lambda_{UV} w} n_o^3 r_{22} = 2\pi b \tag{8.1}$$

Where L is the length of the crystal, V the applied voltage, w the width of the crystal and the distance between the electrodes, n_o the ordinary refractive index, r_{22} the electro-optic coefficient. b represents the ratio $V/V_{2\pi}$ where $V_{2\pi}$ is the voltage required to induce a 2π phase shift. The crystal is affected by environmental conditions and this 2π voltage can change slightly during operation due to temperature (environmental and uv beam induced heating) and charge accumulation from a high DC field. The relation of temperature dependence is as follow:

$$\frac{d\Delta\phi}{dT} = 2\frac{\pi V L n_o^2}{\lambda_{UV} w}\left(3r_{22}\frac{dn_o}{dT} + n_o\frac{dr_{22}}{dT}\right) \tag{8.2}$$

In the last equation, the temperature dependence of the electro-optic coefficient is negligible compared to the thermo-optic coefficient of BBO. As for thermal expansion on the crystal dimension, they cancel out between length L and width w. Therefore equation (8.2) can be simplified to:

$$\frac{d\Delta\phi}{dT} \approx 6\Delta\phi\frac{1}{n_o}\frac{dn_o}{dT} \tag{8.3}$$

This dependence on the environment can induce both a low frequency phase variation (non-linear chirp) or a phase error when a DC voltage is applied to induce a phase shift. Both of these cases were observed experimentally. The latter case is the reason why the phase-shift of DFB FBGs was not reproducible from one hour to another. The solution to this problem, as detailed in article 1, was to induce a phase shift in a different way: by inducing a short wavelength shift. Although this solved the issue of reproducible phase shift, the modulators can still produce non-linear chirp through temperature fluctuation. This can be seen by deriving a wavelength variation as a function of applied voltage from equation (2.37), in the ideal case where the aimed value of b is M (integer number of periods):

$$\Delta\lambda_B = \frac{2\lambda_{B0}}{M}\Delta b \tag{8.4}$$

Where λ_{B0} is the central wavelength defined by the Talbot interferometer. By using equation (8.1) and (8.3) in equation (8.4), while studying a full phase shift $\Delta\phi$ of $2\pi M$, we have:

$$\frac{d\Delta\lambda_B}{dT} = \frac{12\lambda_{B0}}{n_o}\frac{dn_o}{dT} \tag{8.5}$$

Considering the BBO's thermo-optic coefficient of $9.3x10^{-6}$ K^{-1}, this leads to a written wavelength variation of 50 pm/°C, a very important variation considering the narrow bandwidth of ultra-long FBGs.

As mentioned, this problem is inherent to phase-modulator systems due to the lack of feedback, while a piezo, which has an even greater temperature dependence, is mostly immune to such effects thanks to a closed-loop feedback on its actual position. Also, as was observed during the initial trials on phase-shifted DFB FBGs, applying a DC field (~3 kV) on the BBO crystal seems to change considerably the applied phase from one time to another (order of 1-2 radian). This could be due to a charge accumulation effect from a very small current passing in the crystal. Therefore, the solution to such problem on the modulator system is quite obvious: developing a feedback system. This was not implemented during the course of my PhD due to the complexity of such system. The most direct solution is to measure the phase to apply a closed loop correction, which involves building a second sensing interferometer inside the current Talbot interferometer. Another indirect feedback correction would be to precisely measure the temperature on the crystal and apply a correction on the applied voltage. This would solve the issue of temperature induced chirp, which currently remains the main limitation of the overall system.

The next issue to consider in in Table 8.1, which is related to both systems, is perhaps the most damaging defect on FBGs: unintended phase-shifts. As mentioned, vibration can cause high frequency noise during writing. This noise is detrimental to the FBG side-lobes, but does not affect the stop-band, therefore it is not a critical problem for the applications intended in this thesis. However, large amplitude vibration can cause the closed-loop feedback on the translation stage to "lose" its position, thus causing a phase-shift. This issue is easily resolved by ensuring no activity took place on the optical table during FBG writing, a laboratory rule which was generally well respected.

The next potential problem is high frequency phase noise from power fluctuation, vibrations and air currents. These two latter effects are difficult to control and impossible to remove entirely, but with good care, can be minimised. To reduce power fluctuation, the system was upgraded to a faster feedback on the laser power by an electronic closed-loop control comprised of a detector, motorized wave-plate and polarizer. Another source of high-frequency noise is the stage feedback

loop, which adds a slight phase noise, as can be seen in Figure 8.4. This feedback noise is negligible of itself, but the sum of all the other sources mentioned above becomes important on the writing.

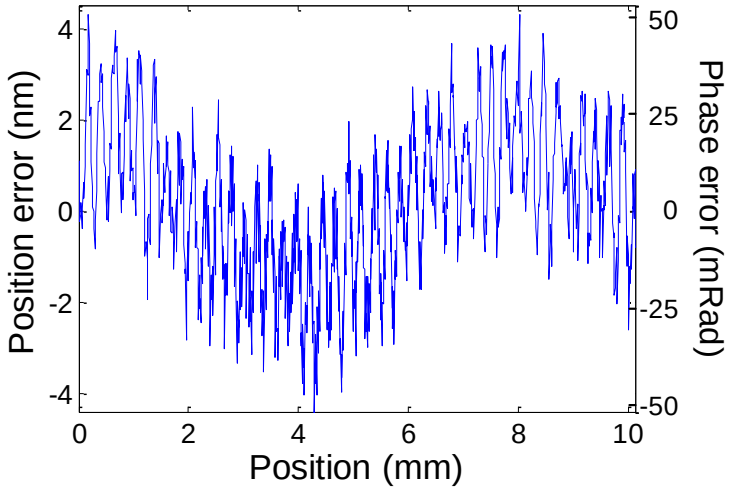

Figure 8.4: Position error noise, hence phase error noise, measured by the stage. The measured data was spatially averaged over the illumination spot size of 120 µm.

One method to reduce this high frequency phase noise is to expand the exposure spot size, which will effectively averaged out that noise. However, expanding the spot size will be detrimental to another limitation of continuous writing: tunability (last element of Table 8.1). Indeed, as described by equation (2.37), the tunability of a continuous writing system is limited by the spot size. A small spot size will increase this tunability range and allow a higher resolution in terms of FBG structure. However, such a small spot size would increase the phase noise (reduced averaging) and decrease the alignment tolerance, making the writing more susceptible to fiber position, a problem discussed below.

The fiber position is itself a critical issue to address. Fiber must remain in the same area inside the overlapping beams (ideally within ±5 µm) throughout the entire length of the grating, else chirp will arise from non-uniform exposure and variation of the fringe pattern phase. One method to address this issue is to map the fiber position with cameras and move the writing head accordingly, as proposed by Gagné *et al.* [11]. However, the alignment of the beam becomes critical: in many cases, such movement of the writing head induces chirp due to angle variation. We came to the conclusion that ensuring fiber flatness is a better solution for reproducible FBGs by properly adjusting the fiber holders) and putting the 1-m of fiber under substantial strain (150 to 200 g).

An important source of non-linear chirp (low-frequency variation of phase) is the variations in environmental conditions on the whole system. Thermal expansion of the structure of the system can change mirror angles, including in the Talbot interferometer. There isn't much that can be done to mitigate this, except limit the sources of heat in the room, ensure good control of the room temperature and avoid the movement of personnel near the system. Heating caused by the beam itself of the optics can be mitigated by a "pre-heating" period in which the interfering beams are sent to the fiber while writing a 100% apodized grating, i.e. no grating. This is equivalent to an initial DC exposure and has negligible impact on the final FBG, but allows the whole beam path to heat-up, thus avoiding an initial thermally induced chirp.

Another very important source of chirp which was observed, is the strain variation from fiber slippage in their clamps. Since a high strain is normally applied on the fiber to keep it flat (ideally, 200g), fibers must be held tightly. The original clamps on the Fabulas proved to be insufficient and caused the fiber to slip very slightly, causing enormous chirp (in the order of 100 pm) on ultra-long FBGs. Reinforcing the clamps with elastic bands proved a good solution. High retention clamps, the FiberVice from Photonova Inc. are planned to be added to the system as a more permanent solution.

Finally, the final issue with ultra-long FBG continuous writing scheme, and an important subject of this thesis, is non-uniformity of the refractive index of the optical fiber, as described in article 2. A solution to this major problem presented in article 3, is to compensate for the calculated Bragg wavelength deviation after measuring the non-uniformity of probe FBGs by OFDR, as described in article 2. Once characterised, the fiber is compensated for the final FBG by adjusting the writing speed along the fiber, therefore adjusting its Bragg wavelength. The method proved extremely successful and led to near perfect FBG.

However, despite this correction, FBGs remained slightly imperfect: slight non-linear chirp persists on some FBGs. Although this chirp does not compromise the operation of FBGs when used for Raman DFB fiber lasers, it does affect laser performance variability. The cause for this has been shown in the above discussion and Table 8.1 and relates to environmental fluctuations. Although an EOM system is more appropriate for ultra-long FBGs, it remains more sensitive to temperature due to lack of feedback. Solutions have been proposed to resolve this in the future. However, the general effect of temperature on the rest of the system's structure and beam path cannot be

completely suppressed. An important lesson learned during this PhD is that great care must be taken when writing ultra-long FBGs. This included a rigorous control of the temperature around the fabrication system.

8.2 Raman and Brillouin gain in DFB lasers

The main application targeted in this thesis is ultra-long FBGs for Raman and Brillouin gain, phase-shifted DFB lasers. This was studied with Brillouin gain in article 1 and Raman gain in article 4. As was mentioned in that article, having a long length FBG reduces the threshold, thus allows the usage of Raman and Brillouin gain. Let us now clarify that advantage of ultra-long FBGs. By viewing the phase-shifted DFB FBG as two sub-FBG reflectors (of reflection R_1 and R_2) separated by a small spacing corresponding to half the period (the phase shift), such a laser can be modeled as a linear dual-mirror cavity. In such case, the pump power threshold can be defined by the following equation:

$$P_{th} = \frac{A_{eff}}{gL_{eff}}\left(\alpha L_{eff} - \ln\left(\sqrt{R_1 R_2}\right)\right) \tag{8.6}$$

Where A_{eff} is the effective mode area, g the Brillouin or Raman gain, α the fiber intrinsic loss, L_{eff} the effective length viewed by a photon for a half roundtrip. This length would normally be the length between the two mirrors in a dual-mirror cavity. However, when considering a DFB FBG, the light enters each sub-FBGs partially dependant on the grating coupling constant. The effective length can be defined as follows:

$$L_{eff} = a\frac{(1 - e^{-\kappa_{ac}L_1})}{\kappa_{ac}} + a\frac{(1 - e^{-\kappa_{ac}L_2})}{\kappa_{ac}} \tag{8.7}$$

Where κ_{ac} is the grating strength and L_1 and L_2 the lengths of each sub-FBG (each half the total length for a centered phase-shift). The constant a was found by simulation to be 0.275 and accounts for the intensity-dependant nature of the gain. This value indicates, for strong gratings ($\kappa_{ac}L \gg 1$), that the effective length includes the fields with an average amplitude of 76% of the maximum, instead of the typical 36% (1/e) from the standard definition of the effective length.

Let us consider such strong gratings, which is the case for Raman and Brillouin gain DFB FBG lasers, with a centered phase-shift (R_1=R_2, L_1=L_2=L/2). The effective length can then be simplified to:

$$L_{eff} = a\frac{2}{\kappa_{ac}} = a\frac{2L}{\sigma} \tag{8.8}$$

Where $\sigma = \kappa_{ac}L$ which represents the grating strength. It is often useful to use a constant FBG strength when comparing different FBG designs, as this strength can be easily tuned through κ_{ac}, as long as κ_{ac} remains below the maximum inscription limit for the considered fiber. Considering equation (8.8) as well as equation (2.16) defining a FBG's reflectivity, equation (8.6) can be rewritten and simplified for the case $\kappa_{ac}L \gg 1$ as the following:

$$P_{th} = \frac{A_{eff}\kappa_{ac}}{2ag}\left(\frac{2\alpha}{\kappa_{ac}} + 4e^{-\kappa_{ac}L}\right) \tag{8.9}$$

Considering only the FBG's design limitations, therefore neglecting the contribution of absorption, the minimum threshold would therefore be:

$$P_{th} = \frac{2A_{eff}\kappa_{ac}}{ag}e^{-\kappa_{ac}L} \tag{8.10}$$

In order to compare the effect of length of a grating, we can compare various design at constant strength. Therefore equation (8.10) can be rewritten as:

$$P_{th} = \frac{2A_{eff}}{agL}\sigma\, e^{-\sigma} \tag{8.11}$$

As can be seen in Figure 8.5, this theoretical analytical threshold fits well with simulation. As was mentioned in article 4, there is an important advantage in increasing the length of the FBG. For one, when comparing constant FBG strength (constant reflectivity), the pump threshold reduces linearly with length. Also, for the same FBG strength, the required Δn to induce the designed $\kappa_{ac}L$ is decreased as length is increased. Therefore, ultra-strong FBGs ($\kappa_{ac}L > 10, T < -80$ dB) can be written easily, but which would normally be difficult in short ~cm length FBGs. However, writing ultra-long FBGs also becomes more difficult as length is increased, for the reasons described in the previous sub-section. Difficulties also arise during operation, as they have to be perfectly stabilised. This is why an optimal length of 300 to 500 mm was proposed in article 4, since the FBG's writing and operation conditions can be still well controlled.

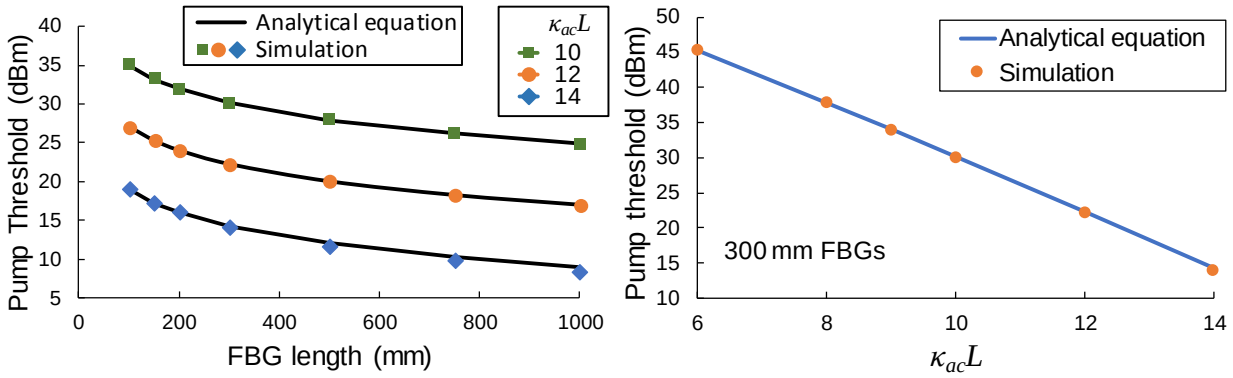

Figure 8.5: Comparison of the proposed equation (8.11) with simulation for no-loss DFB FBGs with a π, centered phase-shift.

Apart from the FBG's design structure, the pump threshold depends on other parameters of which we have less control: transmission loss, mode area and gain. Those parameters were not optimized in the study, as their effect is obvious: loss and mode area should be minimised (not the case for RE dopants in the core alone), while the gain should be maximised. However, there are material or fabrication limits for each which will be detailed below.

Among the 3, loss is perhaps the most detrimental as it limits the improvement offered in performance from the FBG design. If loss could be zero, a strong FBG could compensate for large-core fibers or small gain. However, such utopia is not the case in optical fibers. In our tested fibers, the loss is relatively high due to UV exposure and deuterium loading. Heat treatment is normally used to reduced such loss, a process which was attempted, but not mastered, during the course of the study in this thesis, as it depends on previous fabrication steps (deuterium concentration (if any), exposure, UV wavelength, pulsed or CW regime, fiber dopants, etc.). Since we had no fixed fabrication recipe, as the objective was mostly to study different designs, i.e. different recipes, the heat treatment optimization was not attempted. We did notice performance improvement when using non-deuterium-loaded fibers, relying only on the small-core fiber's photosensitivity and higher exposure values. However, such a method was time consuming (slow writing), and therefore to study multiple FBGs, all lasers were compared using deuterium-loaded fibers.

An interesting effect was observed during Raman laser operation: the pump threshold was normally higher for the first operation, then permanently decreased after tens of minutes, and even further after several hours of operation. Although we observed thresholds in the order of 1-5 W, as shown in article 4, the first activation threshold was often in the 8-11 W range, near the limit of our

1480 nm pump laser. This high initial activation was often a limit in our FBG designs and why we had to rely on high κ_{ac} gratings. We believe that multi-photon absorption could be resulting from the intense intra-cavity fields, which in turn changes the core material of the fiber and reduces losses. This phenomenon is still under investigation.

The second important variable in equation (8.11) which was not optimised is the fiber's mode area. The smaller the mode area, the less power is required for the same intensity. Raman and Brillouin DFB fiber lasers' gain and Kerr effect depend on intensity, thus why the threshold of the above equations depends on the fiber's mode area. The mode area chosen for simulation and experimental testing was for typical small-core fibers, with modes field diameters (MFD) of 3-4 µm. More specialised fibers with 2 µm MFD were recently developed (not yet tested) and photonic crystal fibers with 1.6 µm MFD was proposed by Youfang *et al.* [112]. Reducing core size may also have an advantage in reducing the thermally induced chirp during laser operation: for the same intensity, the power is reduced, therefore reducing absorption generated heating inside the core, which is a linear process.

The choice of fiber core size was experimentally studied. Indeed, in article 1, SMF-28, with a MFD of 10 µm was used for Brillouin generation. Although abundantly available, low cost fiber and easier to fabricate high quality FBG (at the time, at least), such fiber has a threshold 6 times higher than typical small-core fiber. This was observed in article 1, where the threshold to generate SBS was higher than previous experiments in small-core fiber. This was also noted as we were unable to have a DFB laser operating with Raman gain in SMF-28 with our 12 W of available power. Lasing in SMF-28 with Raman gain is likely possible if loss is well optimised and with higher pump power. However, as stated previously, thermal effect could be more important in larger-core fiber. This was observed in article 1, as the thermally induced push-broom effect in SMF-28 allowed a larger tuning than in previous experiments with small-core fiber. A subject which will be discussed in the next paragraphs.

The third parameter of importance for DFB laser performance which was not optimised is the gain itself. As this is a material property, we have very little control over it. However, there are a few cases we can study. First, is the type of gain. SBS has a higher gain than SRS, which is why we were able to demonstrate a working DFB fiber laser in SMF-28 in article 1, while this was not possible with SRS in the same fiber. Another means to change the gain is by polarisation. Both

SBS and SRS are polarisation sensitive. Indeed, for SRS, the gain with polarised light (when optimised) is double that of the non-polarised pump. This was observed by previous authors [127] and by us through a reduction by a factor of 2 of pump threshold. The effect on SBS gain is lower, but still present.

While it has been shown how various parameters and FBG design affect the pump threshold through equation (8.11), the second figure of merit of importance for DFB fiber lasers which was also studied in articles 1 and 4, is the slope efficiency. The slope efficiency is defined as the power produced per power injected in the system *above* the threshold. Slope efficiency is not the efficiency of the laser. Total efficiency depends on the pump power: it increases as the output power increases since the power used to reach threshold becomes less important. Therefore, total efficiency cannot be considered as a figure of merit of the laser, thus the use of slope efficiency. In this thesis, the slope efficiency was generally specified for single-sided operation, i.e. only by one output (the highest) is considered. Theoretically, for ideal Raman and Brillouin gain lasers, the global slope efficiency (both sides) is limited only by the loss and by the quantum defect, i.e. the difference in energy between pump and emitted photons. This was verified through simulation where 90-95 % total slope efficiency can be reached when supposing a relatively low loss. However, this ideal case is only true when Kerr effect is NOT taken into account. Indeed, it was shown from calculations in article 4 that intensity-induced chirp (through Kerr effect and thermal gradient) reduces the slope efficiency significantly. This comes from the fact that any intensity-induced chirp will affect the Q-factor of the cavity by "moving" the DFB mode inside the FBG stop-band, therefore creating a dependence of the Q-factor on the internal intensity. This brings us to the most interesting effect observed in this thesis: the push-broom effect of Raman and Brillouin DFB fiber lasers.

This push-broom effect, is an equilibrium state obtained from two opposing effects: the above-threshold gain induced high intensity in the cavity and the non-linear chirp induced by this same intensity. Non-linear chirp reduces the Q-factor, and hence increases the pump threshold. The term push-broom, introduced by Martijn de Sterke [132], is an effect where a pump "pushes" a signal through non-linear effects (SPM and XPM). In the case of de Sterke, this push-broom was in the temporal domain (a large pulse is "pushed" and compressed by a pump pulse) while in our case it is in the frequency domain (a narrow CW oscillating mode is "pushed" in frequency by SPM/XPM).

The first article showed this push-broom effect when moving the SBS gain spectra with to the lasing line. This could be done with SBS since the gain bandwidth is very narrow (20 MHz) and can be tuned easily by pump modulation. As the gain approaches the lasing line from the high frequency side, the low-frequency tail of the gain interacts with the laser line and pushes that line towards lower-frequencies inside the FBG stop-band (See Figure 4.3). SPM and XPM were known to induce such effects, however according to simulation performed by Winful *et al.* [133], it could not explain the amplitude of the observed push-broom effect. We, as well as other authors [131, 133], supposed it may be from local heating in the core inducing a non-linear thermal gradient. This was the first clue as to why our Raman DFB fiber laser did not perform as expected.

The same effect was indeed observed in Raman DFB fiber laser, although it took simulation to properly understand and quantify the problem. In the case of SRS, the gain bandwidth is much larger and changing the pump frequency does not yield the same effect as for SBS. However, we can observe the same push-broom effect by increasing the pump power: as the pump is increased, the lasing line moves to lower frequency inside the stop-band (higher wavelength), as shown in Figure 7.4. Again, SPM/XPM cannot account as the entire explanation, since simulation showed that DFB gratings should allow for a slope efficiency of ~30-40 % (single-sided output) when including optical non-linearity, while this is far from the observed efficiency (1-5%). As explained in article 4, accounting for heating induced by intra-cavity intensity increases the effective non-linearity and explains the low efficiencies, thus confirming the hypothesis of article 1.

The large non-linear effect induced by a thermal gradient is a major limitation discovered this research concerning Raman and Brillouin gain DFB fiber lasers. This limitation significantly reduces performance (slope efficiency) of such lasers by the push-broom effect described above. One idea that was proposed in article 4 to mitigate this detrimental effect is to reduce the inscribed phase-shift ($<\pi$) to compensate for the induced phase shift during operation. According to simulation, this does increase slope efficiency slightly. However, it comes at the cost of a major increase in activation pump threshold, as the initial (no internal field) Q-factor is reduced due to the non-ideal phase shift. Experimentally, the advantage of such design could not be demonstrated clearly, as the required phase-shift reduction to induce a clear slope efficiency increase ($<0.6\ \pi$) brings the pump threshold above our available pump power.

One potential solution would be to dynamically control the phase-shift *during* operation. With such a solution, the FBG should be written without any phase shift (or with a negative phase-shift). Before starting the laser, an appropriate phase-shift (~ π) can be induced by local heating (such as using a heating wire). Once the FBG is lasing, the heating can be reduced gradually to allow only the internal field as phase-shift inducing mechanism through non-linear effects and thermal gradient. From simulation, an increased slope efficiency is seen, as shown in Figure 8.6. The results shown in this figure can be also interpreted as cooling down the phase-shift area of a written π-phase-shifted DFB FBG to induce a final "inscribed" phase shift (x-axis), but only after the threshold is reached.

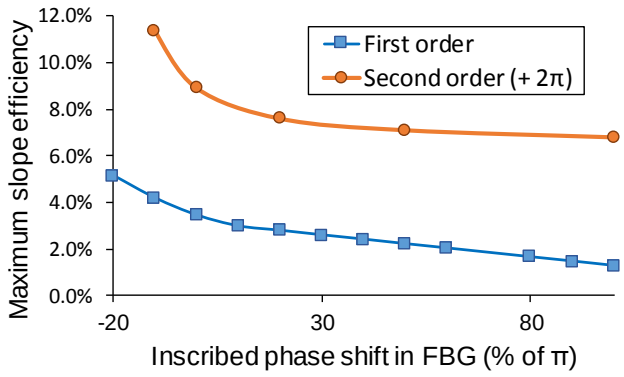

Figure 8.6: Calculated maximum slope efficiency for various centered phase-shifted FBG designs (variation of the inscribed phase-shift value), with thermal non-linearity included. An optimal phase shift (π, for lowest threshold) is dynamically applied through (ex: heating) to "start" the lasing only, then removed to calculate the "maximum slope efficiency".

Interestingly, we can also consider high order field-induced phase shifts, where the fields induce an integrated phase variation over $2\pi m$, where m is an integer describing the high-order. As shown in Figure 8.6, considering such high-order significantly increases the slope efficiency. Because convergence is difficult, we could not consider higher orders in our simulation. The reason for this, is that a high-order field-induced phase-shift also induces non-linear chirp which deforms the stop-band. Although 2nd order phase-shift allows (in most cases) only one mode to lase in the stop-band, higher-order phase-shifts seem to allow several modes with similar Q-factors in the stop-band, which leads to multi-mode operation.

We have shown optimisation mostly for output power in article 4. If threshold is the main requirement, then the minimum is for a centered, π phase-shifted FBG. Non-linearity and loss were

studied mainly to understand what effect each has on the operation of the laser, as it is not possible to eliminate either. Another optimization which can be studied is single-frequency (SF) operation. SF operation was supposed in the simulation of article 4, but it was not optimized (the ideal conditions to ensure SF operation were not studied). However, an experimental study was undertaken in collaboration with MPB Communication Inc. and an article was published showing outstanding SF performance of the Raman DFB laser [128]. Figure 8.7 shows the important results of this article, where all the points are in SF operation, although we suspect that the output over 60 mW (2 W of pump) in (b) is from a high order mode (effective phase-shift > 2π) oscillation. This is still under investigation, especially how to control such high-order stable SF modes, which exhibits higher slope efficiency.

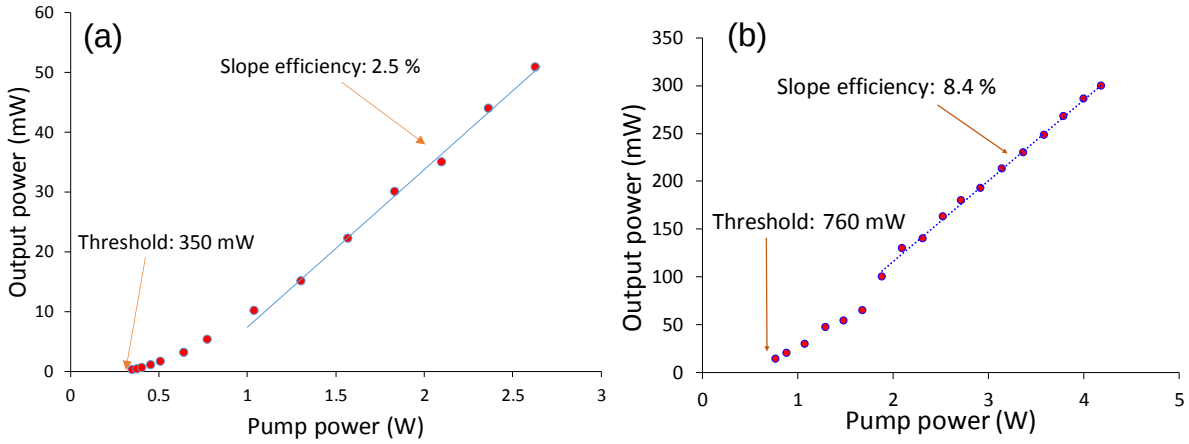

Figure 8.7: Operation results from 300 mm long phase-shifted DFB Raman fiber lasers. (a) Laser operating at 1120 nm (1064 nm pump) and (b) another design operating at 1178 nm (1120 nm pump)

From these experiments, it was observed that Raman DFB fiber lasers do not always operate in the SF mode. Experimentally we observed multi-mode operation at high power (> 2.5 W in Figure 8.7 (a) and > 4.2 W in (b)), with a mode spacing (beat-note) in the hundreds of MHz, therefore relating to several modes lasing inside the stop-band. Although multi-mode operation could not be observed in our simulation, convergence problems were observed for high pump power, at which point more than one mode appears inside the stop-band due to higher non-linear phase.

Another major limitation to SF operation, and for DFB fiber lasers in general, is the surprising generation of SBS for high pump powers. Indeed, at some elevated pump power and when the

grating's environment is optimized (on metal base for heat dissipation), the DFB mode laser line saturates and SBS is generated on the lower frequency *outside* the stop-band, as shown in Figure 8.8. The SBS generation seems to be dependent on temperature, which leads us to believe it comes from an oscillation in a side-mode of the FBG (weak resonance), as the side-mode structure does change with temperature. This SBS generation is likely due to the intense field inside the grating, which gives rise to a high SBS gain, enough to allow lasing under low feedback. This undesired SBS was more present in the FBGs made in the collaborative study with MPB, which were done at 1.12µm and 1.178µm, both of which require the use of our piezo driven writing system. As stated in the last sub-section, this system induces more side-lobe noise, which is why SBS seems occur. The FBG made at 1578 nm with our modulator system did show SBS on some occasions under high pump power, but this was relatively rare.

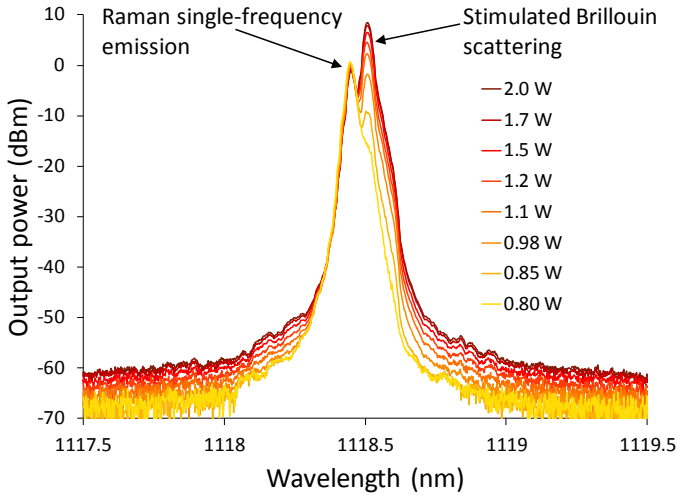

Figure 8.8: Generation of SBS outside of the DFB FBG stop-band during Raman emission.

Nevertheless, this SBS generation is an important problem for DFB fiber laser. If our hypothesis of side-lobe resonance is correct, this detrimental effect can be mitigated with proper apodization (using the modulator writing system). Another means to solve this is to write a grating at the SBS emission wavelength over the strong Raman DFB grating. Apodization was tried on the DBF laser in the MPB study, without much success, as the apodization quality is lacking due to the piezo system. Further investigation on potential solutions is still underway.

CHAPTER 9 CONCLUSION AND RECOMMENDATIONS

The work presented in this thesis showed the realisation and applications of reproducible high-quality ultra-long FBGs. The first objective of the Thesis was to bring a better understanding of ultra-long FBG fabrication, its problems and its limitations, while the second was to find solutions to those problems to ensure the production of reproducible high-quality FBGs. During this study, every aspect and parameter influencing the fabrication system was examined thoroughly to address that first objective. Some new problems were found concerning our recently developed modulator driven Talbot interferometer system for continuous writing, while other intrinsic limitations with ultra-long FBG writing were also discovered. The main limitation that was found in this Thesis, and the subject of 2 articles presented here, is the non-uniformity of the fiber, a limiting issue present in all fibers. Since ultra-long FBGs are very sensitive to phase variation, small changes in the order of 10^{-5} in effective refractive index are sufficient to radically impact the quality of the FBG or even render it to be useless. Such variations in effective refractive index are common and caused by manufacturing imperfection, except perhaps in standard SMF-28 fiber, in which the defects are ~10 times smaller. Solving this issue was proposed in the 3rd article presented here and allowed for the first-time the fabrication of high-quality FBGs reproducibly. This solution involved characterizing the fiber and implementing a Bragg wavelength correction during inscription to compensate for the varying effective refractive index.

This thesis also covers other issues, one of which was related to our continuous writing system using EO modulators. The main issue found was the lack of closed-loop feedback to control the phase, which makes the writing sensitive to the environment when compared with a commercially available closed-loop piezo-driven system used in the interferometer. A solution was proposed, with success, to properly control DC phase variations (for phase-shifted DFB FBGs) by implementing a small wavelength shift. However, no solution has yet been implemented for the modulator's sensitivity to the environment, which could improve the overall quality of ultra-long FBGs, above what is possible with the great care taken to minimise temperature variation during writing. The best solution proposed for this issue is a direct measurement of phase with relevant feedback electronics. However, such a solution requires the use of a second interferometer with the current Talbot interferometer to allow phase measurement, a rather complex implementation.

Another indirect solution would be to precisely measure the crystal temperature and apply a correction to the driving voltage.

Temperature variations around the fabrication system also have an impact on the writing: such fluctuations induce very small changes in the alignment from thermal expansion of all parts along the beam path. Although very small, these alignment changes induce pm variations in Bragg wavelength, sufficient to cause undesirable chirp, which affect the FBG quality. There is unfortunately no solution which can completely resolve this issue at present and may always remain a limitation for ultra-long FBG writing. Great care can be taken to minimise such effects: use of thermally stable optics, stabilising the room temperature, avoiding human proximity to the system, avoiding any source of heat (such as heat gun, or soldering iron) in the vicinity of the FBG writing rig before and during production, etc.

Other minor issues were also found and investigated in this Thesis, which can impact the FBG's quality: phase-shift induced by vibrations, strain variations, power fluctuations, air currents, etc. These issues can all be resolved by taking the greatest care in handling the fabrication process and remembering how ultra-long FBG writing is extremely sensitive to any such parameters.

It can therefore be claimed that the first objective of the Thesis was well met to the best of my knowledge. As for the second objective, it was accomplished sufficiently well to allow reproducible high-quality ultra-long FBG usable in a variety of applications. However, as stated above, there remains some unresolved issues, for which solutions have nevertheless been proposed. Because of these issues, our current ultra-long FBGs are not entirely perfect, but are probably the best reported to date; slight random chirp can appear, but that rarely compromises the FBG when used for DFB lasers.

The 3rd and 4th objectives of this Thesis were to study an application of ultra-long FBGs: phase-shifted DFB Raman and Brillouin gain lasers. The third objective was to develop a model and simulation method which is fast enough to allow an extensive study of all parameters influencing the performance of single-longitudinal-mode DFB fiber lasers. Such a method was detailed in the 4th article presented here and was shown to be quite successful. Thanks to this model and simulations performed with it, a deeper understanding of the behavior of such lasers was possible, correlated with results from Brillouin and Raman gain experiments (1st and 4th papers respectively). The main conclusion of this study is that Brillouin and Raman gain DFB fiber lasers are limited

from thermally induced chirp due to the fiber core heating under intense optical fields. This reduces slope efficiency significantly, increases the push-broom effect of SBS frequency tuning as well as the hysteresis of output vs pump power for phase shifts less then π. The model and simulation was verified experimentally through series of fabricated ultra-long FBGs. Therefore, this objective was also met.

The final objective of the thesis was to optimize and improve the performance of DFB fiber lasers with Brillouin and Raman gain. Such optimisation on the design was first investigated by simulation for ideal FBGs (no thermal gradient): it was shown that for a given pump power and grating strength and length, an optimal position of the phase-shift can be found to maximize the output power. Also, reducing the phase-shift (less then π), compensates for the push-broom effect and allows for a higher slope efficiency, at the cost of increasing the lasing pump threshold. Ideal grating length (~300 mm) and strength ($10 < \kappa_{ac}L < 14$) were then proposed following this optimization procedure. However, this ideal optimization could not be met experimentally within the timeframe of this study, due to the presence of high thermal gradient from core heating.

When considering this thermal non-linearity, the optimal conditions on grating length and strength remain the same. However, under these non-ideal conditions, it was observed experimentally and through simulation a saturation of the slope efficiency as a function of the phase-shift position, leading to an optimal (minimum threshold) position of the shift at the center of the FBGs. The optimization of the phase-shift value could not be demonstrated due to the high activation threshold and the limited pump power available for the experiments, although the hysteresis behavior predicted by simulation was observed. Nevertheless, the experiments led to a better understanding of the limitations of such lasers. A solution can be proposed which could allow the DFB laser to approach the ideal conditions predicted in the simulations.

That solution is to reduce thermal gradient. This can be done passively, by minimising absorption loss (anneal fiber after FBG inscription) and improving thermal conductivity along the fiber during operation. These solutions can lead to an increase in the slope efficiency, but can never eliminate the effect of the thermal gradient. Another proposed solution is to dynamically control the phase-shift during operation, such as by a heating wire or a temperature-controlled cold-finger. By doing so, the optimal conditions (π-phase-shift) can be met for the laser activation, then optimised afterward by reducing the phase shift to compensate for the push-broom effect.

In conclusion, the contributions presented in this thesis have led to a better understanding of ultra-long FBG fabrication, its limitations and how to deal with them. Solutions have been proposed which have led to the production of high quality ultra-long FBGs which can be reproduced in any type of fiber, even those which present large non-uniformity in the spatial effective refractive index. Being able to produce reproducibly high quality ultra-long FBGs is crucial for applications such as Brillouin and Raman gain DFB fiber lasers. Long lengths allow for operation with low pump threshold powers, below sub-watt, with the lowest reported to date demonstrated in this thesis. These contributions could lead to commercial applications, as a Raman DFB fiber laser offering narrow-linewidths, single-frequency emission at any wavelength, with the reproducible production, now possible. Proposals have been made to use such single-frequency sources for guide-star applications, for which a wavelength of the sodium (589 nm) line is required, and which can now be achieved through single frequency lasing with Raman gain. Many other applications of such Raman DFB fiber laser or of ultra-long FBG in general could now be considered, having overcome the severe limitations not only posed by the writing scheme, but also by the poor quality of the fiber, leading to high reliability and reproducibility.

REFERENCES

[1] M. Matsuhara, K. O. Hill, and A. Watanabe, "Optical-waveguide filters: Synthesis," *Journal of the Optical Society of America,* vol. 65, pp. 804-809, 1975.

[2] K. Hill, Y. Fujii, D. C. Johnson, and B. Kawasaki, "Photosensitivity in optical fiber waveguides: Application to reflection filter fabrication," *Applied Physics Letters,* vol. 32, pp. 647-649, 1978.

[3] G. Meltz, W. W. Morey, and W. H. Glenn, "Formation of Bragg gratings in optical fibers by a transverse holographic method," *Optics Letters,* vol. 14, pp. 823-825, 1989.

[4] V. Mizrahi, T. Erdogan, D. DiGiovanni, P. Lemaire, W. MacDonald, S. Kosinski, *et al.*, "Four channel fibre grating demultiplexer," *Electronics Letters,* vol. 30, pp. 780-780, 1994.

[5] G. E. Town, K. Sugden, J. A. R. Williams, I. Bennion, and S. B. Poole, "Wide-band Fabry-Perot-like filters in optical fiber," *IEEE Photonics Technology Letters,* vol. 7, pp. 78-80, 1995.

[6] F. Ouellette, P. A. Krug, T. Stephens, G. Dhosi, and B. Eggleton, "Broadband and WDM dispersion compensation using chirped sampled fibre Bragg gratings," *Electronics Letters,* vol. 31, pp. 899-901, 1995.

[7] B. Eggleton, P. A. Krug, and L. Poladian, "Dispersion compensation by using Bragg-grating filters with self-induced chirp," in *Optical Fiber Communication Conference*, 1994, p. ThK3.

[8] B. J. Eggleton, G. Lenz, N. Litchinitser, D. B. Patterson, and R. E. Slusher, "Implications of fiber grating dispersion for WDM communication systems," *IEEE Photonics Technology Letters,* vol. 9, pp. 1403-1405, 1997.

[9] G. S. Kanter, A. K. Samal, and A. Gandhi, "Electronic dispersion compensation for extended reach," in *Optical Fiber Communication Conference, 2004. OFC 2004*, 2004, p. 419.

[10] S. Tsukamoto, K. Katoh, and K. Kikuchi, "Unrepeated 20-Gbit/s QPSK Transmission over 200-km Standard Single-Mode Fiber Using Homodyne Detection and Digital Signal Processing for Dispersion Compensation," in *Optical Fiber Communication Conference and Exposition and The National Fiber Optic Engineers Conference,* Anaheim, California, 2006, p. OWB4.

[11] M. Gagné, S. Loranger, J. Lapointe, and R. Kashyap, "Fabrication of high quality, ultra-long fiber Bragg gratings: up to 2 million periods in phase," *Optics Express,* vol. 22, pp. 387-398, 2014.

[12] M. Gagné, L. Bojor, R. Maciejko, and R. Kashyap, "Novel custom fiber Bragg grating fabrication technique based on push-pull phase shifting interferometry," *Optics Express,* vol. 16, pp. 21550-21557, 2008.

[13] Y. Feng, L. R. Taylor, and D. B. Calia, "25 W Raman-fiber-amplifier-based 589 nm laser for laser guide star," *Optics Express,* vol. 17, pp. 19021-19026, 2009.

[14] D. Gloge, "Weakly Guiding Fibers," *Applied Optics,* vol. 10, pp. 2252-2258, 1971.

[15] R. Kashyap, *Fiber bragg gratings (Second Edition)*. Boston: Academic press, 2010.

[16] D. Marcuse, *Theory of dielectric optical waveguides*: Elsevier, 2013.

[17] E. Kreyszig, "Matrix Eigenvalue Problems," in *Advanced Engineering Mathematics*, 5th edition ed New York: Wiley, 2011, p. 322.

[18] H. A. Haus and Y. Lai, "Theory of cascaded quarter wave shifted distributed feedback resonators," *IEEE journal of Quantum Electronics,* vol. 28, pp. 205-213, 1992.

[19] M. Yamada and K. Sakuda, "Analysis of almost-periodic distributed feedback slab waveguides via a fundamental matrix approach," *Applied optics*, vol. 26, pp. 3474-3478, 1987.

[20] E. Chehura, S. W. James, and R. P. Tatam, "Rouard's method as a modelling tool for the sensing characteristics of complex fibre Fabry-Perot interferometers formed between chirped fibre Bragg gratings," in *17th International Conference on Optical Fibre Sensors*, Bruges, 2005.

[21] E. J. Friebele, D. L. Griscom, and G. H. S. Jr., "Defect centers in a germanium-doped silica-core optical fiber," *Journal of Applied Physics*, vol. 45, pp. 3424-3428, 1974.

[22] T. E. Tsai, D. L. Griscom, E. J. Friebele, and J. W. Fleming, "Radiation-induced defect centers in high-purity GeO2 glass," *Journal of Applied Physics*, vol. 62, pp. 2264-2268, 1987.

[23] M. Gagné and R. Kashyap, "New nanosecond Q-switched Nd:VO4 laser fifth harmonic for fast hydrogen-free fiber Bragg gratings fabrication," *Optics Communications,* vol. 283, pp. 5028-5032, 2010.

[24] D. Williams, B. Ainslie, J. Armitage, R. Kashyap, and R. Campbell, "Enhanced UV photosensitivity in boron codoped germanosilicate fibres," *Electronics Letters*, vol. 29, pp. 45-47, 1993.

[25] L. Dong, J. L. Cruz, L. Reekie, M. G. Xu, and D. N. Payne, "Large photo-induced index changes in Sn-doped germanosilicate fibres," presented at the Topical Meeting Photosensitivity and Quadratic Nonlinearity in Glass Waveguide Fundamentals and Applications, 1995.

[26] P. Lemaire, A. Vengsarkar, W. Reed, V. Mizrahi, and K. Kranz, "Refractive-index changes in optical fibers sensitized with molecular hydrogen," in *Optical Fiber Communication Conference*, 1994, p. TuL1.

[27] P. J. Lemaire, R. M. Atkins, V. Mizrahi, and W. A. Reed, "High pressure H2 loading as a technique for achieving ultrahigh UV photosensitivity and thermal sensitivity in GeO2 doped optical fibres," *Electronics Letters*, vol. 29, pp. 1191-1193, 1993.

[28] R. M. Atkins, P. J. Lemaire, T. Erdogan, and V. Mizrahi, "Mechanisms of enhanced UV photosensitivity via hydrogen loading in germanosilicate glasses," *Electronics Letters,* vol. 29, pp. 1234-1235, 1993.

[29] B. Poumellec and P. Niay, "About writing mechanism of UV induced refractive index change in H2 loaded Ge doped SiO2," in *Photorefractive Effects, Materials, and Devices 2003*, La Colle sur Loup, France, 2003, p. 283.

[30] J. Stone, "Interactions of hydrogen and deuterium with silica optical fibers: A review," *Lightwave Technology, Journal of,* vol. 5, pp. 712-733, 1987.

[31] A. Saliminia, N. T. Nguyen, S. L. Chin, and R. Vallée, "The influence of self-focusing and filamentation on refractive index modifications in fused silica using intense femtosecond pulses," *Optics Communications,* vol. 241, pp. 529-538, 2004.

[32] A. P. Joglekar, H.-h. Liu, E. Meyhöfer, G. Mourou, and A. J. Hunt, "Optics at critical intensity: Applications to nanomorphing," *Proceedings of the National Academy of Sciences of the United States of America,* vol. 101, pp. 5856-5861, April 20, 2004.

[33] D. Du, X. Liu, G. Korn, J. Squier, and G. Mourou, "Laser-induced breakdown by impact ionization in SiO2 with pulse widths from 7 ns to 150 fs," *Applied Physics Letters,* vol. 64, pp. 3071-3073, 1994.

[34] A. Martinez, I. Y. Khrushchev, and I. Bennion, "Direct inscription of Bragg gratings in coated fibers by an infrared femtosecond laser," *Optics Letters,* vol. 31, pp. 1603-1605, 2006.

[35] C. W. Smelser, S. J. Mihailov, and D. Grobnic, "Formation of Type I-IR and Type II-IR gratings with an ultrafast IR laser and a phase mask," *Optics Express,* vol. 13, pp. 5377-5386, 2005.

[36] J. Albert, B. Malo, K. O. Hill, F. Bilodeau, D. C. Johnson, and S. Thériault, "Comparison of one-photon and two-photon effects in the photosensitivity of germanium-doped silica optical fibers exposed to intense ArF excimer laser pulses," *Applied Physics Letters,* vol. 67, pp. 3529-3531, 1995.

[37] J. L. Archambault, L. Reekie, and P. S. J. Russell, "100% reflectivity Bragg reflectors produced in optical fibres by single excimer laser pulses", *Electronics Letters 29(5),* pp. 453-455, 1993.

[38] D. L. Williams, S. T. Davey, R. Kashyap, J. R. Armitage, and B. J. Ainslie, "Direct observation of UV induced bleaching of 240 nm absorption band in photosensitive germanosilicate glass fibres," *Electronics Letters,* vol. 28, pp. 369-371, 1992.

[39] L. Dong, J. L. Archambault, P. S. J. Russell, and D. N. Payne, "Strong UV absorption in germanosilicate fibre preforms induced by exposure to 248nm radiation," presented at the ECOC '94: 20th European Conference on Optical Communications, 1994.

[40] H. Patrick and S. L. Gilbert, "Growth of Bragg gratings produced by continuous-wave ultraviolet light in optical fiber," *Optics Letters,* vol. 18, pp. 1484-1486, 1993.

[41] J. R. Armitage, "Fibre Bragg reflectors written at 262 nm using a frequency quadrupled diode-pumped Nd3+:YLF laser," *Electronics Letters,* vol. 29, 1993.

[42] J. Blows and D. Y. Tang, "Gratings written with tripled output of Q-switched Nd:YAG laser," *Electronics Letters,* vol. 36, pp. 1837-1839, 2000.

[43] V. L. Iezzi, J.-S. Boisvert, S. Loranger, and R. Kashyap, "3D printed long period gratings for optical fibers," *Optics Letters,* vol. 41, pp. 1865-1868, 2016.

[44] J. Martin and F. Ouellette, "Novel writing technique of long and highly reflective in-fibre gratings," *Electronics Letters,* vol. 30, pp. 811-812, 1994.

[45] M. J. Cole, W. H. Loh, R. I. Laming, M. N. Zervas, and S. Barcelos, "Moving fibre/phase mask-scanning beam technique for enhanced flexibility in producing fibre gratings with uniform phase mask," *Electronics Letters,* vol. 31, pp. 1488-1490, 1995.

[46] R. Kashyap, P. F. McKee, R. J. Campbell, and D. L. Williams, "Novel method of producing all fibre photoinduced chirped gratings," *Electronics Letters,* vol. 30, pp. 996-998, 1994.

[47] J. Albert, S. Theriault, F. Bilodeau, D. C. Johnson, K. O. Hill, P. Sixt, *et al.*, "Minimization of phase errors in long fiber Bragg grating phase masks made using electron beam lithography," *IEEE Photonics Technology Letters,* vol. 8, pp. 1334-1336, 1996.

[48] W. H. Loh, M. J. Cole, M. N. Zervas, and R. I. Laming, "Compensation of imperfect phase mask with moving fibre-scanning beam technique for production of fibre gratings," *Electronics Letters,* vol. 31, pp. 1483-1485, 1995.

[49] G. A. Miller, G. M. H. Flockhart, and G. A. Cranch, "Technique for correcting systematic phase errors during fibre Bragg grating inscription," *Electronics Letters,* vol. 44, pp. 1399-1400, 2008.

[50] M. Bernier, Y. Sheng, and R. Vallée, "Ultrabroadband fiber Bragg gratings written with a highly chirped phase mask and Infrared femtosecond pulses," *Optics Express,* vol. 17, pp. 3285-3290, 2009.

[51] C. W. Smelser, S. J. Mihailov, and D. Grobnic, "Hydrogen loading for fiber grating writing with a femtosecond laser and a phase mask," *Optics Letters,* vol. 29, pp. 2127-2129, 2004.

[52] M. Bernier, D. Faucher, R. Vallée, A. Saliminia, G. Androz, Y. Sheng, *et al.*, "Bragg gratings photoinduced in ZBLAN fibers by femtosecond pulses at 800 nm," *Optics Letters,* vol. 32, pp. 454-456, 2007.

[53] S. J. Mihailov, C. W. Smelser, D. Grobnic, R. B. Walker, P. Lu, H. Ding, *et al.*, "Bragg Gratings Written in All-SiO2 and Ge-Doped Core Fibers With 800-nm Femtosecond Radiation and a Phase Mask," *Journal of Lightwave Technology,* vol. 22, p. 94, 2004.

[54] D. Grobnic, S. J. Mihailov, R. B. Walker, and C. W. Smelser, "Strong Bragg Gratings made with IR Femtosecond Radiation in Heavily Doped Er3+and Yb3+Silica Fibers," in *Bragg Gratings, Photosensitivity, and Poling in Glass Waveguides*, Quebec City, 2007, p. BTuC4.

[55] R. Kashyap, "Assessment of tuning the wavelength of chirped and unchirped fibre Bragg grating with single phase-masks," *Electronics Letters 34(21),* 2025-2027, 1998.

[56] C. Martinez and P. Ferdinand, "Analysis of phase-shifted fiber Bragg gratings written with phase plates," *Applied Optics,* vol. 38, pp. 3223-3228, 1999.

[57] Q. Zhang, D. A. Brown, L. Reinhart, and T. F. Morse, "Simple prism-based scheme for fabricating Bragg gratings in optical fibers," *Optics Letters,* vol. 19, pp. 2030-2032, 1994.

[58] M. Gagné and R. Kashyap, "Random fiber Bragg grating Raman fiber laser," *Optics Letters,* vol. 39, pp. 2755-2758, 2014.

[59] M. Gagné and R. Kashyap, "Demonstration of a 3 mW threshold Er-doped random fiber laser based on a unique fiber Bragg grating," *Optics express,* vol. 17, pp. 19067-19074, 2009.

[60] S. J. Mihailov and M. C. Gower, "Recording of efficient high-order Bragg reflectors in optical fibres by mask image projection and single pulse exposure with an excimer laser," *Electronics Letters,* vol. 30, pp. 707-709, 1994.

[61] D. C. Johnson, P. G. J. Wigley, G. I. Stegeman, F. Bilodeau, B. Malo, and K. O. Hill, "Long-length, long-period rocking filters fabricated from conventional monomode telecommunications optical fiber," *Optics Letters,* vol. 17, pp. 1635-1637, 1992.

[62] B. A. Childers, M. E. Froggatt, S. G. Allison, S. T. C. Moore, D. A. Hare, C. F. Batten, *et al.*, "Use of 3000 Bragg grating strain sensors distributed on four 8-m optical fibers during static load tests of a composite structure," in *Smart Structures and Materials 2001*, 2001, pp. 133-142.

[63] R. Stubbe, B. Sahlgren, S. Sandgren, and A. Asseh, "Novel technique for writing long superstructured fiber Bragg gratings," *Photosensitivity and quadratic nonlinearity in glass waveguides: Fundamentals and applications,* vol. 22, 1995.

[64] R. Kashyap, H. G. Froehlich, A. Swanton, and D. J. Armes, "1.3 m long super-step-chirped fibre Bragg grating with a continuous delay of 13.5 ns and bandwidth 10 nm for broadband dispersion compensation," *Electronics Letters,* vol. 32, pp. 1807-1809, 1996.

[65] I. Petermann, B. Sahlgren, S. Helmfrid, A. T. Friberg, and P.-Y. Fonjallaz, "Fabrication of advanced fiber Bragg gratings by use of sequential writing with a continuous-wave ultraviolet laser source," *Applied Optics,* vol. 41, pp. 1051-1056, 2002.

[66] M. Durkin, M. Ibsen, M. J. Cole, and R. I. Laming, "1 m long continuously-written fibre Bragg gratings for combined second- and third-order dispersion compensation," *Electronics Letters,* vol. 33, pp. 1891-1893, 1997.

[67] K. M. Chung, L. Dong, C. Lu, and H. Y. Tam, "Novel fiber Bragg grating fabrication system for long gratings with independent apodization and with local phase and wavelength control," *Optics Express,* vol. 19, pp. 12664-12672, 2011.

[68] R. Kashyap, A. Swanton, and R. P. Smith, "Infinite length fibre gratings," *Electronics Letters,* vol. 35, pp. 1871-1872, 1999.

[69] S. Roy Choudhury and Y. Jaluria, "Practical aspects in the drawing of an optical fiber," *Journal of Materials Research,* vol. 13, pp. 483-493, 1998.

[70] F. El-Diasty, A. Heaney, and T. Erdogan, "Analysis of fiber Bragg gratings by a side-diffraction interference technique," *Applied Optics,* vol. 40, pp. 890-896, 2001.

[71] P.-Y. Fonjallaz and P. Börjel, "Interferometric side diffraction technique for the characterization of fibre gratings," in *OSA Tech. Dig. Series*, 1999, pp. 179-182.

[72] P. Ingemar, H. Sten, and F. Pierre-Yves, "Fibre Bragg grating characterization with ultraviolet-based interferometric side diffraction," *Journal of Optics A: Pure and Applied Optics,* vol. 5, p. 437, 2003.

[73] A. Sherman, A. Rosenthal, and M. Horowitz, "Extracting the structure of highly reflecting fiber Bragg gratings by measuring both the transmission and the reflection spectra," *Optics Letters,* vol. 32, pp. 457-459, 2007.

[74] K.-C. Hsu, L.-G. Sheu, W.-W. Hsiang, and Y. Lai, "Methods of achieving linear index-change response for narrow-band fiber Bragg grating sequential writing," *Optics Communications,* vol. 277, pp. 310-314, 2007.

[75] L. M. Baskin, M. Sumetsky, P. S. Westbrook, P. I. Reyes, and B. J. Eggleton, "Accurate characterization of fiber Bragg grating index modulation by side-diffraction technique," *IEEE Photonics Technology Letters,* vol. 15, pp. 449-451, 2003.

[76] A. D. Yablon, "Multi-Wavelength Optical Fiber Refractive Index Profiling by Spatially Resolved Fourier Transform Spectroscopy," *Journal of Lightwave Technology,* vol. 28, pp. 360-364, 2010.

[77] W. Margulis, B. Lesche, I. C. S. Carvalho, and P. M. P. Gouvêa, "Heat scan: a simple technique to study gratings infibers," *Optics Letters,* vol. 18, pp. 1016-1018, 1993.

[78] Z. Zhaowei, C. Tian, M. A. F. Roelens, M. R. Mokhtar, P. Petropoulos, D. J. Richardson, *et al.*, "Direct characterization of the spatial effective refractive index profile in Bragg gratings," *IEEE Photonics Technology Letters,* vol. 17, pp. 2685-2687, 2005.

[79] E. P. Alcusa-Sáez, A. Díez, M. González-Herráez, and M. V. Andrés, "Time-resolved acousto-optic interaction in single-mode optical fibers: characterization of axial nonuniformities at the nanometer scale," *Optics Letters,* vol. 39, pp. 1437-1440, 2014.

[80] W. Eickhoff and R. Ulrich, "Optical frequency domain reflectometry in single-mode fiber," *Applied Physics Letters,* vol. 39, pp. 693-695, 1981.

[81] U. Glombitza and E. Brinkmeyer, "Coherent frequency-domain reflectometry for characterization of single-mode integrated-optical waveguides," *Journal of Lightwave Technology,* vol. 11, pp. 1377-1384, 1993.

[82] M. Froggatt and J. Moore, "High-spatial-resolution distributed strain measurement in optical fiber with Rayleigh scatter," *Applied Optics,* vol. 37, pp. 1735-1740, 1998.

[83] M. Froggatt, R. J. Seeley, and D. K. Gifford, "High resolution interferometric optical frequency domain reflectometry (OFDR) beyond the laser coherence length," United States Patent, 2009.

[84] R. I. Woodward, E. J. R. Kelleher, T. H. Runcorn, S. Loranger, D. Popa, V. J. Wittwer, *et al.*, "Fiber grating compression of giant-chirped nanosecond pulses from an ultra-long nanotube mode-locked fiber laser," *Optics Letters,* vol. 40, pp. 387-390, 2015.

[85] M. C. Farries, K. Sugden, D. C. J. Reid, I. Bennion, A. Molony, and M. J. Goodwin, "Very broad reflection bandwidth (44 nm) chirped fibre gratings and narrow bandpass filters produced by the use of an amplitude mask," *Electronics Letters,* vol. 30, pp. 891-892, 1994.

[86] S. Lewis, M. Guy, J. Taylor, and R. Kashyap, "All-fibre periodic spectral filter for simultaneous generation of multiple WDM channels from broad bandwidth pulsed sources," *Electronics Letters,* vol. 34, pp. 1247-1249, 1998.

[87] R. Kashyap, "A new class of fibre grating based band-pass filters: The asymmetric interferometer," *Optics Communications,* vol. 153, pp. 14-18, 1998.

[88] S. Loranger, M. Gagné, and R. Kashyap, "Delay enhancement : A Cavity with an extended broad-band mode using chirped fiber-Bragg gratings," presented at the Photonic West, San Francisco, 2015.

[89] J. Zheng, R. Wang, T. Pu, L. Lu, T. Fang, Y. Su, *et al.*, "Phase-controlled superimposed FBGs and their applications in spectral-phase en/decoding," *Optics Express*, vol. 19, pp. 8580-8595, 2011.

[90] X. Dong, W. Liu, D. Wang, and M. Wu, "Study on Fabry–Perot cavity consisting of two chirped fiber Bragg gratings," *Optical Fiber Technology*, vol. 18, pp. 209-214, 2012.

[91] B. Lee, "Review of the present status of optical fiber sensors," *Optical Fiber Technology*, vol. 9, pp. 57-79, 2003.

[92] W. W. Morey, G. Meltz, and W. H. Glenn, "Fiber optic Bragg grating sensors," in *Proc. SPIE*, 1989, p. 106.

[93] A. J. Rogers and V. A. Handerek, "Frequency-derived distributed optical-fiber sensing: Rayleigh backscatter analysis," *Applied Optics*, vol. 31, pp. 4091-4095, 1992.

[94] Y. Koyamada, M. Imahama, K. Kubota, and K. Hogari, "Fiber-Optic Distributed Strain and Temperature Sensing With Very High Measurand Resolution Over Long Range Using Coherent OTDR," *Journal of Lightwave Technology*, vol. 27, pp. 1142-1146, 2009.

[95] Y. Koyamada, H. Nakamoto, and N. Ohta, "High performance coherent OTDR enhanced with erbium doped fiber amplifiers," *Journal of optical communications*, vol. 13, pp. 127-133, 1992.

[96] Y. Wang, J. Gong, B. Dong, D. Y. Wang, T. J. Shillig, and A. Wang, "A Large Serial Time-Division Multiplexed Fiber Bragg Grating Sensor Network," *Journal of Lightwave Technology*, vol. 30, pp. 2751-2756, 2012.

[97] B. A. Childers, M. E. Froggatt, S. G. Allison, T. C. Moore Sr, D. A. Hare, C. F. Batten, *et al.*, "Use of 3000 Bragg grating strain sensors distributed on four eight-meter optical fibers during static load tests of a composite structure," NASA Langley Research Center; Hampton, VA, United States, Technical Report 20040086084, 2001.

[98] H. Igawa, K. Ohta, T. Kasai, I. Yamaguchi, H. Murayama, and K. Kageyama, "Distributed measurements with a long gauge FBG sensor using optical frequency domain reflectometry," *Journal of Solid Mechanics and Materials Engineering*, vol. 2, pp. 1242-1252, 2008.

[99] S. Loranger, M. Gagné, V. Lambin-Iezzi, and R. Kashyap, "Rayleigh scatter based order of magnitude increase in distributed temperature and strain sensing by simple UV exposure of optical fibre," *Sci. Rep.*, vol. 5, 2015.

[100] D. Johlen, F. Knappe, H. Renner, and E. Brinkmeyer, "UV-induced absorption, scattering and transition losses in UV side-written fibbers," in *Optical Fiber Communication Conference 1999*, 1999, pp. ThD1-ThD1.

[101] D. W. Hahn, "Light scattering theory," *Department of Mechanical and Aerospace Engineering, Florida*, 2006.

[102] F. Parent, S. Loranger, K. K. Mandal, V. L. Iezzi, J. Lapointe, J.-S. Boisvert, *et al.*, "Enhancement of accuracy in shape sensing of surgical needles using optical frequency domain reflectometry in optical fibers," *Biomedical Optics Express*, vol. 8, pp. 2210-2221, 2017.

[103] H. Haus and C. V. Shank, "Antisymmetric taper of distributed feedback lasers," *Quantum Electronics, IEEE Journal of,* vol. 12, pp. 532-539, 1976.

[104] K. Utaka, S. Akiba, K. Sakai, and Y. Matsushima, "λ/4-shifted InGaAsP/InP DFB lasers by simultaneous holographic exposure of positive and negative photoresists," *Electronics Letters 20(24),* 1008-1010, 1984.

[105] M. Nakamura, K. Aiki, J. Umeda, A. Katzir, A. Yariv, and H. Yen, "GaAs GaAlAs double-heterostructure injection lasers with distributed feedback," *IEEE Journal of Quantum Electronics,* vol. 11, pp. 436-439, 1975.

[106] F. K. Reinhart, R. A. Logan, and C. V. Shank, "GaAs-AlxGa1-xAs injection lasers with distributed Bragg reflectors," *Applied Physics Letters,* vol. 27, pp. 45-48, 1975.

[107] D. R. Scifres, R. D. Burnham, and W. Streifer, "Distributed-feedback single heterojunction GaAs diode laser," *Applied Physics Letters,* vol. 25, pp. 203-206, 1974.

[108] K. Tada and A. Suzuki, "Integrated lasers with intracavity distributed Bragg reflector and phase modulation," in *Proc. Monthly Meet. Microwave Group, IECE,* 1977.

[109] M. Sejka, P. Varming, J. Hubner, and M. Kristensen, "Distributed feedback Er³⁺-doped fibre laser," *Electronics Letters,* vol. 31, pp. 1445-1446, 1995.

[110] C. Spiegelberg, G. Jihong, H. Yongdan, Y. Kaneda, J. Shibin, and N. Peyghambarian, "Low-noise narrow-linewidth fiber laser at 1550 nm (June 2003)," *Journal of Lightwave Technology,* vol. 22, pp. 57-62, 2004.

[111] J. Geng, Q. Wang, T. Luo, S. Jiang, and F. Amzajerdian, "Single-frequency narrow-linewidth Tm-doped fiber laser using silicate glass fiber," *Optics Letters,* vol. 34, pp. 3493-3495, 2009.

[112] Y. Hu and N. G. R. Broderick, "Improved design of a DFB Raman fibre laser," *Optics Communications,* vol. 282, pp. 3356-3359, 2009.

[113] H. Kogelnik and C. V. Shank, "Coupled-Wave Theory of Distributed Feedback Lasers," *Journal of Applied Physics,* vol. 43, pp. 2327-2335, 1972.

[114] C. M. de Sterke, K. R. Jackson, and B. D. Robert, "Nonlinear coupled-mode equations on a finite interval: a numerical procedure," *Journal of the Optical Society of America B,* vol. 8, pp. 403-412, 1991.

[115] V. E. Perlin and H. G. Winful, "Distributed feedback fiber Raman laser," *IEEE Journal of Quantum Electronics,* vol. 37, pp. 38-47, 2001.

[116] Y.-H. Liao and H. G. Winful, "Dynamics of distributed-feedback fiber lasers: effect of nonlinear refraction," *Optics Letters,* vol. 21, pp. 471-473, 1996.

[117] J. T. Kringlebotn, J. L. Archambault, L. Reekie, and D. N. Payne, "Er3+:Yb3+-codoped fiber distributed-feedback laser," *Optics Letters,* vol. 19, pp. 2101-2103, 1994.

[118] H. Asseh, H. Storoy, J. Kringlebotn, W. Margulis, B. Sahlgren, and S. Sandgren, "cm long Yb q DFB fibre laser with perma-Ž. nent phase shifted grating," *Electron Lett,* vol. 31, p. 969970, 1995.

[119] M. Ibsen, E. Ronnekieiv, G. J. Cowle, M. O. Berendt, O. Hadeler, M. N. Zervas, *et al.*, "Robust high power (>20 mW) all-fibre DFB lasers with unidirectional and truly single

polarisation outputs," in *Lasers and Electro-Optics, 1999. CLEO '99. Summaries of Papers Presented at the Conference on*, 1999, pp. 245-246.

[120] S. Yamashita and G. J. Cowle, "Single-polarization operation of fiber distributed feedback (DFB) lasers by injection locking," *Journal of Lightwave Technology*, vol. 17, pp. 509-513, 1999.

[121] M. N. Zervas, R. Wilmshurst, and L. M. B. Walker, "Twisted hi-bi fiber distributed-feedback lasers with controllable output state of polarization," *Optics Letters*, vol. 38, pp. 1533-1535, 2013.

[122] R. E. Bartolo, G. A. Cranch, and C. K. Kirkendall, "The nature of the polarization beat frequency as a function of twist for DFB fiber lasers," 2003, pp. 96-105.

[123] P. S. Westbrook, K. S. Abedin, J. W. Nicholson, T. Kremp, and J. Porque, "Demonstration of a Raman fiber distributed feedback laser," in *CLEO:2011 - Laser Applications to Photonic Applications*, Baltimore, Maryland, 2011, p. PDPA11.

[124] P. S. Westbrook, K. S. Abedin, J. W. Nicholson, T. Kremp, and J. Porque, "Raman fiber distributed feedback lasers," *Optics Letters*, vol. 36, pp. 2895-2897, 2011.

[125] J. Shi, S.-u. Alam, and M. Ibsen, "High Power, Low Threshold, Raman DFB Fibre Lasers," in *Proceedings of the International Quantum Electronics Conference and Conference on Lasers and Electro-Optics Pacific Rim 2011*, Sydney, 2011, p. C1174.

[126] J. Shi, S.-u. Alam, and M. Ibsen, "Highly efficient Raman distributed feedback fibre lasers," *Optics Express*, vol. 20, pp. 5082-5091, 2012.

[127] J. Shi, S.-u. Alam, and M. Ibsen, "Sub-watt threshold, kilohertz-linewidth Raman distributed-feedback fiber laser," *Optics Letters*, vol. 37, pp. 1544-1546, 2012.

[128] S. Loranger, V. Karpov, G. W. Schinn, and R. Kashyap, "Single-Frequency Low Threshold Linearly Polarized DFB Raman Fiber Lasers," *Optics Letters*, vol. 42, pp. 3864-3867, 2017.

[129] J. Shi, "Effects of Phase and Amplitude Noise on? Phase-Shifted DFB Raman Fibre Lasers," in *Bragg Gratings, Photosensitivity, and Poling in Glass Waveguides*, 2011, p. JThA30.

[130] J. Shi, P. Horak, S.-u. Alam, and M. Ibsen, "Detailed study of four-wave mixing in Raman DFB fiber lasers," *Optics Express*, vol. 22, pp. 22917-22924, 2014.

[131] K. S. Abedin, P. S. Westbrook, J. W. Nicholson, J. Porque, T. Kremp, and X. Liu, "Single-frequency Brillouin distributed feedback fiber laser," *Optics Letters*, vol. 37, pp. 605-607, 2012.

[132] C. M. de Sterke, "Optical push broom," *Optics Letters*, vol. 17, pp. 914-916, 1992.

[133] H. G. Winful, I. V. Kabakova, and B. J. Eggleton, "Model for distributed feedback Brillouin lasers," *Optics Express*, vol. 21, pp. 16191-16199, 2013.

[134] S. Loranger, V. Lambin-Iezzi, M. Wahbeh, and R. Kashyap, "Stimulated Brillouin scattering in ultra-long distributed feedback Bragg gratings in standard optical fiber," *Optics Letters*, vol. 41, pp. 1797-1800, 2016.

[135] S. Loranger and R. Kashyap, "Are optical fibers really uniform? Measurement of refractive index on a centimeter scale," *Optics Letters*, vol. 42, pp. 1832-1835, 2017.

[136] S. Loranger, V. Lambin-Iezzi, and R. Kashyap, "Reproducible ultra-long FBGs in phase corrected non-uniform fibers," *Optica,* vol. 4, pp. 1143-1146, 2017.

[137] S. Loranger, A. Tehranchi, H. Winful, and R. Kashyap, "Optimization and Realization of phase-shifted Distributed Feedback Fiber Bragg Grating Raman lasers," *Optica,* 2017.

[138] J. Sun, D. Yitang, C. Xiangfei, Z. Yejin, and X. Shizhong, "Stable Dual-Wavelength DFB Fiber Laser With Separate Resonant Cavities and Its Application in Tunable Microwave Generation," *Photonics Technology Letters, IEEE,* vol. 18, pp. 2587-2589, 2006.

[139] V. C. Lauridsen, J. H. Povlsen, and P. Varming, "Design of DFB fibre lasers," *Electronics Letters,* vol. 34, pp. 2028-2030, 1998.

[140] R. Kashyap, H.-G. Froehlich, A. Swanton, and D. J. Armes, "1.3 m long super-step-chirped fibre Bragg grating with a continuous delay of 13.5 ns and bandwidth 10 nm for broadband dispersion compensation," *Electronics Letters,* vol. 32, pp. 1807-1809, 1996.

[141] S. Le Floch and P. Cambon, "Study of Brillouin gain spectrum in standard single-mode optical fiber at low temperatures (1.4–370 K) and high hydrostatic pressures (1–250 bars)," *Optics Communications,* vol. 219, pp. 395-410, 2003.

[142] H. Rokhsari and K. J. Vahala, "Observation of Kerr nonlinearity in microcavities at room temperature," *Optics Letters,* vol. 30, pp. 427-429, 2005.

[143] N. Lizárraga, N. P. Puente, E. I. Chaikina, T. A. Leskova, and E. R. Méndez, "Single-mode Er-doped fiber random laser with distributed Bragg grating feedback," *Optics Express,* vol. 17, pp. 395-404, 2009.

[144] S. Loranger and R. Kashyap, "Are optical fibers really uniform? Measurement of refractive index on a centimeter scale " *Opt. Lett.,* 2017.

[145] G. A. Miller, J. R. Peele, C. G. Askins, and G. A. Cranch, "Characterization of strong fiber Bragg gratings using an applied thermal chirp and iterative algorithm," *Applied Optics,* vol. 50, pp. 6617-6626, 2011/12/20 2011.

[146] G. A. Miller, G. M. Flockhart, and G. A. Cranch, "Reducing Phase Errors during the Inscription Process of Distributed Feedback Fiber Lasers," in *Conference on Lasers and Electro-Optics/International Quantum Electronics Conference*, Baltimore, Maryland, 2009, p. CThE6.

APPENDIX A - LIST OF PUBLICATION AND AWARDS

Publications

1- V. Lambin-Iezzi, **S. Loranger**, and R. Kashyap, " High sensitivity distributed temperature fiber sensor using stimulated Brillouin scattering," *Optics Express*, 2017 (submitted 31/10/2017).
2- **S. Loranger**, A. Tehranchi, H. Winful, and R. Kashyap, "Optimization and Realization of phase-shifted Distributed Feedback Fiber Bragg Grating Raman lasers," *Optica*, 2017 (submitted 15/09/2017).
3- **S. Loranger**, V. Karpov, G. W. Schinn, and R. Kashyap, "Single-Frequency Low Threshold Linearly Polarized DFB Raman Fiber Lasers," *Optics Letters*, vol. 42, pp. 3864-3867, 2017.
4- **S. Loranger**, V. Lambin-Iezzi, and R. Kashyap, "Reproducible ultra-long FBGs in phase corrected non-uniform fibers," *Optica*, vol. 4, pp. 1143-1146, 2017.
5- F. Parent, **S. Loranger**, K. K. Mandal, V. L. Iezzi, J. Lapointe, J.-S. Boisvert, *et al.*, "Enhancement of accuracy in shape sensing of surgical needles using optical frequency domain reflectometry in optical fibers," *Biomedical Optics Express*, vol. 8, pp. 2210-2221, 2017.
6- **S. Loranger** and R. Kashyap, "Are optical fibers really uniform? Measurement of refractive index on a centimeter scale," *Optics Letters*, vol. 42, pp. 1832-1835, 2017.
7- V. L. Iezzi, T. F. S. Büttner, A. Tehranchi, **S. Loranger**, I. V. Kabakova, B. J. Eggleton, *et al.*, "Temporal characterization of a multi-wavelength Brillouin–erbium fiber laser," *New Journal of Physics*, vol. 18, p. 055003, 2016.
8- **S. Loranger**, V. Lambin-Iezzi, M. Wahbeh, and R. Kashyap, "Stimulated Brillouin scattering in ultra-long distributed feedback Bragg gratings in standard optical fiber," *Optics Letters*, vol. 41, pp. 1797-1800, 2016.
9- J. Lapointe, Y. Ledemi, **S. Loranger**, V. L. Iezzi, E. Soares de Lima Filho, F. Parent, *et al.*, "Fabrication of ultrafast laser written low-loss waveguides in flexible As2S3 chalcogenide glass tape," *Optics Letters*, vol. 41, pp. 203-206, 2016.
10- V. L. Iezzi, J.-S. Boisvert, **S. Loranger**, and R. Kashyap, "3D printed long period gratings for optical fibers," *Optics Letters*, vol. 41, pp. 1865-1868, 2016.
11- R. I. Woodward, E. J. R. Kelleher, T. H. Runcorn, **S. Loranger**, D. Popa, V. J. Wittwer, *et al.*, "Fiber grating compression of giant-chirped nanosecond pulses from an ultra-long nanotube mode-locked fiber laser," *Optics Letters*, vol. 40, pp. 387-390, 2015.
12- **S. Loranger**, M. Gagné, V. Lambin-Iezzi, and R. Kashyap, "Rayleigh scatter based order of magnitude increase in distributed temperature and strain sensing by simple UV exposure of optical fibre," *Sci. Rep.*, vol. 5, 2015.
13- J. Lapointe, F. Parent, E. Soares de Lima Filho, **S. Loranger**, and R. Kashyap, "Toward the integration of optical sensors in smartphone screens using femtosecond laser writing," *Optics Letters*, vol. 40, pp. 5654-5657, 2015.
14- **S. Loranger**, M. Gagné, and R. Kashyap, "Capacitors go optical: wavelength independent broadband mode cavity," *Optics Express*, vol. 22, pp. 14253-14262, 2014.
15- V. L. Iezzi, **S. Loranger**, M. Marois, and R. Kashyap, "High-sensitivity temperature sensing using higher-order Stokes stimulated Brillouin scattering in optical fiber," *Optics letters*, vol. 39, pp. 857-860, 2014.

16- M. Gagné, **S. Loranger**, J. Lapointe, and R. Kashyap, "Fabrication of high quality, ultra-long fiber Bragg gratings: up to 2 million periods in phase," *Optics Express,* vol. 22, pp. 387-398, 2014.
17- E. S. d. L. Filho, G. Nemova, **S. Loranger**, and R. Kashyap, "Laser-induced cooling of a Yb:YAG crystal in air at atmospheric pressure," *Optics Express,* vol. 21, pp. 24711-24720, 2013.
18- **S. Loranger**, V. L. Iezzi, and R. Kashyap, "Demonstration of an ultra-high frequency picosecond pulse generator using an SBS frequency comb and self phase-locking," *Opt. Express,* vol. 20, pp. 19455-19462, 2012.
19- V. Lambin-Iezzi, S**. Loranger**, M. Saad, and R. Kashyap, "Stimulated Brillouin scattering in SM ZBLAN fiber," *Journal of non-crystalline solids,* vol. 359, pp. 65-68, 2013.
20- **S. Loranger**, V. L. Iezzi, A. Harhira, M. Saad, A. Gomes, S. Rehman, *et al.*, "Stimulated Brillouin Scattering in Multimode Optical Fibers for Sensing Applications," *Photon,* vol. 9, pp. 17-20, 2011.
21- D. Seddaoui, **S. Loranger**, M. Malatek, Me, x, D. nard, *et al.*, "The Nonlinear Landau-Lifshitz Equation: Ferromagnetic Resonance, Giant Magnetoimpedance, and Related Effects," *Magnetics, IEEE Transactions on,* vol. 47, pp. 279-283, 2011.
22- D. Seddaoui, **S. Loranger**, D. Ménard, and A. Yelon, "Landau-Lifshitz equation for magnetization dynamics of thin films: Failure of the linear approximation at low effective fields," *Physical Review B,* vol. 82, p. 134430, 2010.
23- C. Santato, L. Favaretto, M. Melucci, A. Zanelli, M. Gazzano, M. Monari, D. Isik, D. Banville, S. Bertolazzi, **S. Loranger**, F. Cicoira, "Influence of the oxidation level on the electronic, morphological and charge transport properties of novel dithienothiophene S-oxide and S,S-dioxide inner core oligomers," *Journal of Materials Chemistry,* vol. 20, pp. 669-676, 2010.

Patents submitted

1- **Loranger, S.**, and Kashyap, R. "Correcting long Fibre Bragg Gratings," provisional submitted patent # US 62/483,437, 2017.
2- Lambin-Iezzi. V., **Loranger, S.**, and Kashyap, R., "Method for generating optical pulses and optical pulse generator," submitted patent # CA 2,823,462 & US 14/454,220, 2013.

Conferences (presenter only)

1- **S. Loranger**, V. L. Iezzi, and R. Kashyap, "All-in-phase ultralong Bragg gratings in non-uniform fiber by complete phase correction," presented at the 5th Workshop on Specialty Optical Fibers and Their Applications, Limassol, 2017. (**Invited Oral**)
2- **S. Loranger** and R. Kashyap, "Fiber Imperfections and their Impact on the Performance of Fiber Grating DFB Raman Lasers," presented at the Nonlinear Optics (NLO), Waikoloa, 2017. (Poster)
3- **S. Loranger**, A. Tehranchi, H. Winful, and R. Kashyap, "Parameter optimisation of pi-shifted Distributed Feedback Fiber Bragg Grating Raman lasers," presented at the The European Conference on Lasers and Electro-Optics (CLEO Europe), Munich, Germany, 2017. (Poster)
4- **S. Loranger**, V. L. Iezzi, and R. Kashyap, "Ultra-Long DFB Fiber Bragg Grating for Stimulated Brillouin Scattering in Standard Fiber," presented at the Frontiers in Optics/Laser Science, Rochester, 2016. (Oral)

5- **S. Loranger**, F. Parent, V. Lambin-Iezzi, and R. Kashyap, "Rayleigh scatter based distributed sensing enhancement by simple UV exposure of fiber," presented at the 7th International Conference on Optical, Optoelectronic and Photonic Materials and Applications, Montreal, 2016. (Oral)
6- **S. Loranger**, F. Parent, V. Lambin-Iezzi, and R. Kashyap, "Enhancement of Rayleigh scatter in optical fiber by simple UV treatment: an order of magnitude increase in distributed sensing sensitivity," 2016, pp. 97440E-97440E-7. (Oral)
7- **S. Loranger**, M. Gagné, and R. Kashyap, "Delay enhancement : A Cavity with an extended broad-band mode using chirped fiber-Bragg gratings," presented at the Photonic West, San Francisco, 2015. (Oral)
8- **S. Loranger**, M. Gagné, and R. Kashyap, "The Optical Capacitor: A Cavity with an extended broad-band mode using chirped fiber-Bragg gratings," in *Frontiers in Optics*, 2014, p. FW4D. 1. (Oral)
9- **S. Loranger**, E. S. de Lima Filho, G. Nemova, and R. Kashyap, "Thermal study of laser cooling in rhodamine dye using a Bragg grating," in *SPIE OPTO 9000*, 2014, p. 304. (Poster)
10- **S. Loranger**, E. Soares, G. Nemova, C. Allen, S. Lamarre, and R. Kashyap, "Spectroscopy and Efficiency of Colloidal CdSe Quantum Dots in Liquids for Laser Cooling," presented at the Photonic North, Ottawa, 2013. (Oral)
11- **S. Loranger**, A. Lesage-Landry, E. S. de Lima Filho, G. Nemova, N. O. Dantas, P. C. Morais, *et al.*, "Spectroscopic and life-time measurements of quantum dot doped glass for optical refrigeration: a feasibility study," in *SPIE OPTO*, 2013, pp. 86380I-86380I-8. (Oral)
12- **S. Loranger**, V. Lambin-Iezzi, M. Saad, and R. Kashyap, "Characterisation of internal damage and artifact in ZBLAN fiber by using stimulated Brillouin and Rayleigh scattering," presented at Photonic North, Montreal, July 2012. (Poster)

Awards

1- 2017: Best student oral presentation award, WSOF2017, Limassol, Cyprus
2- 2016: 2nd place for best student oral presentation, ICOOPMA2016, Montreal, Canada
3- 2013-2016: Vanier Scholarship, Canada
4- 2013: NSERC Alexander Graham Bell Scholarship (declined), Canada
5- 2013: 3rd place for best student oral presentation, Photonic North, Ottawa, Canada
6- 2012: Acceptance to SAMPA summer school, Araraquare, Brazil
7- 2012: FQRNT masters Scholarship, Québec
8- 2011: NSERC Julie-Payette Scholarship, Canada
9- 2011: NSERC André Hamer Postgraduate Prize, Canada
10- 2011: Profil De Vinci award, Polytechnique Montréal